

AD-A133 935

INITIATION GROWTH AND COALESCENCE OF SMALL FATIGUE  
CRACKS(U) PURDUE UNIV LAFAYETTE IN SCHOOL OF  
AERONAUTICS AND ASTRONAUTICS A F GRANDT MAY 83

1/1

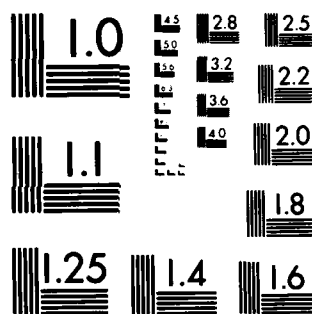
UNCLASSIFIED

AFOSR-TR-83-0867 AFOSR-82-0041

F/G 20/11

NL

END  
DATE  
FILMED  
11-83  
DTIC



MICROCOPY RESOLUTION TEST CHART  
NATIONAL BUREAU OF STANDARDS-1963-A

AFOSR-TR- 83 - 0867



AD-A133935

PURDUE UNIVERSITY

SCHOOL OF AERONAUTICS AND ASTRONAUTICS

DTIC FILE COPY



DTIC  
ELECTE  
OCT 21 1983  
S D D

Approved for public release  
distribution unlimited.

West Lafayette, Indiana 47907

83 10 20 034

4

Initiation, Growth, and  
Coalescence of Small  
Fatigue Cracks

Annual Scientific Report of  
Research conducted during  
period 15 January 1982 to  
15 January 1983 under  
Air Force Grant No.  
AFOSR-82-0041

AIR FORCE OFFICE OF SCIENTIFIC RESEARCH (AFOSR)  
NOTICE OF TRANSMITTAL TO DTIC  
This technical report has been reviewed and is  
approved for public release in accordance with  
Distribution is unlimited.  
MATTHEW J. KERTER  
Chief, Technical Information Division

Accession For	
NTIS GRA&I	<input checked="checked" type="checkbox"/>
DTIC TAB	<input type="checkbox"/>
Unannounced	<input type="checkbox"/>
Justification	
By	
Distribution/	
Availability Codes	
Dist and/or	
Dist	Special
A	

Prepared by

A.F. Grandt, Jr.  
School of Aeronautics and Astronautics  
Purdue University  
West Lafayette, Indiana 47907

DTIC  
ELECTE  
S OCT 21 1983 D  
D

UNCLASSIFIED

SECURITY CLASSIFICATION OF THIS PAGE (When Data Entered)

REPORT DOCUMENTATION PAGE		READ INSTRUCTIONS BEFORE COMPLETING FORM	
1. REPORT NUMBER <b>AFOSR-TR- 83-0867</b>	2. GOVT ACCESSION NO. <b>AD-A133935</b>	3. RECIPIENT'S CATALOG NUMBER	
4. TITLE (and Subtitle) <b>Initiation, Growth and Coalescence of Small Fatigue Cracks</b>		5. TYPE OF REPORT & PERIOD COVERED <b>Annual Scientific Report 15 Jan. 1982 - 15 Jan. 1983</b>	
7. AUTHOR(s) <b>A.F. Grandt, Jr.</b>		6. PERFORMING ORG. REPORT NUMBER	
9. PERFORMING ORGANIZATION NAME AND ADDRESS <b>School of Aeronautics and Astronautics Purdue University West Lafayette, IN 47907</b>		8. CONTRACT OR GRANT NUMBER(s) <b>AFOSR-82-0041</b>	
11. CONTROLLING OFFICE NAME AND ADDRESS <b>Air Force Office of Scientific Research AFOSR/NA Bolling Air Force Base, D.C. 20332</b>		10. PROGRAM ELEMENT, PROJECT, TASK AREA & WORK UNIT NUMBERS <b>611024 2307/B2</b>	
14. MONITORING AGENCY NAME & ADDRESS (if different from Controlling Office)		12. REPORT DATE <b>May 1983</b>	
		13. NUMBER OF PAGES <b>78</b>	
		15. SECURITY CLASS. (of this report) <b>Unclassified</b>	
		15a. DECLASSIFICATION/DOWNGRADING SCHEDULE	
16. DISTRIBUTION STATEMENT (of this Report) <b>Approved for public release; distribution unlimited.</b>			
17. DISTRIBUTION STATEMENT (of the abstract entered in Block 20, if different from Report)			
18. SUPPLEMENTARY NOTES			
19. KEY WORDS (Continue on reverse side if necessary and identify by block number) <b>Fatigue, Fracture Mechanics, Crack Coalescence, Notches, Polymethylmethacrylate</b>			
20. ABSTRACT (Continue on reverse side if necessary and identify by block number) <b>→ This interim report summarizes the first year's progress on a research effort directed at studying the initiation, growth, and coalescence of small fatigue cracks at notches. A fracture mechanics based model is described to predict the growth and coalescence of multiple cracks located at notches. Stress intensity factors are presented for interacting cracks located at holes. The predictive model is compared with experimental results obtained with multiply cracked specimens made from a transparent polymer. Current efforts and future goals are also briefly described.</b>			

UNCLASSIFIED

## Contents

	Page
1.0 Introduction. . . . .	1
2.0 Summary of Progress and Accomplishments . . . . .	3
2.1 Task I Progress - Crack Growth Algorithm. . . . .	3
2.2 Task II Progress - Crack Initiation Analysis . . . . .	3
2.3 Task III Progress - Crack Coalescence Experiments. . . . .	5
2.3.1 Single Crack Verification . . . . .	5
2.3.2 Multiply Cracked Holes in PMMA Plates . . . . .	6
2.3.3 Multiple Cracks in PMMA Bend Specimens. . . . .	7
2.3.4 Multiple Cracks in Metal Edge Notch Specimens . . . . .	7
2.4 Task IV Progress - Characterization of Small Cracks . . . . .	8
3.0 Current and Planned Research. . . . .	11
4.0 Professional Personnel, Publications and Presentations. . . . .	13
5.0 References. . . . .	15
6.0 Figures . . . . .	16
7.0 Appendix A, "Stress Intensity Factors for Coalescing and Single Corner Flaws Along a Hole Bore in a Plate". . . . .	54

## 1.0 INTRODUCTION

This Annual Scientific Report summarizes research accomplished during the first year (January 82 to January 83) of AFOSR Grant No. AFOSR-82-0041. The objective of this effort is to determine the manner in which "small" fatigue cracks initiate at notches, extend by cyclic loading, interact with adjacent flaws, and coalesce into a single dominant crack which controls final fracture. The desired product is a predictive scheme capable of analyzing the early stages of fatigue crack growth which are characterized by the growth and link-up of small cracks. Research toward this goal is directed at the following tasks.

- I. Crack Growth Predictive Algorithm. A computer program will be developed to predict the growth and coalescence of multiple cracks located at notches.
- II. Crack Interaction Analysis. Stress intensity factors solutions will be computed for multiple cracks located at an open hole. These solutions are required for the multiple crack growth algorithm.
- III. Crack Coalescence Experiments. Fatigue tests will be conducted with multiply cracked specimens to provide a data base to evaluate the predictive model. Initially the model will be verified with "large crack" results directed toward coalescence aspects of the problem. Subsequent experiments will focus on coalescence of "small" cracks.
- IV. Characterization of Small Cracks. This phase of the effort is directed toward the growth and coalescence of physically small cracks.

These data will be used to characterize the growth of "small" flaws, which are expected to behave differently than "large" cracks.

Additional details of these goals and progress to date are described in the remaining sections of this report.



## 2.0 SUMMARY OF PROGRESS AND ACCOMPLISHMENTS

### 2.1 Task I Progress - Crack Growth Algorithm

A computer program has been written to analyze the multiple crack configurations shown in Fig. 1. Various combinations of surface and/or corner flaws are assumed to be located along the bore of a circular hole. It is assumed that linear elastic fracture mechanics are valid and that crack growth rates are controlled by the stress intensity factor  $K$ . Stress intensity factors are estimated at the major and minor crack axes (locations 1 to 6 in Fig. 1) by modifying the solutions for single cracks in a large body (1) with an interaction factor (2) developed here for coalescing cracks. (The interaction solution is discussed in the Task II progress section.) The crack tips are allowed to grow independently at their major and minor axes without specifying crack shape changes. The multi-degree of freedom program predicts the growth of the separate initial cracks and their coalescence into single surface corner, or through-the-thickness flaws as shown in Fig. 2. Sample predictions and comparisons with test data are described in the Task III progress section.

### 2.2 Task II Progress - Crack Interaction Analysis

A key element of the overall predictive scheme is determining the interaction between adjacent cracks prior to their actual coalescence. It is expected, for example, that the presence of a nearby flaw will cause an increased crack growth rate. Although a few authors have studied the magnification in stress intensity factors due to coalescing cracks (3-6), solutions were not available for multiple cracks at notches. Thus, one phase of the current effort is directed toward obtaining stress

intensity factor solutions for coalescing cracks at fastener holes, a geometry which is also studied experimentally in the current program.

The three-dimensional finite element-alternating method (7-9) was used to compute stress intensity factors for symmetric corner cracks located at opposite sides of a plate containing a hole loaded in remote tension as shown in Fig. 3. Although the analysis was limited to symmetric corner cracks, several flaw shapes and sizes were considered. By comparing the double crack results with corresponding solutions for single cracks, it was possible to determine the effect of the second crack on the stress intensity factor as the two flaws grow toward each other and eventually touch. The influence of the adjacent flaw was represented as an interaction factor  $\gamma$ . The  $\gamma$  factor is defined as the ratio of the double crack  $K$  divided by the single crack result, and is given in Figs. 4 and 5 for two positions along the crack border.

Note in Fig. 4 that a significant increase in  $K$  ( $\gamma > 1$ ) occurs at the hole bore position ( $\phi = 90^\circ$  in Fig. 3) as the adjacent cracks approach each other (as the dimensionless crack separation distance  $t_{sep}/a \rightarrow 0$ ). This increased stress intensity factor is quite localized along the crack perimeter, however, and as shown in Fig. 5, is much less significant at the front surface location ( $\phi = 0$  in Fig. 3). Note in Fig. 5, for example, that there is actually a slight reduction in  $K$  ( $\gamma < 1$ ) at the free surface as the flaws approach each other. Although the interaction is a strong function of crack spacing (as represented by dimensionless spacing  $t_{sep}/a$  in Figs. 4 and 5), crack shape  $a/c$  has relatively little effect for the cases examined here.

Additional details of the crack interaction analysis are given in Refs. 2 and 10. Reference 2 is included in this report as Appendix A. The interaction factors obtained in this Task are incorporated in the computer program described in Task I to account for crack coalescence in the overall prediction scheme. Experimental verification of the crack coalescence predictions are described in the following section.

### 2.3 Task III Progress - Crack Coalescence Experiments

This phase of the effort is aimed at evaluating the numerical scheme described in Task I for predicting the initial growth and coalescence of multiple cracks located at notches. In order to separate crack coalescence aspects from "small crack" phenomena, the initial work has involved experiments with coalescence of relatively "large" cracks. Current work deals with the small crack problem and is described separately in the Task IV section.

#### 2.3.1 Single Crack Verification

Prior to describing crack coalescence experiments, initial verification of the predictive model for single flaws will be discussed. In an earlier program, fatigue crack growth tests were conducted with large specimens machined from polymethylmethacrylate (PMMA), a transparent polymer. The test specimen, mounted in loading grips, is shown schematically in Fig. 6. The specimens were 0.7 in. thick, 8.0 in. wide, contained a 0.75 in. hole, and were loaded in remote tension. Semielliptical surface cracks or quarter elliptical corner cracks were located along the hole bore in the configuration shown in Fig. 2. A camera viewed the

crack plane through the transparent specimen by means of a mirror placed in the cutout area of the grips. Crack growth was photographed as a function of elapsed cycles, and the photos were measured to give the crack dimensions.

Typical results for a semielliptical crack located midway along the hole bore are given in Fig. 7. Fig. 7a presents crack growth prior to penetration through the specimen thickness by the hole bore crack dimension  $2a$ . (Thickness penetration occurs when  $a = \frac{T}{2} \approx 0.35$  inch in Fig. 7a.) Figure 7b describes crack growth during the transition period when the part-through crack grows into a uniform through-the-thickness flaw. The experimental measurements are represented by open symbols in Fig. 7, while predictions based on a single crack version of the predictive program are given by the solid lines. Note that the numerical algorithm predicts the crack growth, including shape changes, quite well. Additional comparisons with single surface and corner crack tests are given in Ref. 11.

Thus, confident that single cracks could be predicted fairly well, the present program is studying the coalescence problem. The following subtasks are being examined.

### 2.3.2 Multiply Cracked Holes in PMMA Plates

Several fatigue tests have been conducted with PMMA specimens modeled after the double corner crack geometry studied by the finite element-alternating method described in Task II. The test specimens were 3.5 inches wide, had a 0.375 inch diameter hole, and were 0.7 inch thick. Two corner cracks were introduced on opposite sides of the plate thickness to match the symmetric corner crack configuration shown in Fig. 3.

The specimens were fastened to metal grips similar to those described previously in Fig. 6, and crack growth was again photographed through the transparent end of the specimen. Fatigue crack growth curves are shown for two specimens in Figs. 8 and 9. Here  $a_1$  and  $c_1$  represent the hole bore and free surface dimension of one crack (see Fig. 1c), while  $a_2$  and  $c_2$  are the corresponding dimensions for the second flaw. Note that the two cracks were quite symmetric in these two tests, as assumed in the Task II stress intensity factor analysis. After crack coalescence ( $a_1 + a_2 = T = \text{specimen thickness}$ ), only the free surface dimensions ( $c_1$  and  $c_2$ ) are given in Figs. 8 and 9.

The solid and dashed lines give predictions by the multiple degree of freedom model described earlier. The dashed lines predict the  $c$  dimensions prior to crack coalescence, while the solid lines represent predictions for the  $a$  dimension. The single solid line following predicted coalescence give the estimated growth of a single through-the-thickness flaw. Although the predictions are somewhat conservative, they provide a reasonable estimate for total specimen life. It is planned to conduct additional tests with nonsymmetric corner cracks.

### 2.3.3 Multiple Cracks in PMMA Bend Specimens

Several crack coalescence tests have been conducted with the semi-circular notched bend geometry shown in Fig. 10. The bend geometry was selected since loading can be applied without bonding grips to the specimen ends, and the crack plane can be observed directly through the transparent PMMA without use of a viewing mirror. Again corner cracks were located on opposite sides of the notch (see Fig. 10b) and

time lapse photography was used to measure and record crack growth.

A typical set of photographs showing initial crack growth and coalescence is given in Fig. 11. Note that crack coalescence occurs at approximately 11,890 cycles. The cusp dimension  $h$  (see Fig. 10c) then grows very rapidly until a fairly uniform through-the-thickness crack front is achieved at approximately 12,200 cycles. Typical plots of measured crack dimensions are given as functions of elapsed cycles in Figs. 12-15. It is interesting to note that in several experiments the crack tips did not coalesce immediately, but grew past each other in slightly different planes to form the overlapped configuration shown schematically in Fig. 16. Current efforts are directed toward estimating stress intensity factors for the notched bend geometry so that the life prediction model can be applied to this series of tests.

#### 2.3.4 Multiple Cracks in Metal Edge Notch Specimens

The multi-degree of freedom fatigue crack growth model has also been evaluated with experimental data provided by Dr. A. Thakker (12). He conducted a series of tests with the double notched specimen shown in Fig. 17. The specimens were made from Waspalloy, a turbine disk alloy, and were tested at 400°F. Small initial cracks were introduced along the bore of one of the semicircular edge notches, and heat tinting techniques were used to periodically mark the fatigue crack fronts. Crack length and shape measurements were then made on the fracture surface following final failure.

The specimen dimensions, load history, and crack growth properties were provided along with the measured crack lengths. The open hole stress intensity factor solution employed in the original crack growth model was modified here to reflect the fact that the cracks occurred at edge notches rather than central holes. The multiple crack computer program was then used to predict the growth of the individual cracks, coalescence, and final fracture.

The results for several specimens are given in Figs. 18-23. Note that since fracture surface markings were used to determine the crack lengths, relatively few experimental data points are shown. In addition, few details are known regarding crack coalescence and flaw shape changes. Nevertheless, when the total crack growth picture is viewed, the predictive model generally does an excellent job in predicting total specimen life.

#### 2.4 Task IV Progress - Characterization of Small Cracks

It is commonly known that physically small cracks (less than 0.10 inch long) may grow faster than larger flaws subjected to similar stress intensity factor levels. The assumptions regarding continuum behavior and linear elastic material response may lose validity as crack lengths become increasingly small. The problem is further complicated by the presence of adjacent flaws which often initiate simultaneously and which interact prior to the coalescence process. The preceding sections have described tasks directed toward the coalescence problem. This prior work has concentrated on relatively large flaws in order

to separate small crack behavior from coalescence phenomena. This section briefly outlines work aimed at the "small crack problem."

A series of fatigue tests have been conducted with V-notched PMMA specimens as shown schematically in Fig. 24. Again 4-point bending was applied to simplify specimen loading and crack plane observation. Natural fatigue cracks were allowed to develop naturally along the V-notch and to coalesce into a single flaw. Time lapse photography was used to record and measure the individual and coalescing flaws.

Typical results for two of the crack initiation tests are given in Figs. 25 and 26. Note that width and depth measurements are given as functions of elapsed cycles for the naturally occurring cracks. Crack spacing is also measured (not shown in Figs. 25 and 26) so that coalescence behavior can be studied as well. Flaw sizes less than 0.005 inches are routinely observed and measured.

*In several tests, multiple cracks formed uniformly along the notch and quickly joined to form a short through-the-thickness crack. Results for two of these experiments is given in Figs. 27 and 28. Here the initial through-the-thickness cracks size is on the order of 0.003 in.*

Analysis of these small crack experiments is currently in progress. Analysis of the notched specimen are being performed to determine the notch tip stresses. It is hoped that the through-crack results can be used to determine baseline properties for small crack behavior and that the Task I predictive algorithm can be modified to predict the multiple crack growth and coalescence results. It is recognized that this goal could be complicated by nonlinear plastic zone effects which could limit the LEFM approach for the small crack tests.



### 3.0 CURRENT AND PLANNED RESEARCH

As indicated, current efforts are directed toward analysis of the semicircular notch coalescence experiments (2.3.3) and the small crack results (2.4). It is also planned to conduct additional tests with cracked hole specimens (2.3.2) which contain nonsymmetric corner cracks.

The prior results have all been obtained with PMMA specimens. Since PMMA is a relatively brittle material, tests will also be conducted with polycarbonate, a more ductile polymer, in order to emphasize the plasticity problem. A sheet of polycarbonate has been purchased and several preliminary characterization tests have been conducted. It is planned to repeat the PMMA coalescence experiments with the polycarbonate specimens. A modified V-notch specimen, with a slightly larger notch radius, is being considered to minimize variations in the current "sharp" V-notch.

Following the remaining analysis of the PMMA results and the polycarbonate tests, it was originally planned to conduct a small study with metal specimens. Since the current predictive model has matched existing metal results quite well (2.3.4), and since it is much more difficult to measure internal crack dimensions with metal specimens, it may be desirable to continue the transparent polymer study. Overload/retardation experiments could be conducted with the polycarbonate material, for example, to determine load history effects on the coalescence process. (All tests conducted to date have employed constant amplitude cyclic loads). Since the crack tip plastic zone varies through the specimen thickness, and crack interaction effects vary along the flaw perimeter (2.2), one would expect crack coalescence to be a more complex three-dimensional problem in ductile materials subjected to variable load

histories. The decision to conduct variable load tests will be discussed with the project monitor following the outcome of the current PMMA and polycarbonate tests.

#### 4.0 PROFESSIONAL PERSONNEL, PUBLICATIONS, AND PRESENTATIONS

##### 4.1 Personnel

A.F. Grandt, Jr. has served as principal investigator for the research effort. He has been assisted by the following graduate research assistants.

B.J. Heath Mr. Heath completed a Masters Thesis entitled "Stress Intensity Factors for Coalescing and Single Corner Flaws Along A Hole Bore in a Plate" in January of 1983 and was officially awarded the Degree of Master of Science in Aeronautics and Astronautics in May of 1983.

R. Perez expects to complete requirements for the Master of Science Degree in Aeronautics and Astronautics in May of 1983 with the Thesis entitled "Cyclic Growth and Coalescence of Multiple Fatigue Cracks Located at Notches."

J.E. Pope Mr. Pope is currently pursuing a Ph.D. program in Aeronautics and Astronautics.

D.E. Tritsch, a Teaching Assistant supported by other School of Aeronautics and Astronautics Department funds, has also worked on a Masters Thesis which supports the goals of this research grant.

##### 4.2 Publications and Presentations

The following reports have been prepared for publication

B.J. Heath and A.F. Grandt, Jr., "Stress Intensity Factors for Coalescing and Single Corner Flaws Along a Hole Bore in a Plate," Engineering Fracture Mechanics, (in press).

B.J. Heath, "Stress Intensity Factors for Coalescing and Single Corner Flaws Along a Hole Bore in a Plate," M.S. Thesis, Purdue University, May 1983.

R. Perez and A.F. Grandt, Jr., "Coalescence of Multiple Fatigue Cracks at a Notch," Proceedings of the American Society of Civil Engineers Engineering Mechanics Division Speciality Conference, Purdue University, May 1983. Paper to be presented 24 May 1983.

The following publications are in preparation.

A.F. Grandt, Jr., R. Perez, D. Tritzsch, and A. Thakker, "Fatigue Life Predictions for Multiply Cracked Notches," planned for submission to Journal of Engineering Materials and Technology.

D.E. Tritzsch, "Fatigue Crack Size and Shape Predictions," M.S. Thesis, Purdue University, expected May 1983.

R. Perez and A.F. Grandt, "Initiation, Growth, and Coalescence of Small Fatigue Cracks in Polymethylmethacrylate," planned for submission to 5th International Congress on Experimental Mechanics.

R. Perez, "Cyclic Growth and Coalescence of Multiple Fatigue Cracks Located at Notches," M.S. Thesis, Purdue University, expected May 1983.

## 5.0 REFERENCES

1. Newman, J.C. and Raju, I.S., "Stress Intensity Factor Equations for Cracks in Three-Dimensional Finite Bodies," NASA Technical Memorandum 83200, Langley Research Center, August 1981.
2. Heath, B.J. and Grandt, A.F., "Stress Intensity Factors for Coalescing and Single Corner Flaws along a Hole Bore in a Plate," Engineering Fracture Mechanics (in press).
3. Kamei, A., and Yokoburi, T., "Two Collinear Asymmetrical Elastic Cracks," Rep. Res. Inst. Strength Materials, Tohoku Univ., Vol. 10, Dec. 1974.
4. Benthem, J.P. and Koiter, W.T., results reported in Compendium of Stress Intensity Factors, by D.P. Rooke and D.J. Cartwright, The Hillingdon Press, 1976, p. 110.
5. Murakami, Y., Nemat-Nasser, S., "Interacting Dissimilar Semi-elliptical Surface Flaws Under Tension and Bending," Engineering Fracture Mechanics, Vol. 16, No. 3, pp. 373-386, 1982.
6. Murakami, Y., and Nemat-Nasser, S., "Growth and Stability of Interacting Surface Flaws of Arbitrary Shape," Engineering Fracture Mechanics, Vol. 17, No. 3, pp. 193-210, 1983.
7. Smith, F.W., Kullgren, T.E., "Theoretical and Experimental Analysis of Surface Cracks Emanating from Fastener Holes," AFFDL-TR-76-104, Feb. 1977.
8. Grandt, A.F., Jr., and Kullgren, T.E., "Stress Intensity Factors for Corner Cracked Holes Under General Loading Conditions," Journal of Engineering Materials and Technology, Vol. 103, No. 2, April 1981, pp. 171-176.
9. Grandt, A.F., Jr., "Crack Face Pressure Loading of Semielliptical Cracks Located Along the Bore of a Hole," Engineering Fracture Mechanics, Vol. 14, No. 4, 1981, pp. 843-852.
10. Heath, B.J., "Stress Intensity Factors for Coalescing and Single Corner Flaws Along a Hole Bore in a Plate," M.S. Thesis, Purdue University, May 1983.
11. Tritsch, D.E., "Fatigue Crack Size and Shape Predictions," M.S. Thesis, Purdue University, in preparation.
12. Private Correspondence with Dr. A.S. Thakker, Pratt & Whitney Aircraft Corporation.

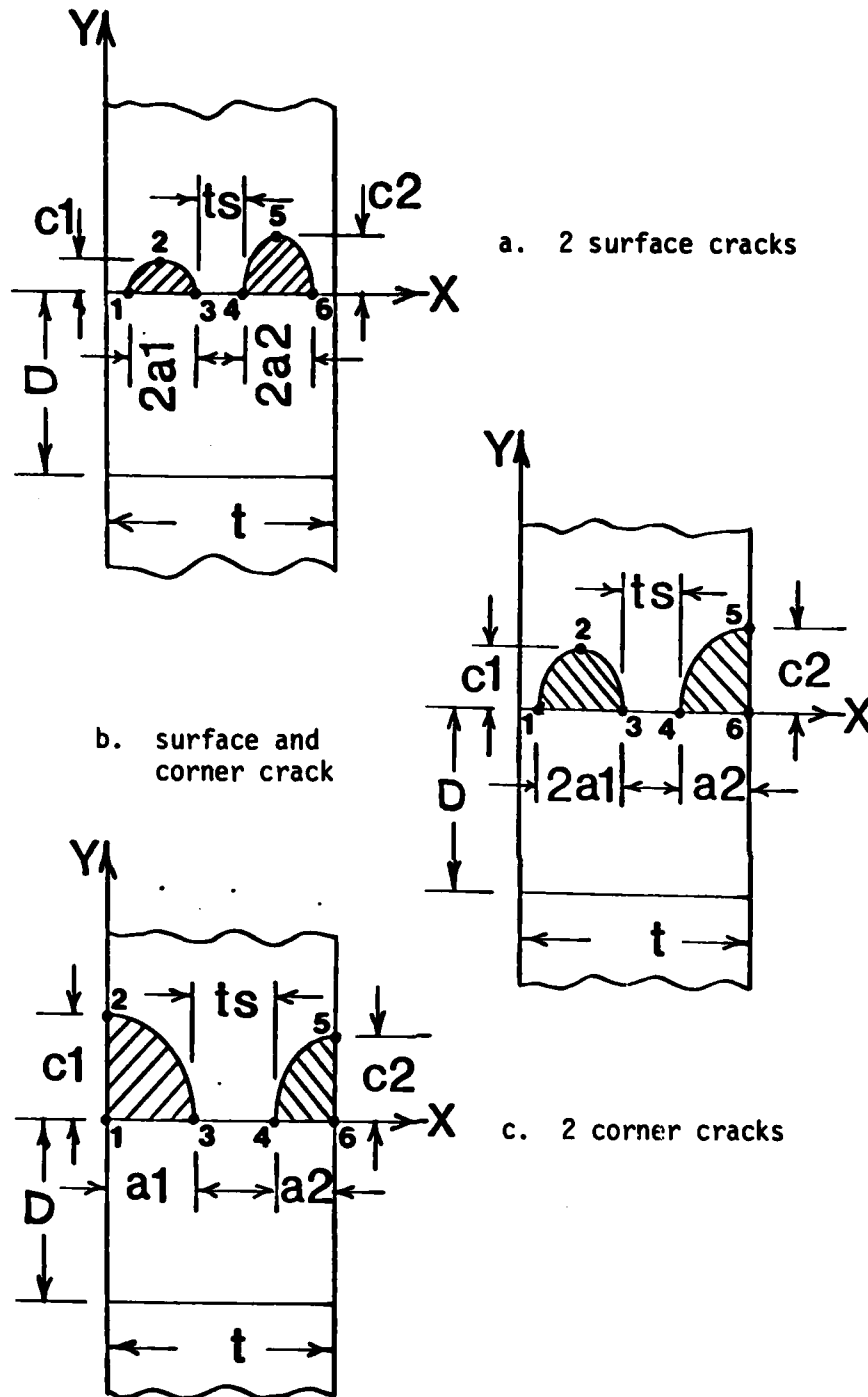


Figure 1 Schematic of multiple cracks located along bore of a hole in a large plate. Hole diameter is  $D$ , plate thickness is  $t$ , and remote tensile stress is applied in  $z$  direction.

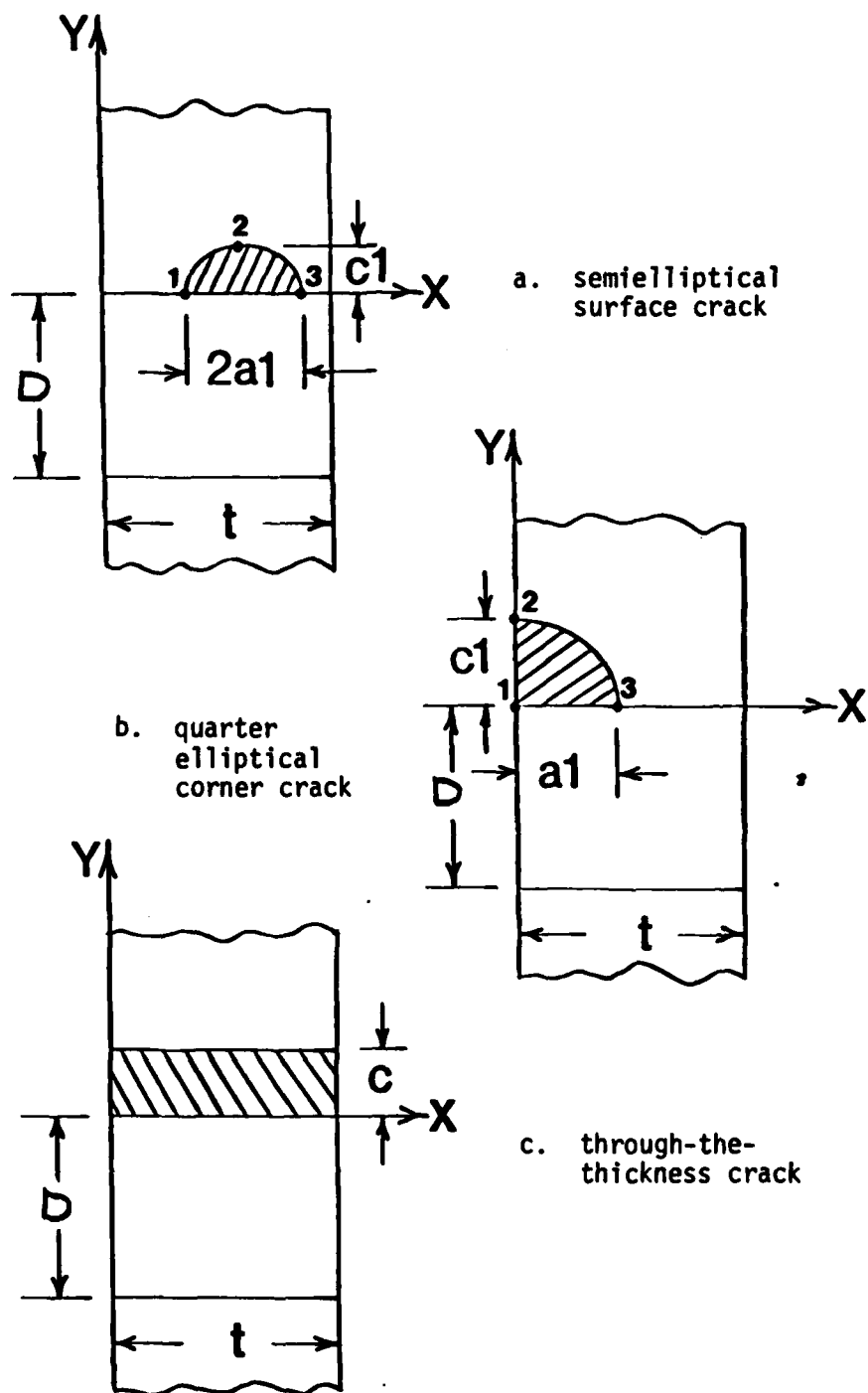
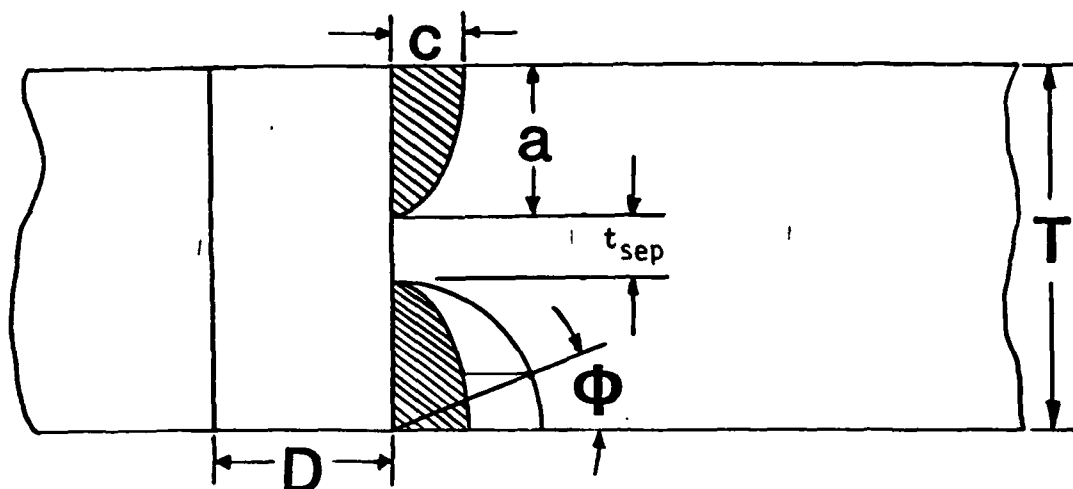


Figure 2 Schematic representation of semielliptical, corner, and through the thickness crack located along the bore of a hole with diameter  $D$  in a plate with thickness  $t$ .

## Symmetric Corner Crack Configuration



## Single Corner Crack Configuration

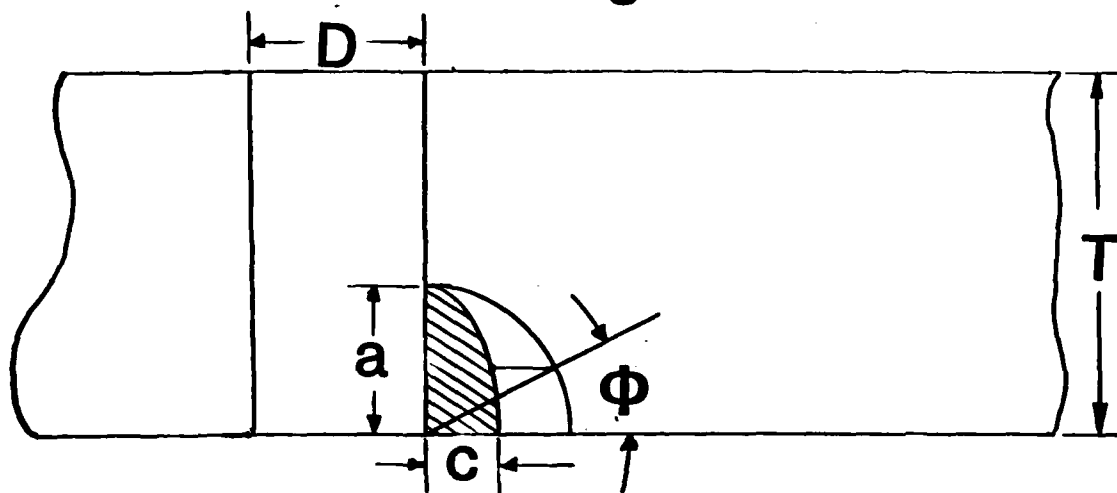


Figure 3 Schematic drawing of crack plane showing location of single and symmetric corner cracks located at bore of hole.



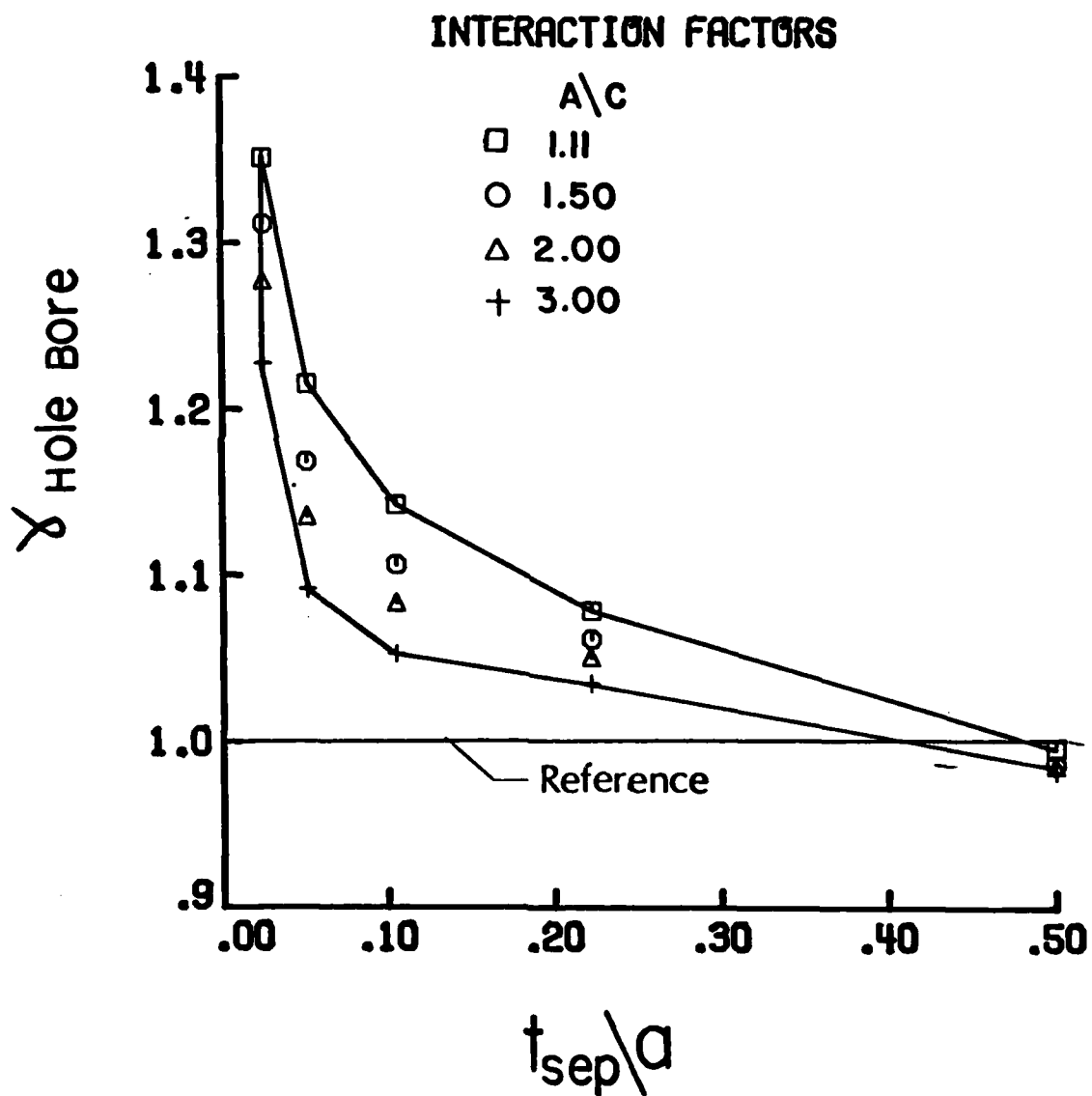


Figure 4 Summary of the effect of crack spacing  $t_{\text{sep}}/a$  and crack shape  $a/c$  on stress intensity factor interaction at hole bore crack location ( $\phi = 90^\circ$ ).

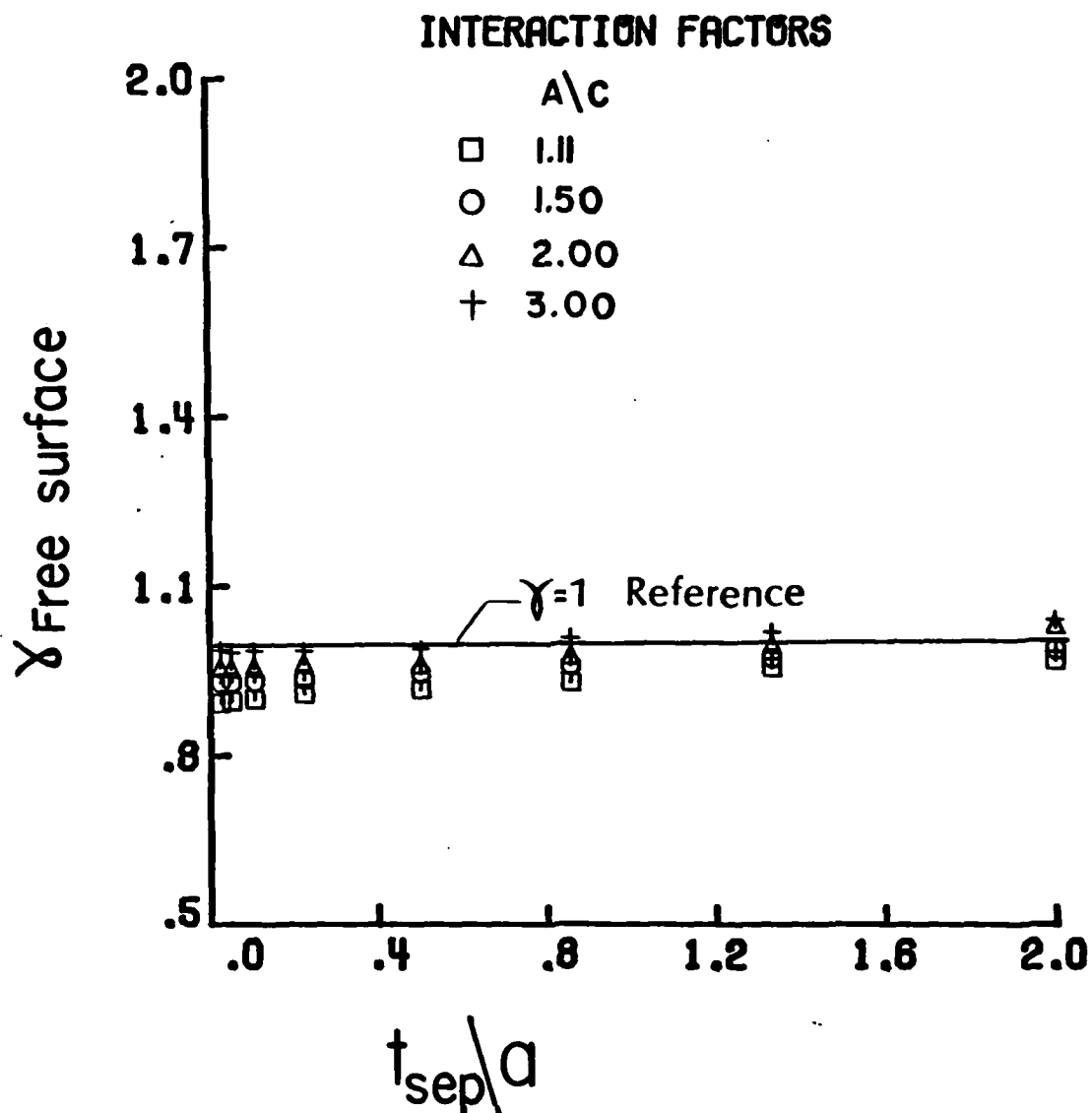


Figure 5 Summary of the effect of crack spacing  $t_{sep}/a$  and crack shape  $a/c$  on stress intensity factor interaction at front surface location ( $\phi = 0$ ) for corner cracked hole.

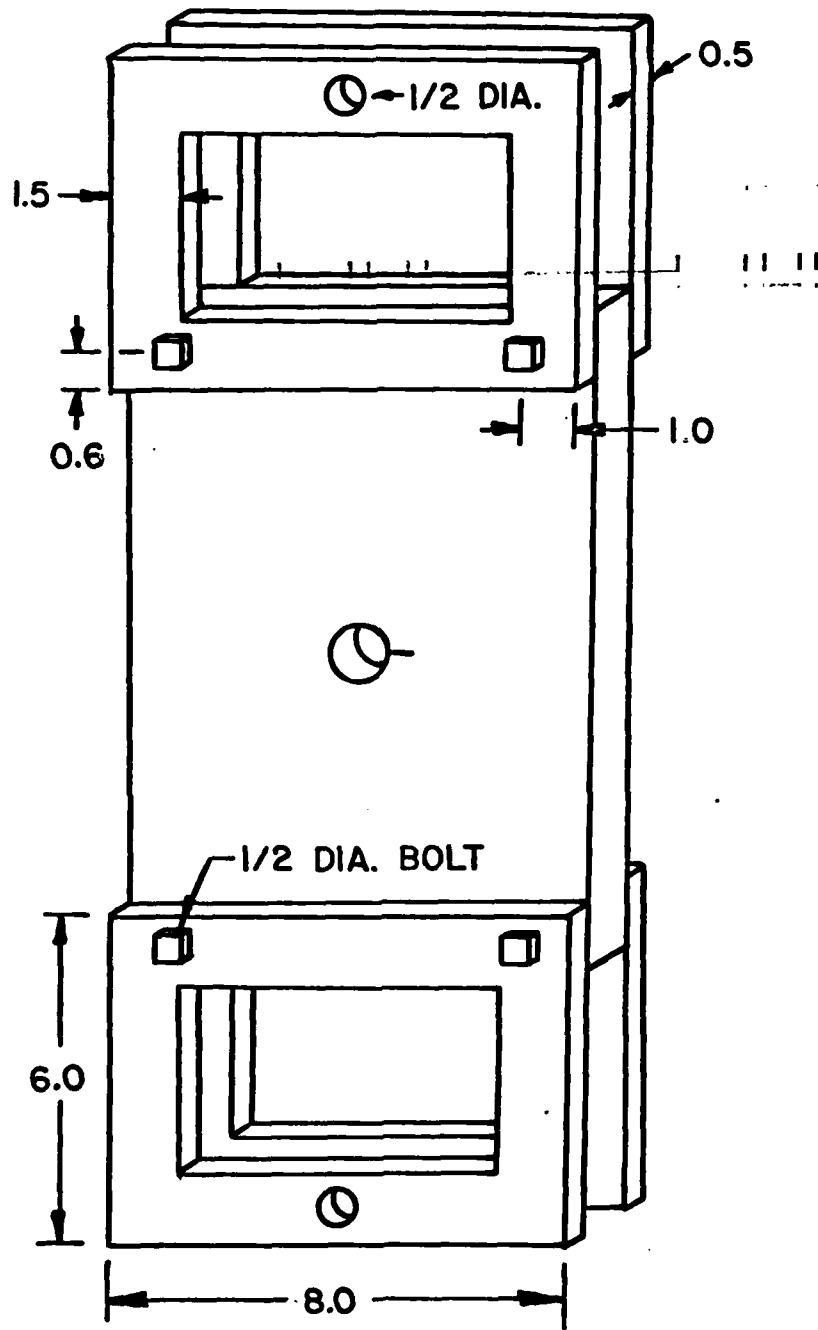


Figure 6 Schematic View of a Plate Specimen Fastened to the Test Grips (All Dimensions in Inches)

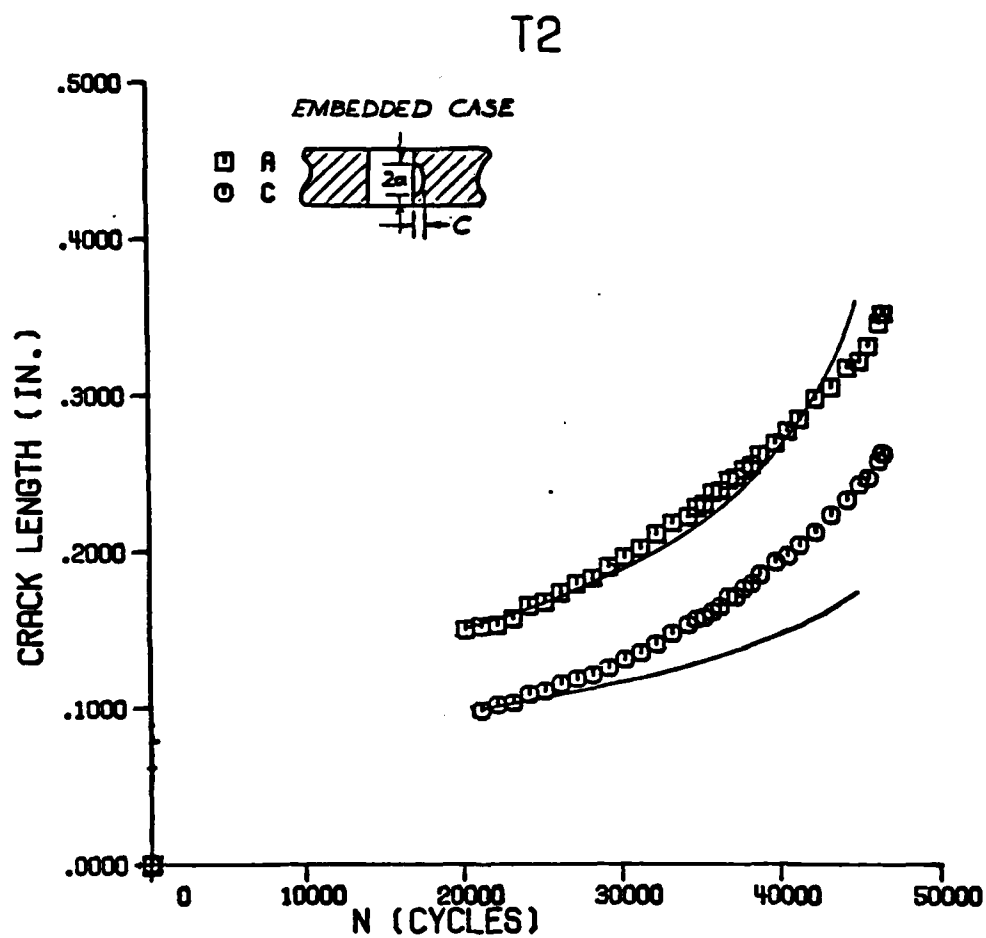


Figure 7a Comparison of Predicted and Actual Crack Growth Prior to Penetration for Plate Specimen T2

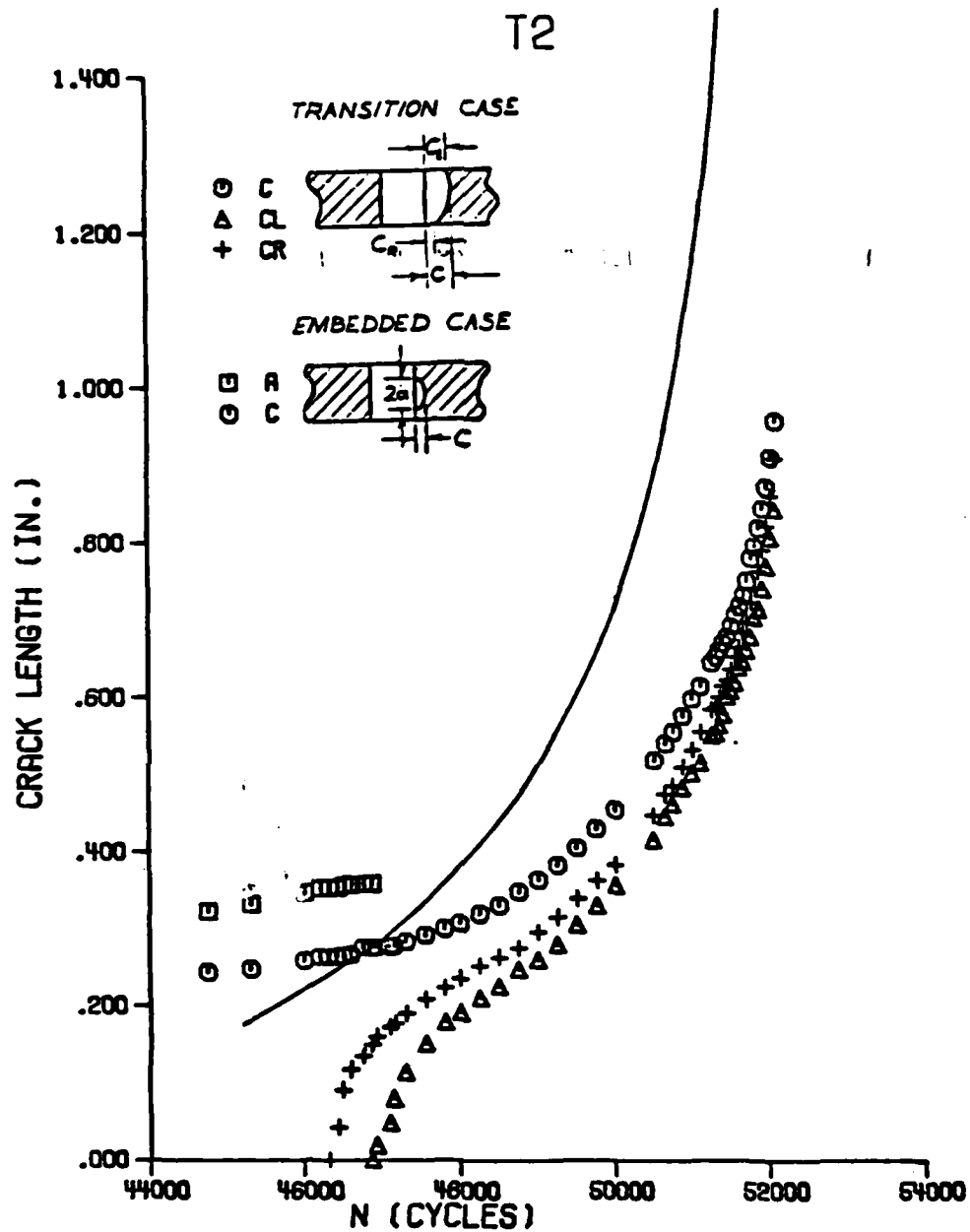


Figure 7b Comparison of Predicted and Actual Crack Growth During Transition Period for Plate Specimen T2

# TEST PT2 : PLATE WITH A HOLE 2 SYMMETRIC CORNER CRACKS.

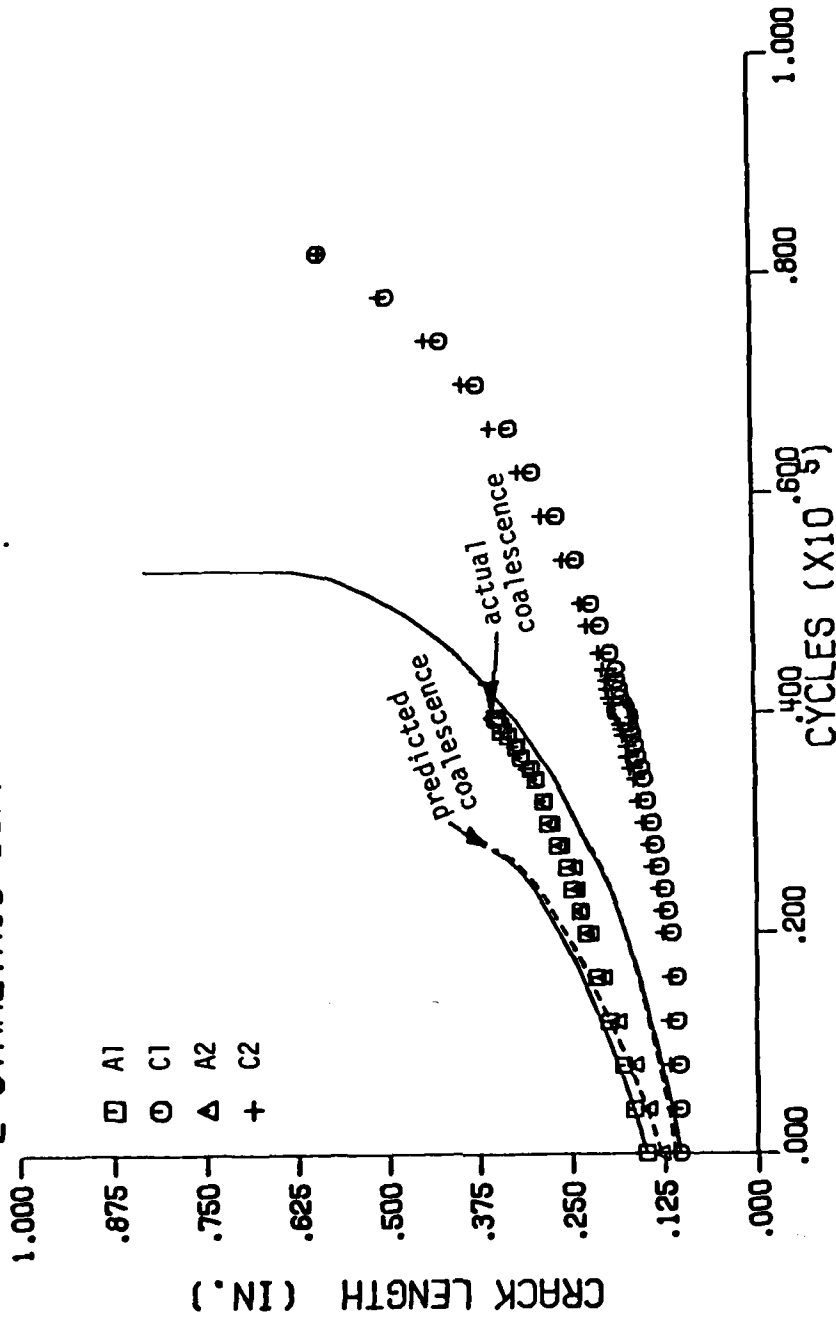


Figure 8 Comparison of predicted and experimental fatigue crack growth for two coalescing corner cracks located at a hole in a PMMA plate loaded in cyclic tension

# TEST PT3 : PLATE WITH A HOLE 2 SYMMETRIC CORNER CRACKS

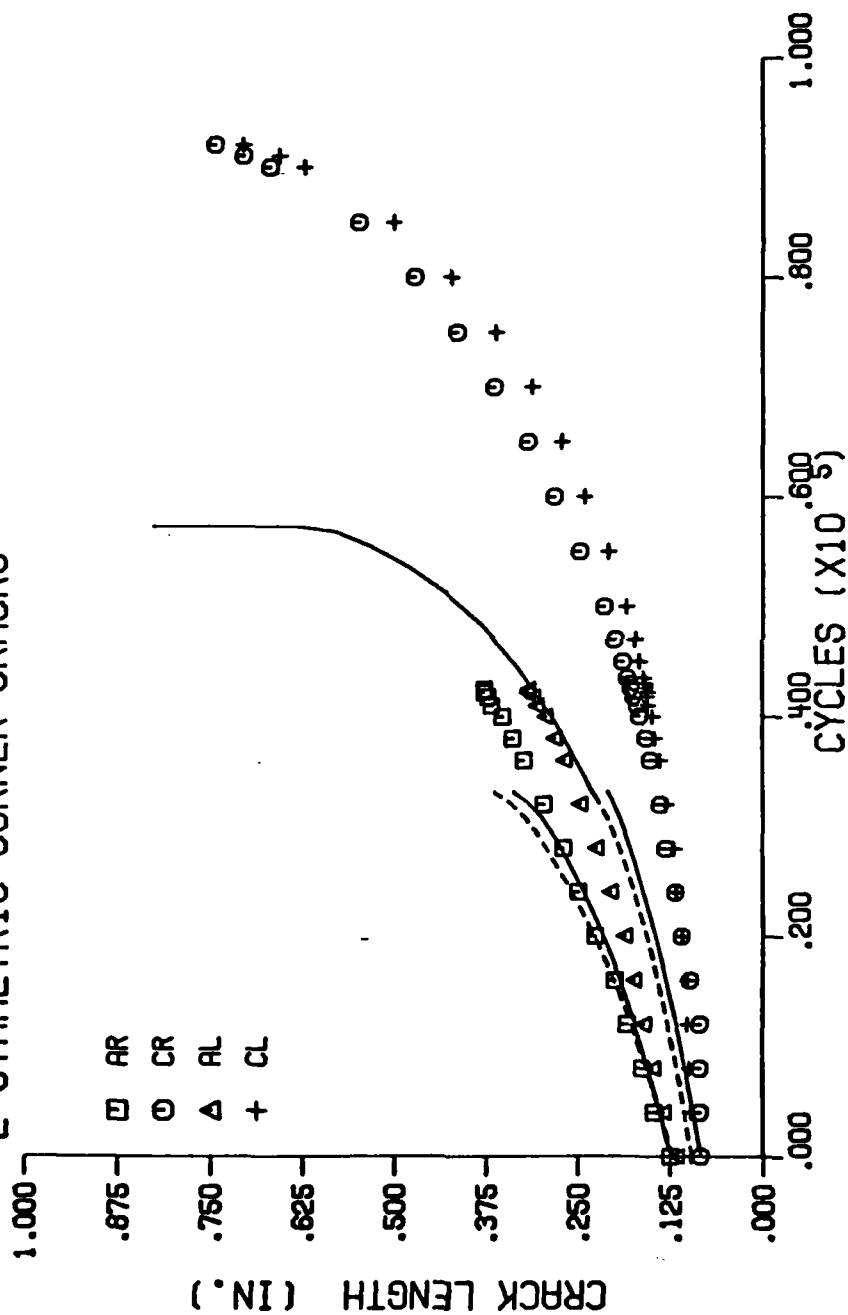
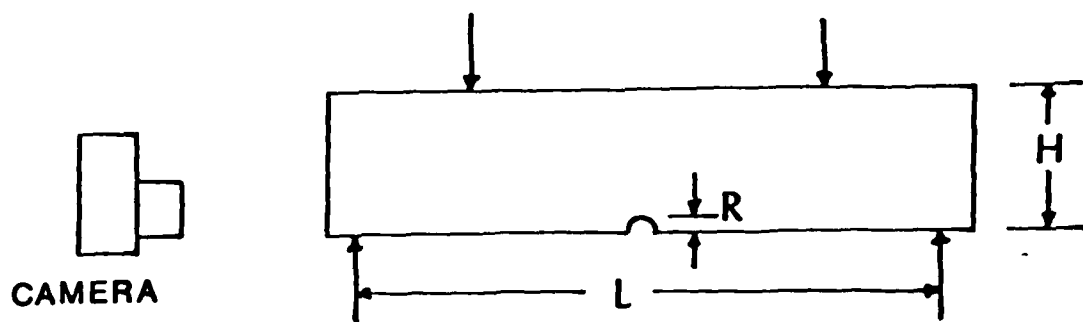
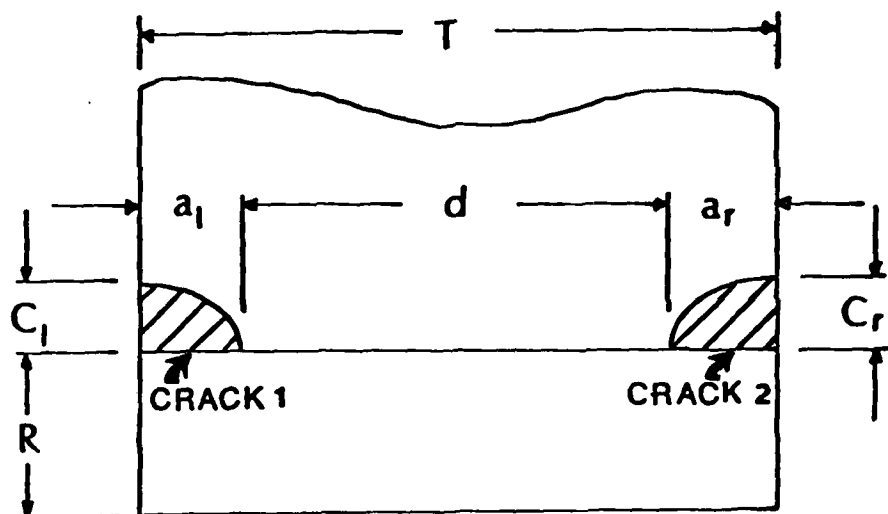


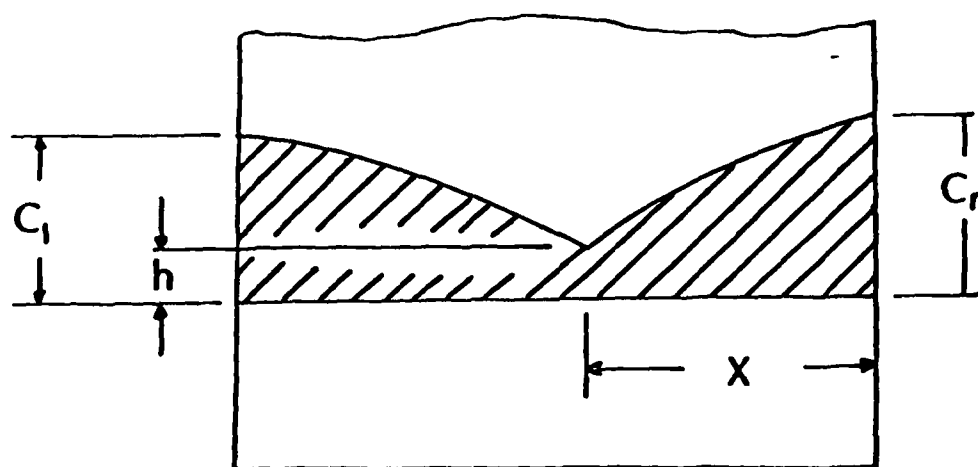
Figure 9 Comparison of predicted and experimental fatigue crack growth for two coalescing corner cracks located at a hole in a PMMA plate loaded in remote tension.



a. Four-Point Bend Specimen



b. Corner crack dimensions before coalescence



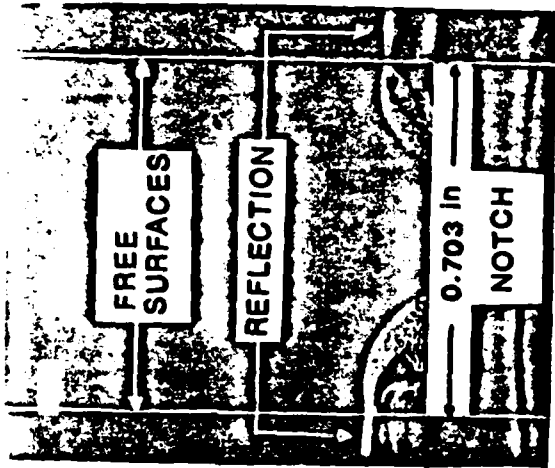
c. Crack dimensions after coalescence

Fig. 10 Specimen geometry showing location of the camera and schematic views of the crack plane.





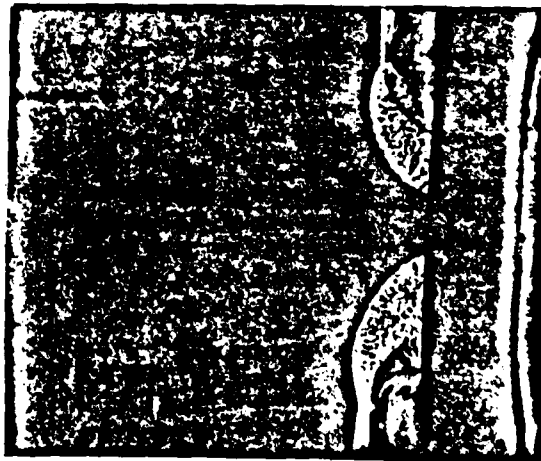
0 cycles



5000



7500



10,000



11,500

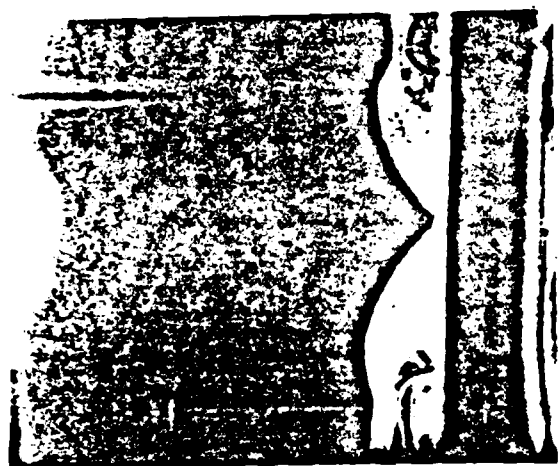


11,820

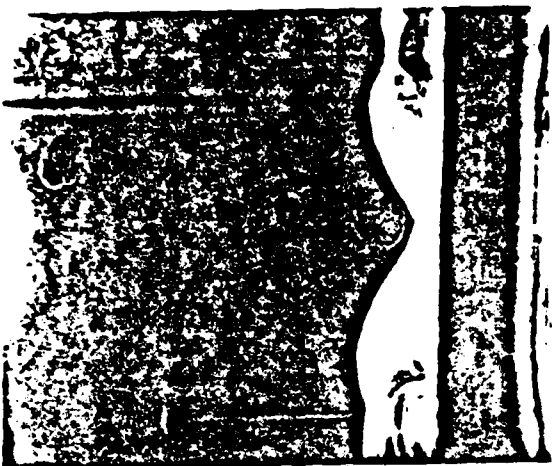
Figure 11 Typical photographs showing growth and coalescence of two fatigue cracks at a circular hole in a PMMA specimen



11,890



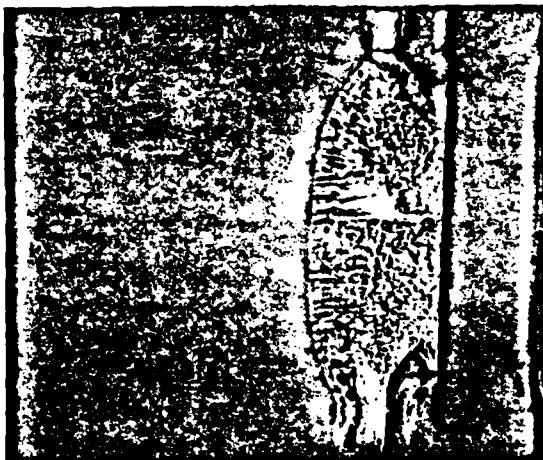
11,900



11,940



12,170



12,270



12,295

Figure 11 continued

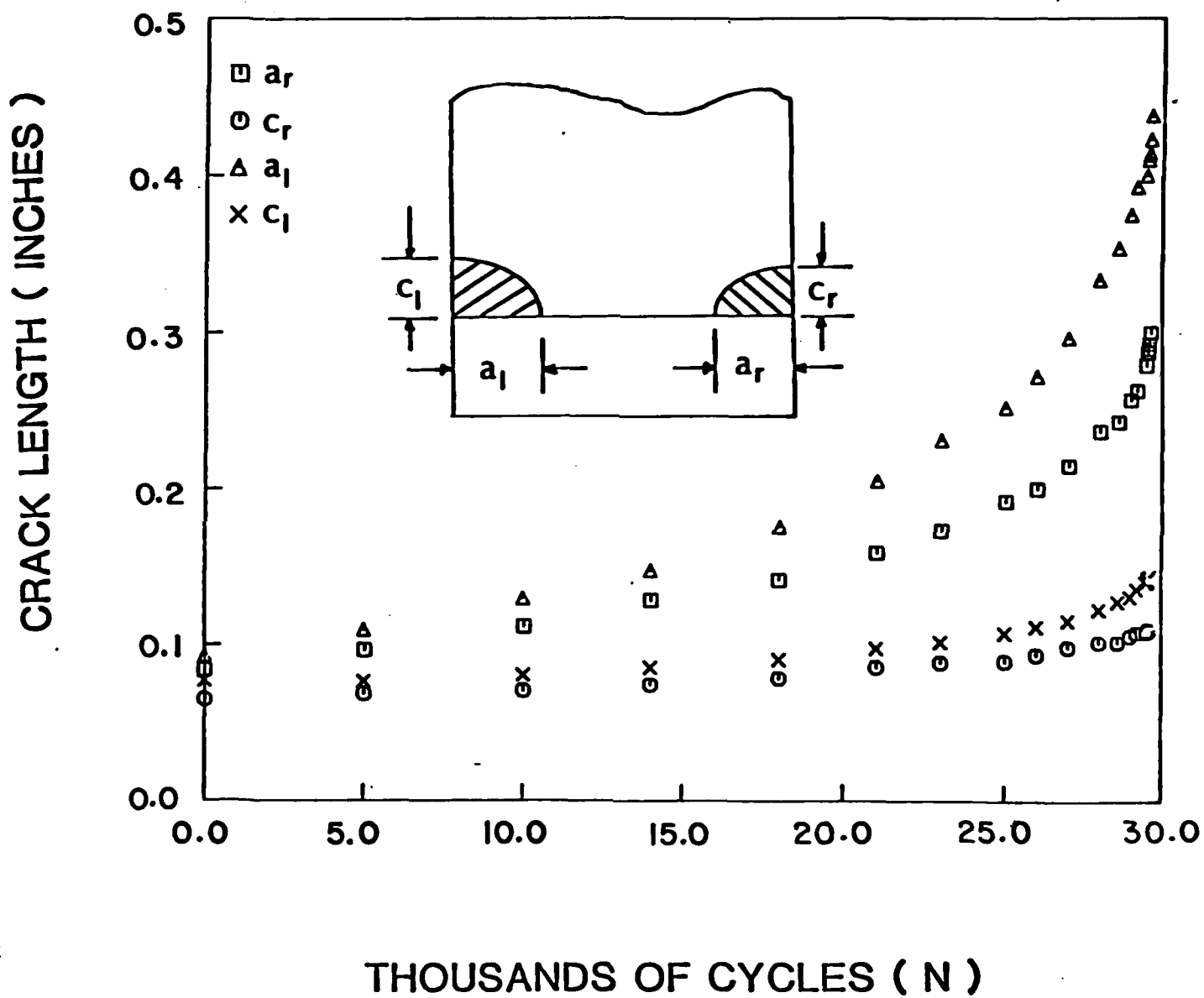


Fig. 12 Crack growth before coalescence as a function of elapsed cycles for nonsymmetric out-of-plane crack test T-2.

CRACK LENGTH ( INCHES )

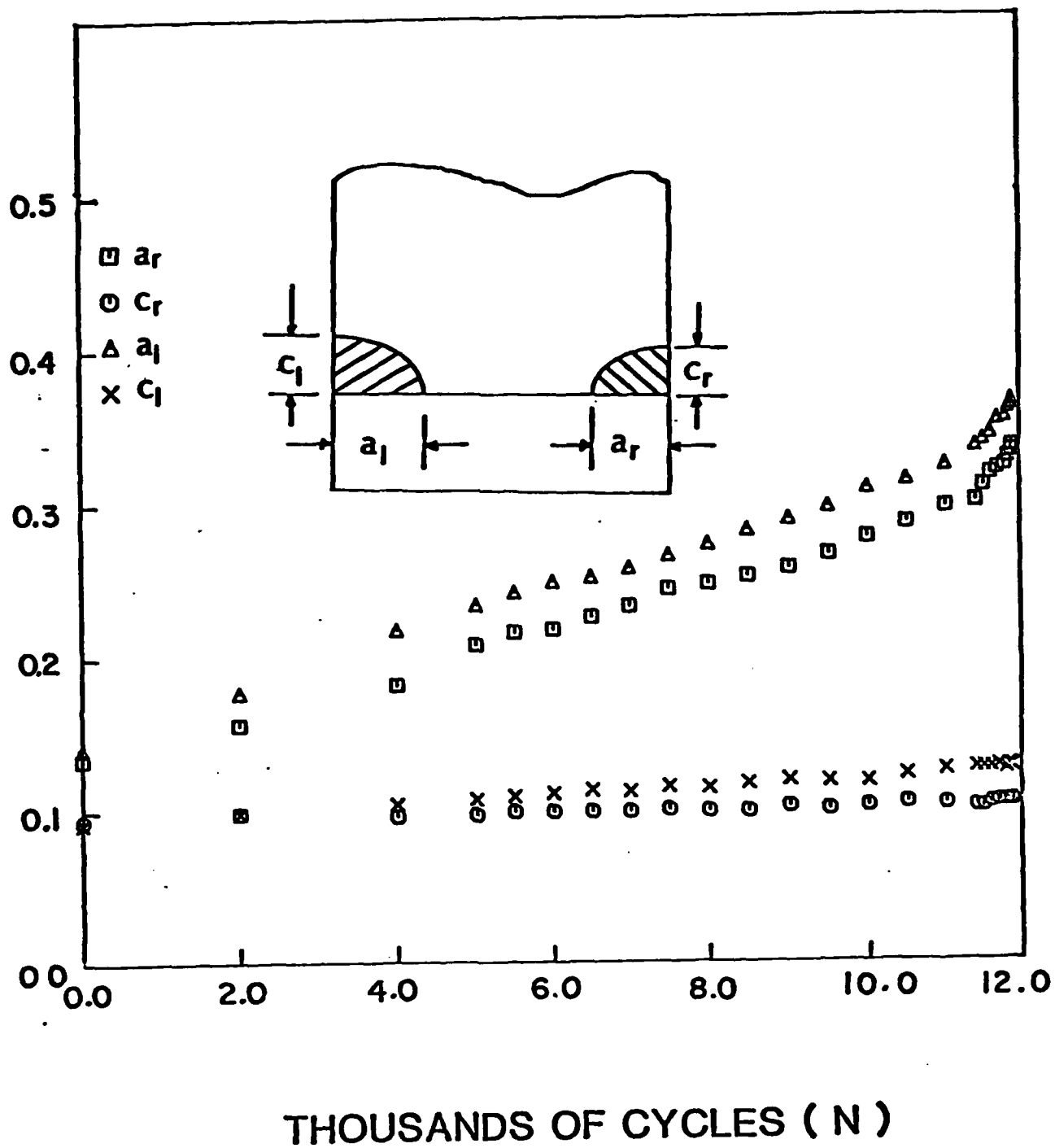


Fig. 13a Crack growth before coalescence as a function of elapsed cycles for symmetric in plane crack test T-3.

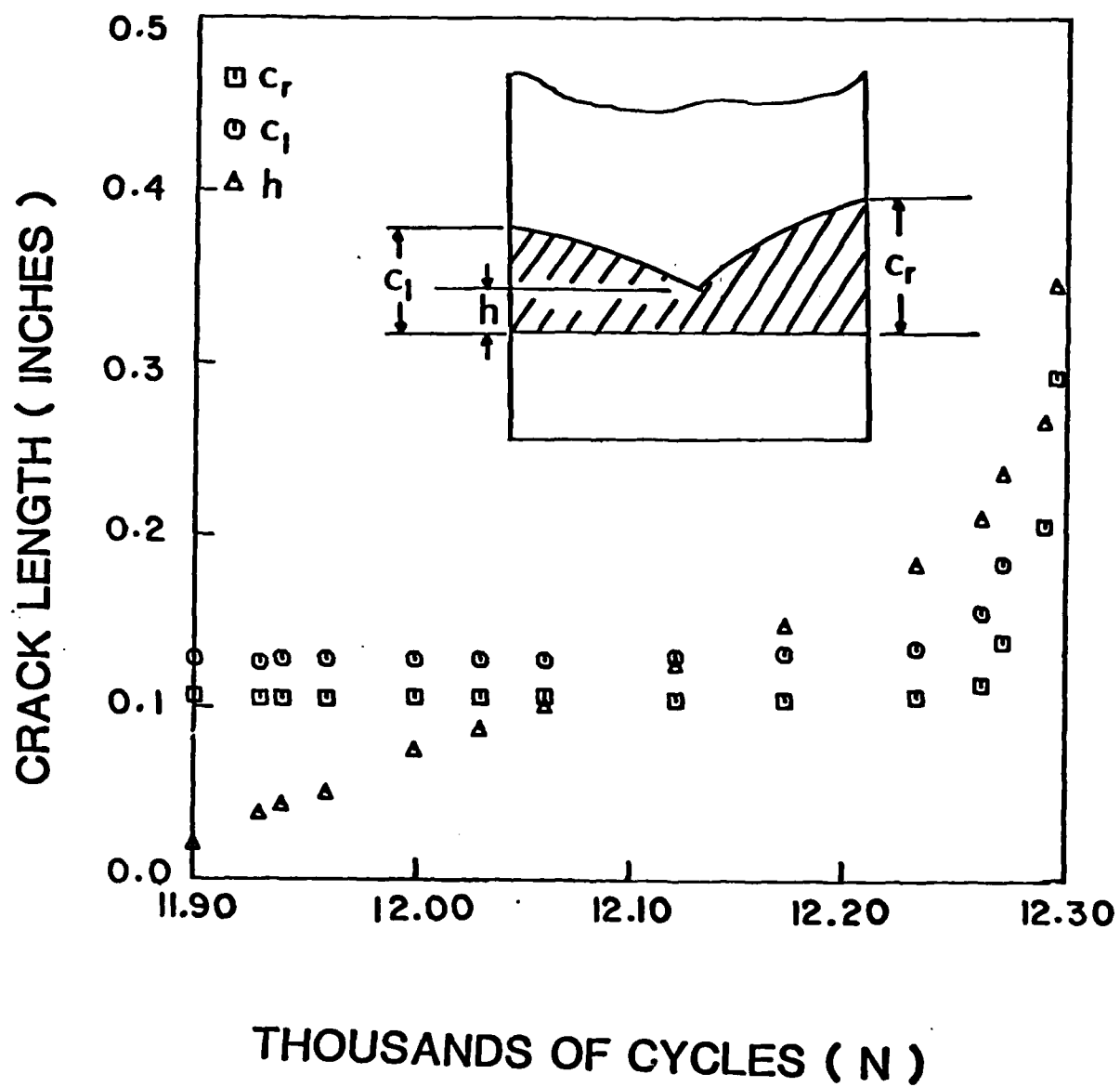


Fig. 13b Crack growth after coalescence as a function of elapsed cycles for symmetric in-plane crack test T-3.

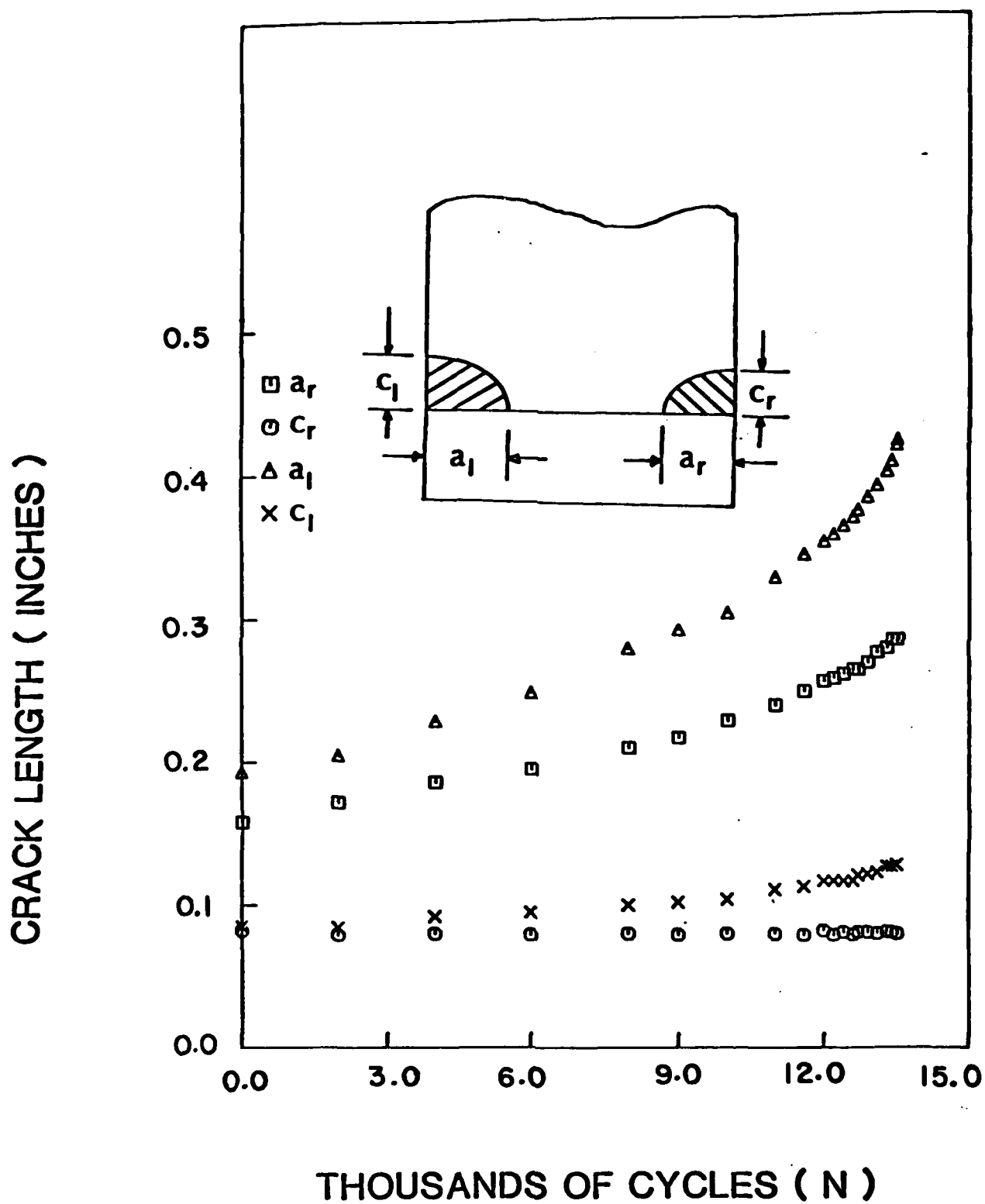


Fig.14a Crack growth before coalescence as a function of elapsed cycles for nonsymmetric out-of-plane crack test T-4.

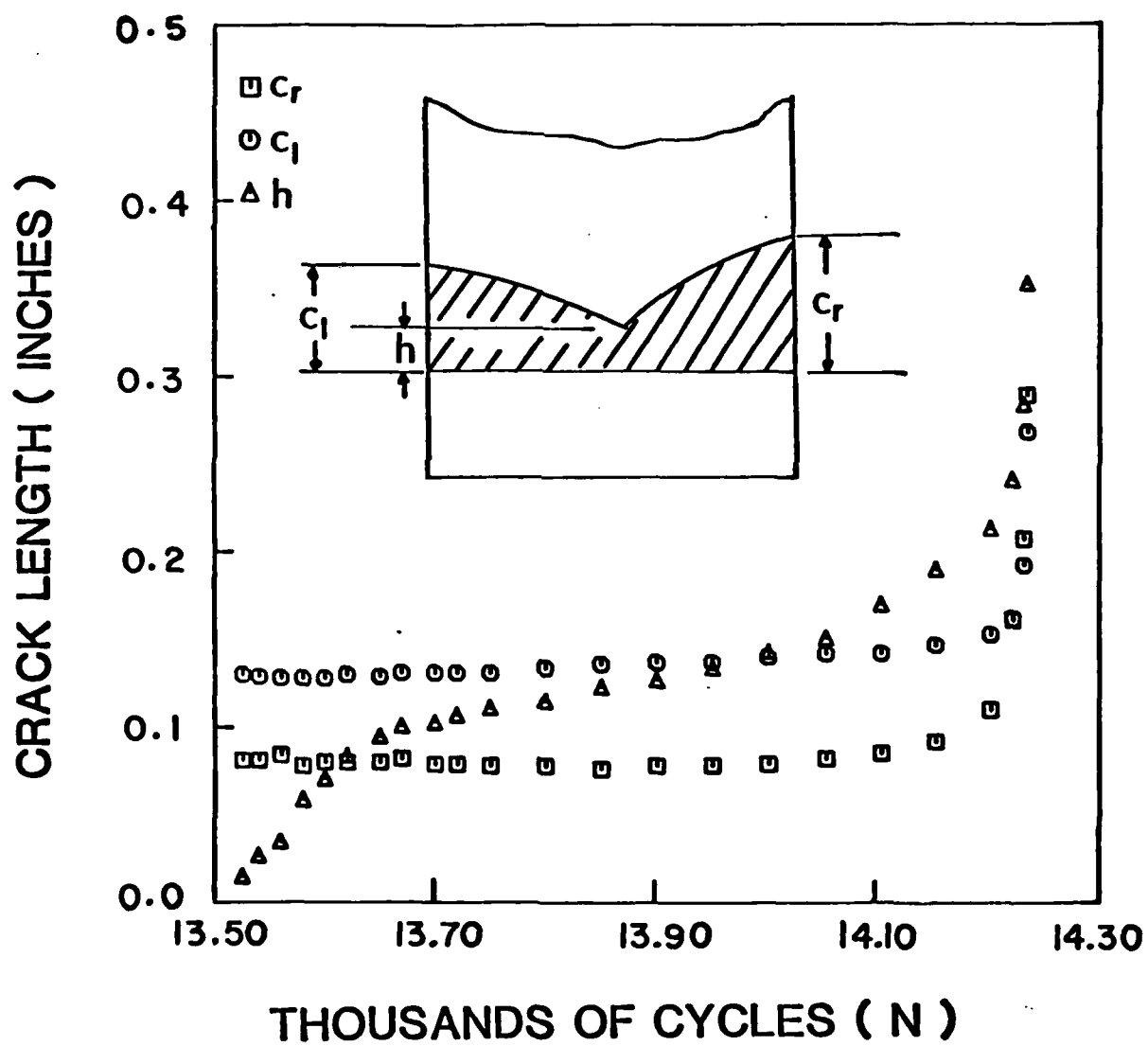


Fig. 14b Crack growth after encounter and coalescence as a function of elapsed cycles for nonsymmetric out-of-plane crack test T-4.

CRACK LENGTH (INCHES)

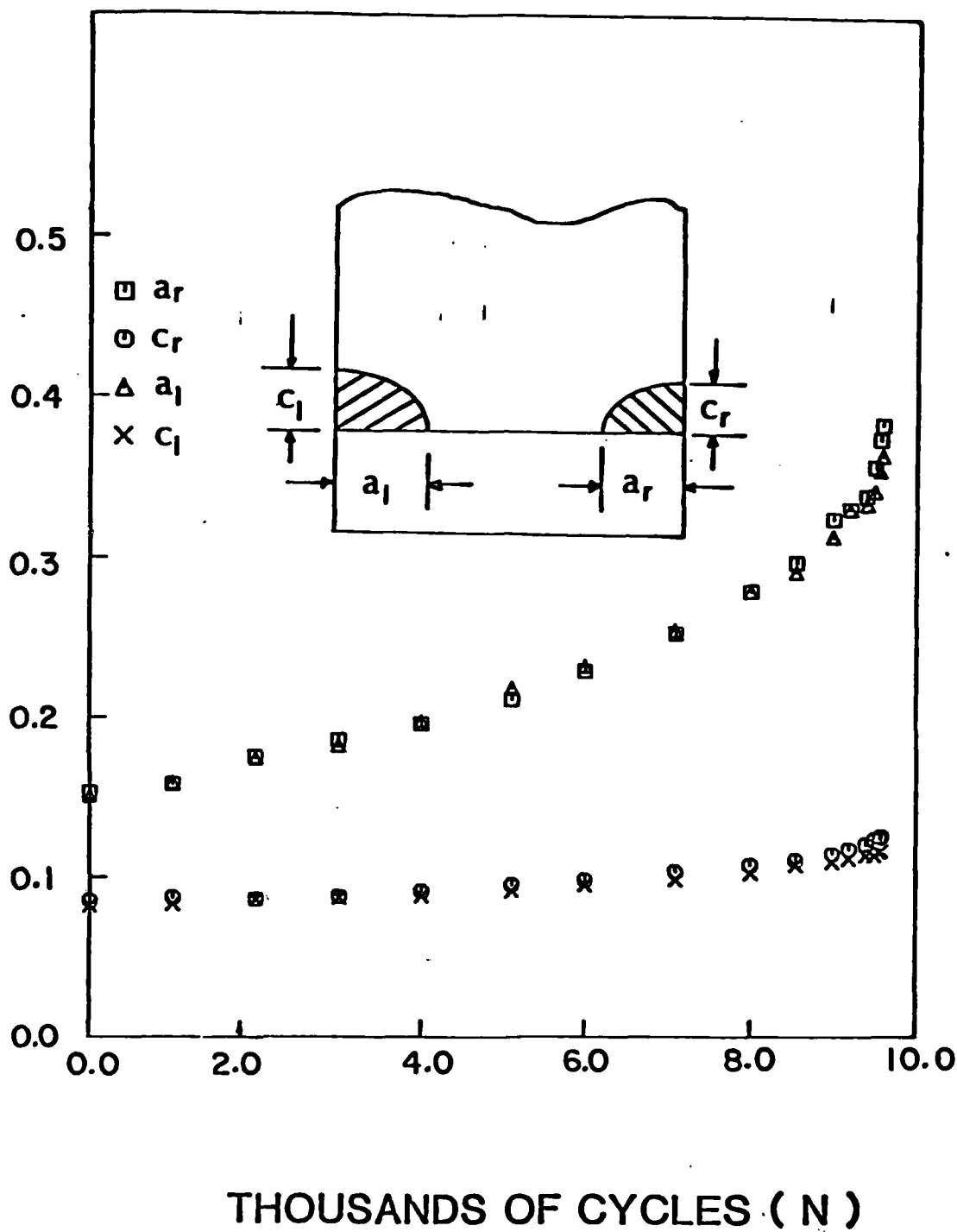
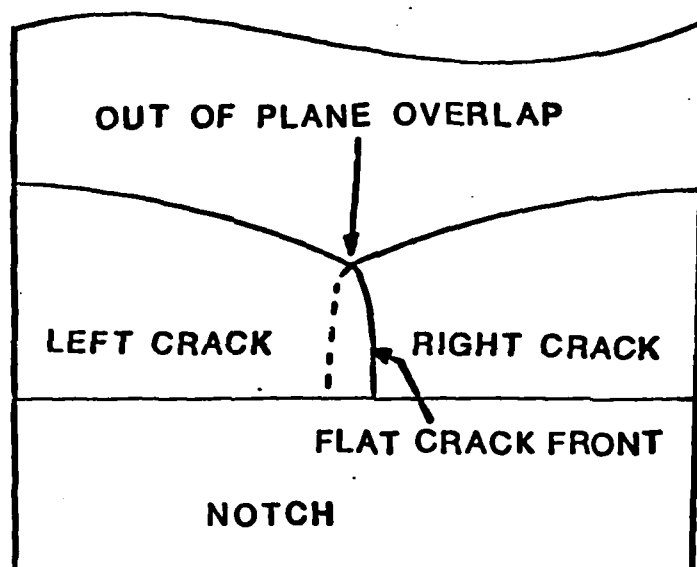
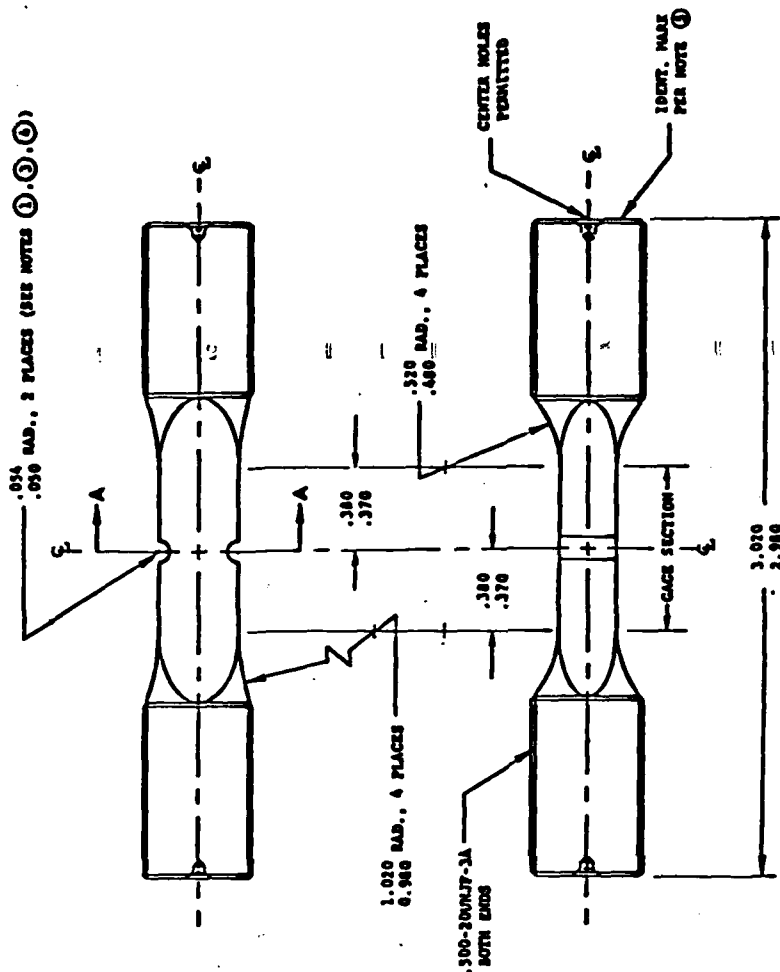
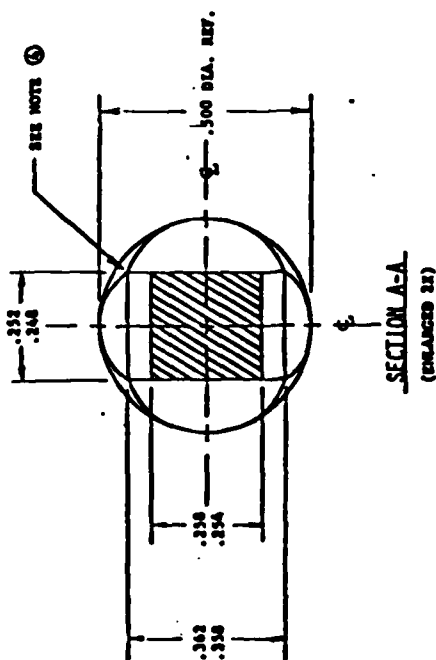


Fig.15 Crack growth before coalescence as a function of elapsed cycles for symmetric out of plane crack test T-5.





**Fig. 16** Crack configuration after the out of plane overlap occurred before coalescence.




## NOTES

- ① SEMICIRCULAR NOTCH (.032) SHALL BE GROUND WITH 320 GRIT WHEEL.
- ② GRIND FINISH GAGE SECTION. POLISH GAGE SECTION (INCLUDING NOTCHES) IN LONGITUDINAL DIRECTION TO 6 RMS MICROFINISH OR BETTER, WITH ALL EDGES BOUNDED TO .010 - .013 RADII.
- ③ SEMICIRCULAR NOTCH  $\frac{1}{8}$ "S MUST BE PARALLEL WITH EACH OTHER WITHIN .002 FIS, AND LOCATED WITHIN .002 OF GAGE SECTION TRANSVERSE  $\frac{1}{8}$ ".
- ④ FLAT FACES OF GAGE SECTION AND NOTCH SLOTTIONS MUST BE SYNETHIC WITHIN .002 FIS.
- ⑤ IDENTIFICATION MARKINGS PERMITTED ONLY ON BONES OF SPECIMENS.

**ALL DIMENSIONS ARE IN INCHES**

[illegible]

NAME J. R. MARCH		EMPLOYED	TITLE	
DATE 8-8-78		DOUBLE NOTCH LCF SPECIMEN		
 PRATT & WHITNEY AIRCRAFT GROUP <small>WALLINGFORD, CONNECTICUT 06495</small>		RESEARCH	SPEC.	QUANTITY 25.000
		AS SPECIFIED		PWL 96201
			ORDER	DATE 8-22-78

**Figure 17 DOUBLE NOTCH LOAD CONTROL LCF SPECIMEN**

# METAL SPECIMEN 3A 2 INTERACTING SURFACE CRACKS

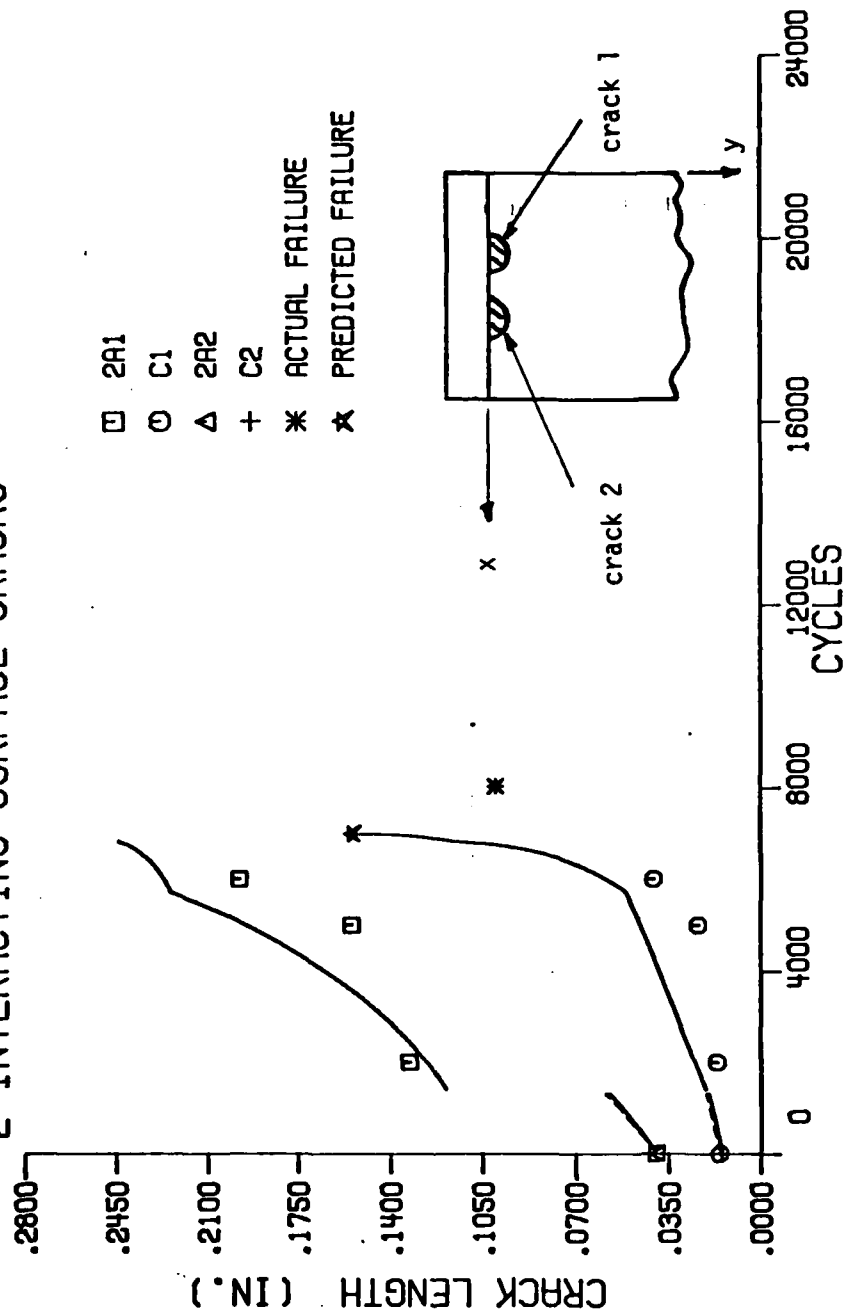


Figure 18 Comparison of predicted and experimental growth and coalescence of two surface cracks at semicircular notch in Waspalloy specimen

# METAL SPECIMEN 7A 2 INTERACTING SURFACE CRACKS

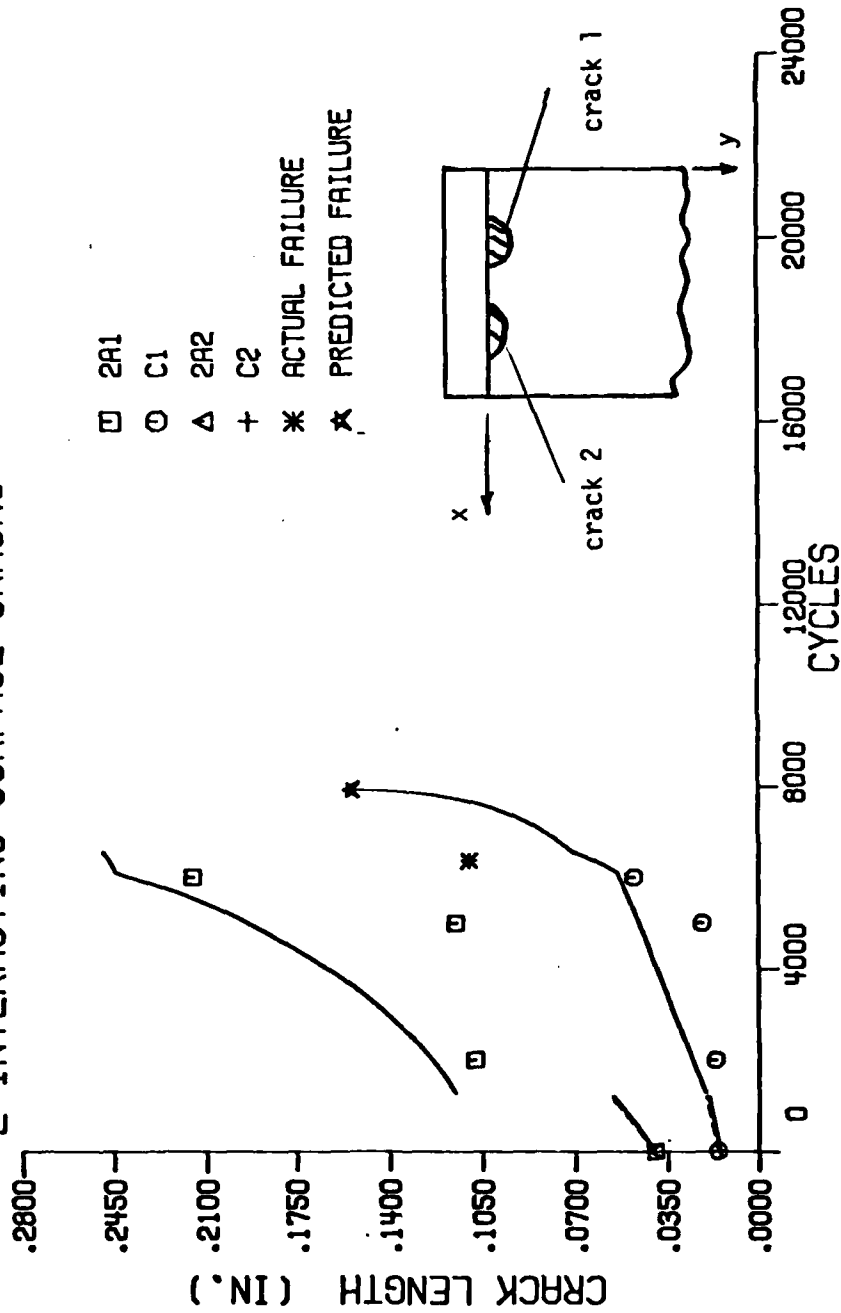


Figure 19 Comparison of predicted and experimental growth and coalescence of two surface cracks at semicircular notch in Waspaloy specimen

# METAL SPECIMEN 8A 2 UNSYMMETRIC NON INTERACTING SURFACE CRACKS

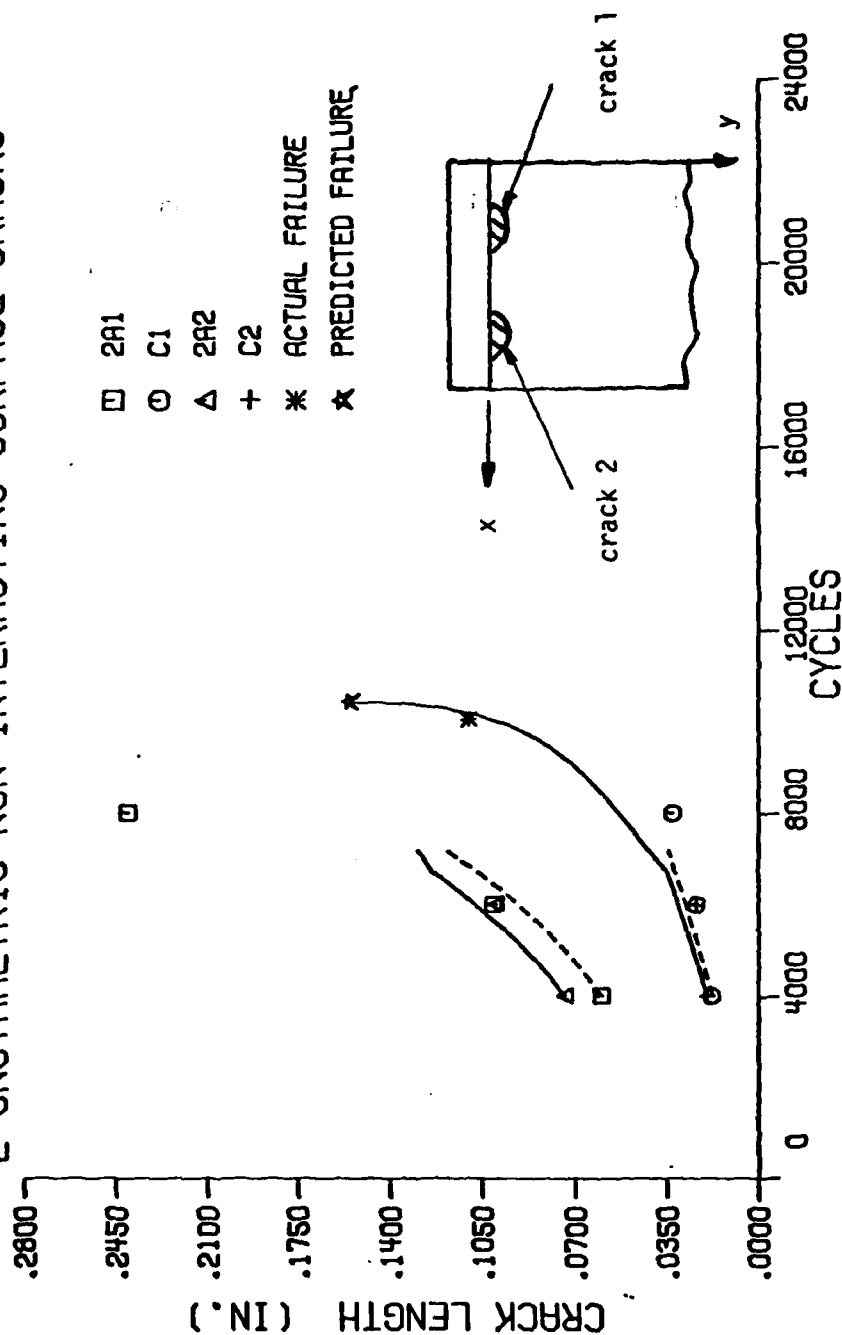


Figure 20 Comparison of predicted and experimental growth and coalescence of two surface cracks at semicircular notch in Waspalloy specimen.

METAL SPECIMEN 10A  
2 UNSYMMETRIC NON INTERACTING SURFACE CRACKS

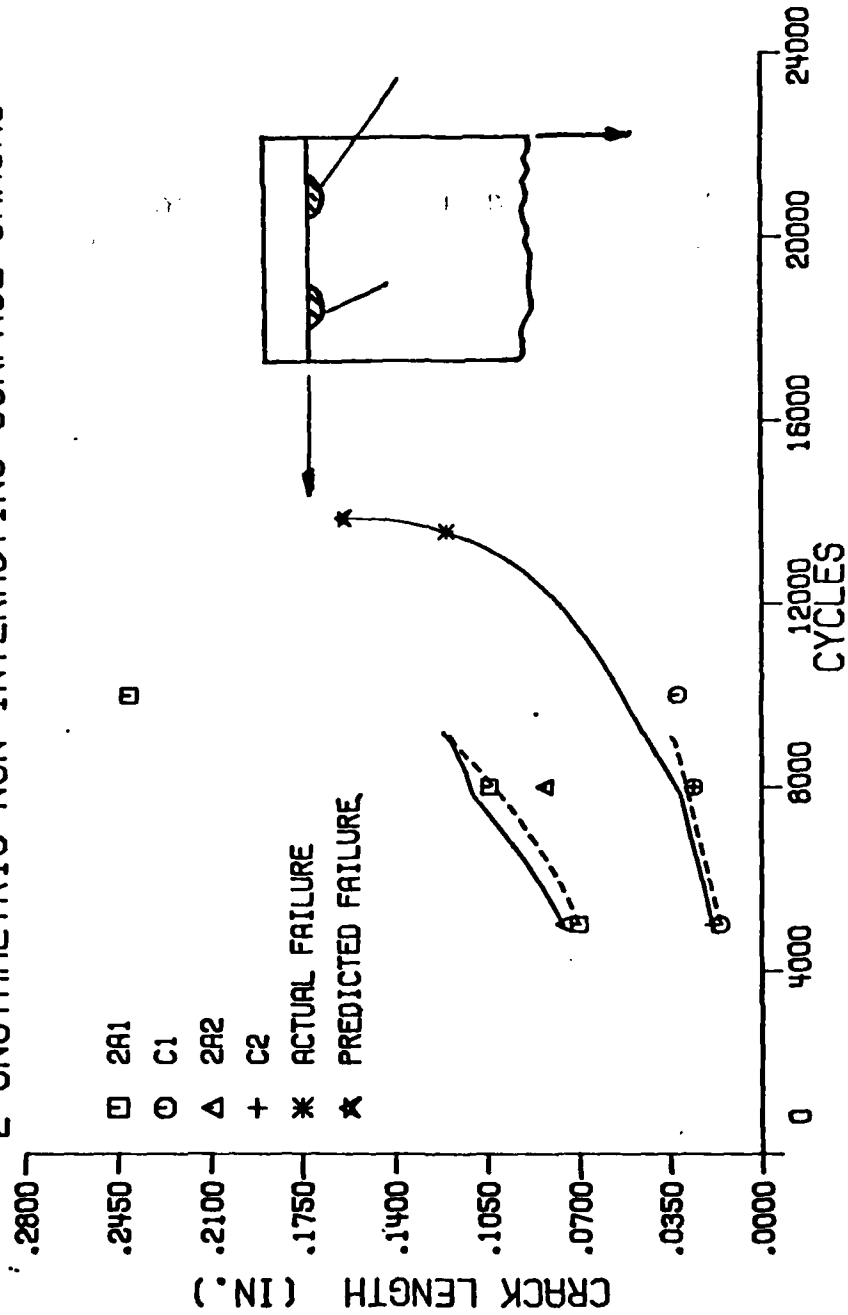


Figure 21 Comparison of predicted and experimental growth and coalescence of two surface cracks at semicircular notch in Waspaloy specimen

# METAL SPECIMEN 17 2 NON INTERACTING SURFACE CRACKS

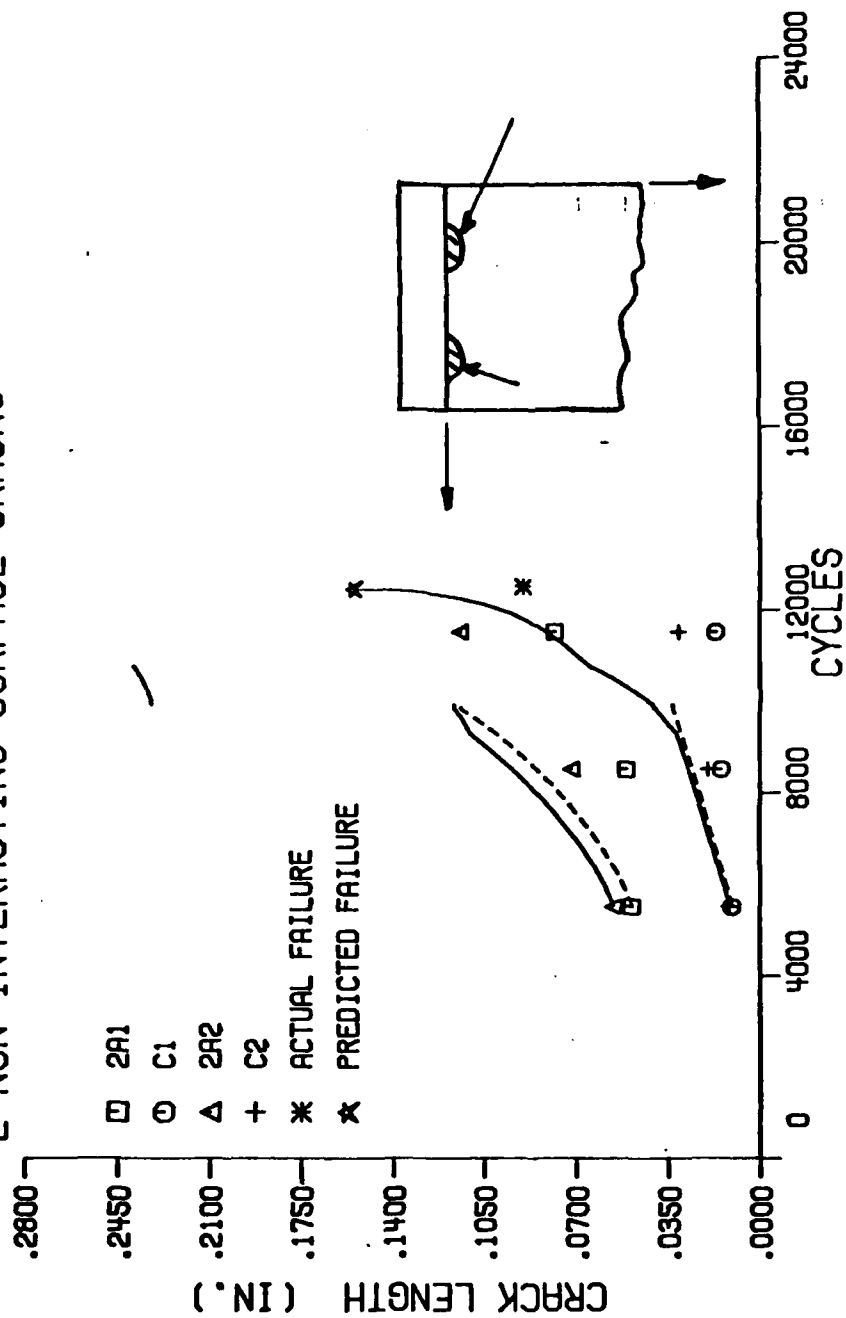


Figure 22 Comparison of predicted and experimental growth and coalescence of two surface cracks at semicircular notch in Waspaloy specimen

# METAL SPECIMEN 18 2 NON INTERACTING SURFACE CRACKS

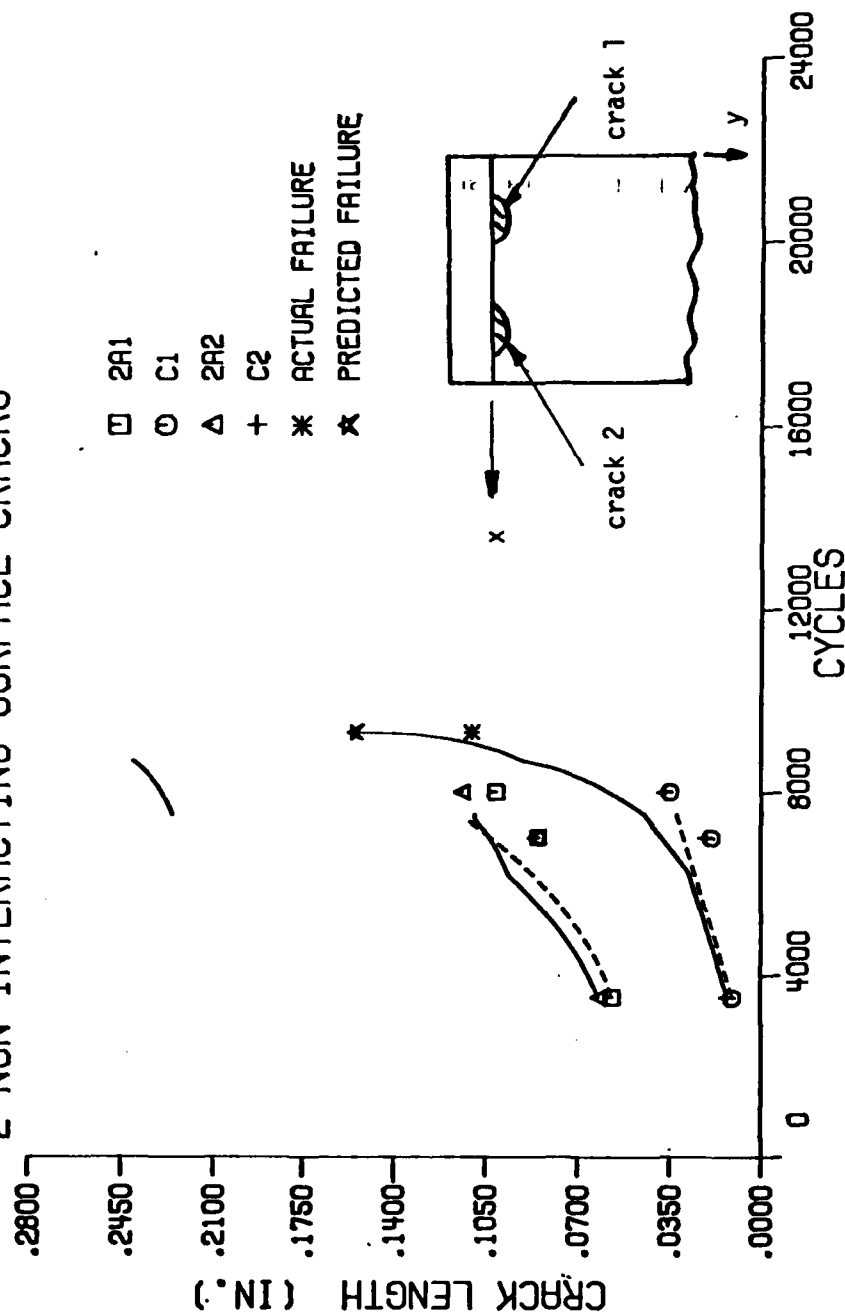
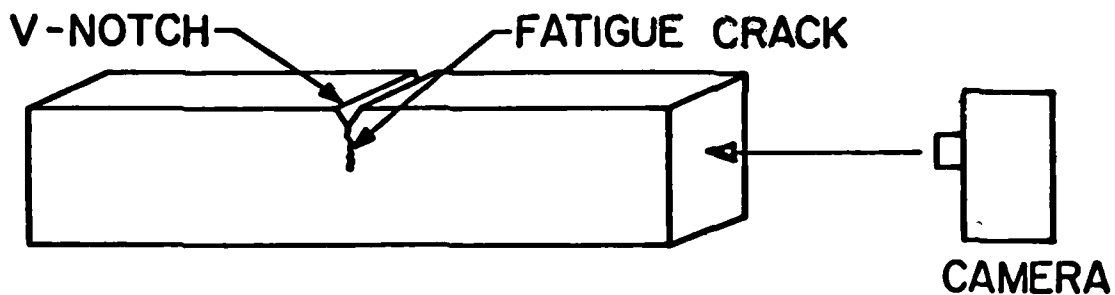
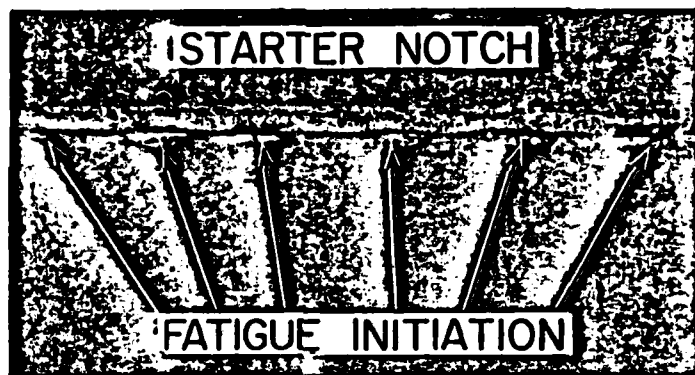


Figure 23 Comparison of predicted and experimental growth and coalescence of two surface cracks at semicircular notch in Waspalloy specimen.

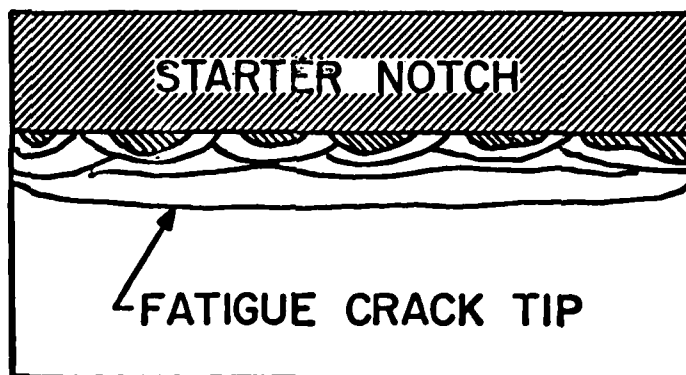




a. SPECIMEN - CAMERA ARRANGEMENT



b. CRACK INITIATION AT V-NOTCH



c. INITIATION SITES UNITED INTO  
UNIFORM CRACK FRONT

Figure 24 Schematic view of fatigue crack initiation at V-notch and coalescence into a single flaw

TEST ST-5

MAX LOAD=600 LB. MIN LOAD=30 LB.

45 DEG. V-NOTCH FREQUENCY 3 HZ.

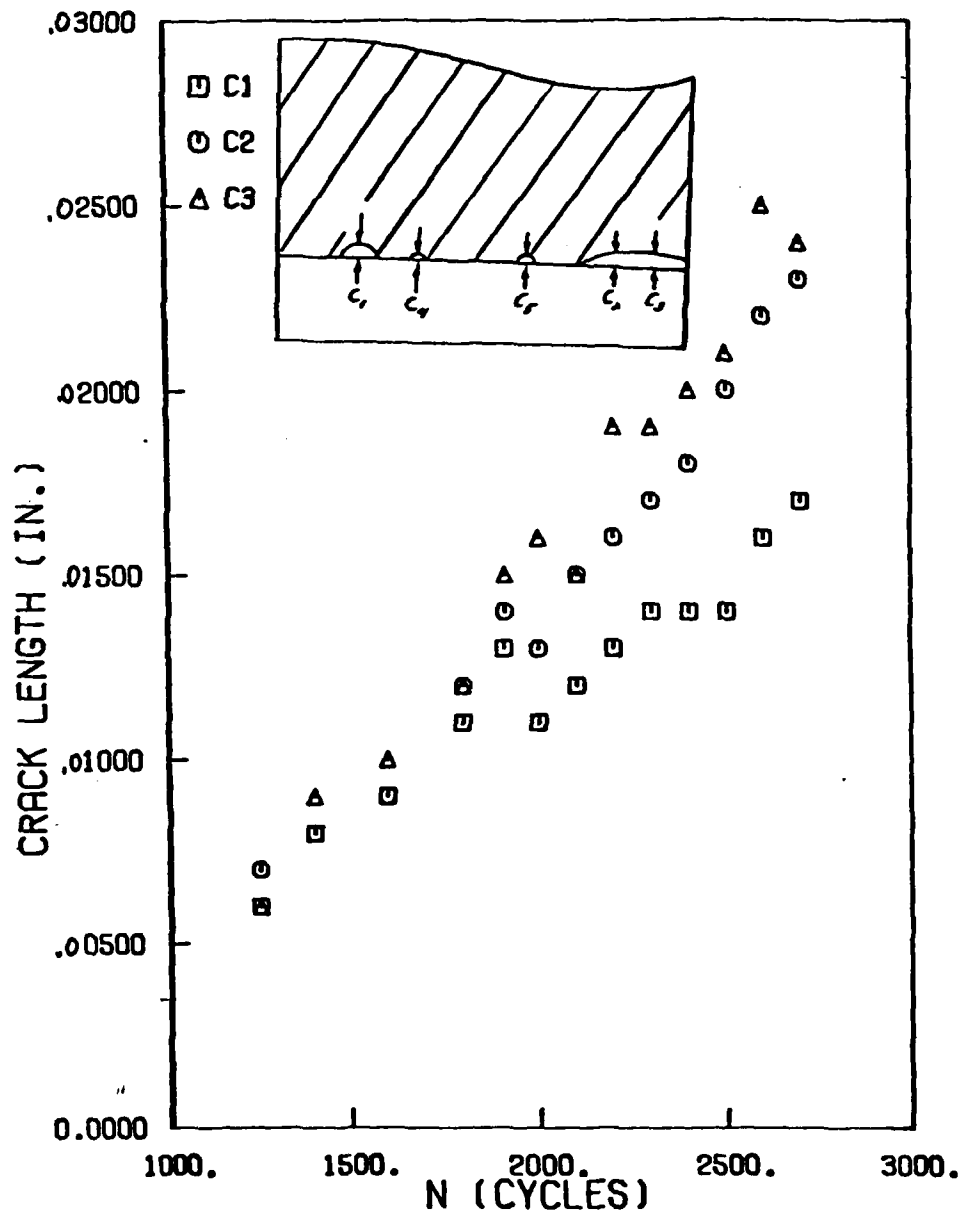


Figure 25a Growth of small fatigue cracks at V-notch in PMMA bend specimen

TEST ST-5

MAX LOAD=600 LB. MIN LOAD=30 LB.

45 DEG. V-NOTCH FREQUENCY 3 HZ.

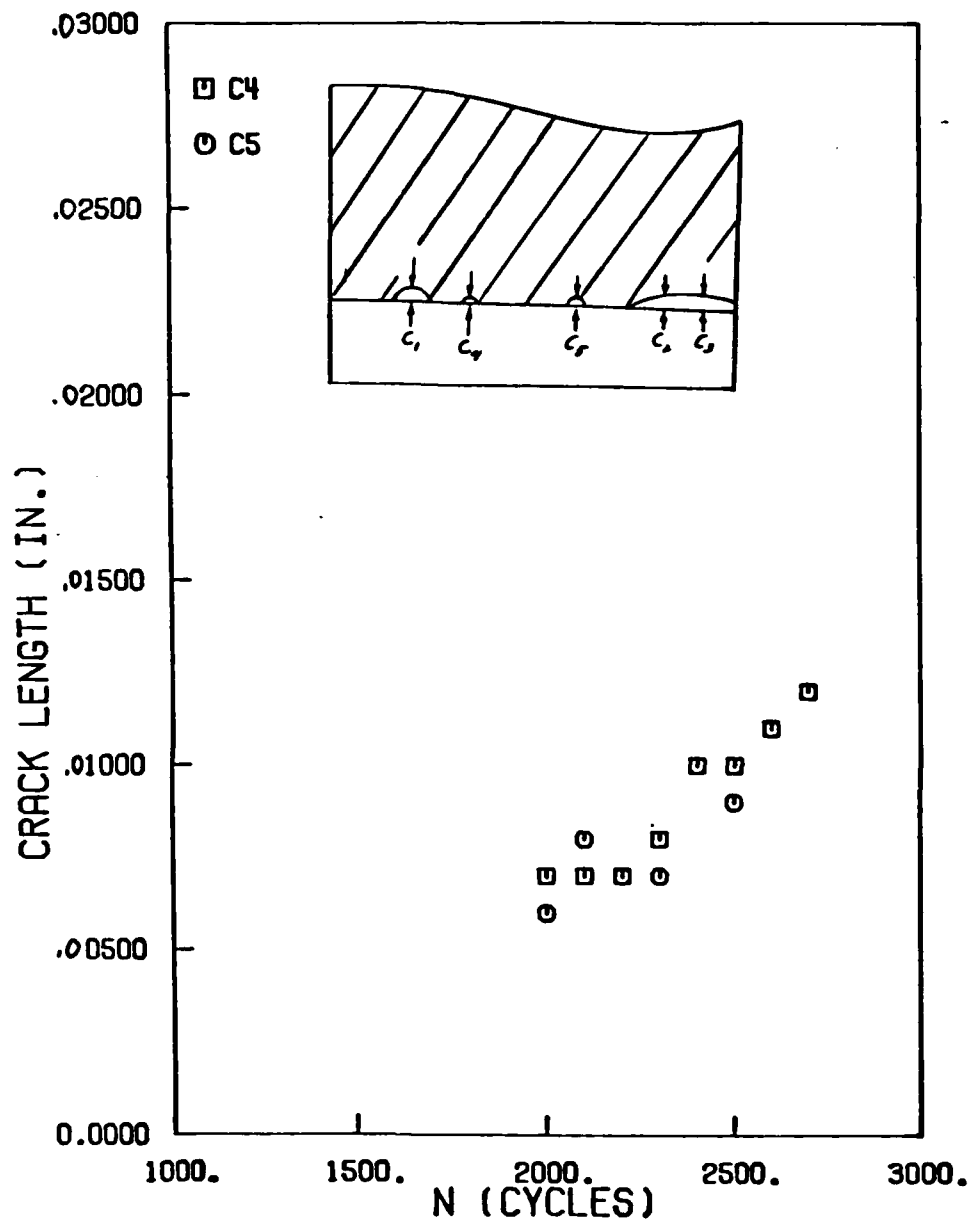


Figure 25b Growth of small fatigue cracks at V-notch in PMMA bend specimen

TEST ST-5

MAX LOAD=600 LB. MIN LOAD=30 LB.

45 DEG. V-NOTCH FREQUENCY 3 HZ.

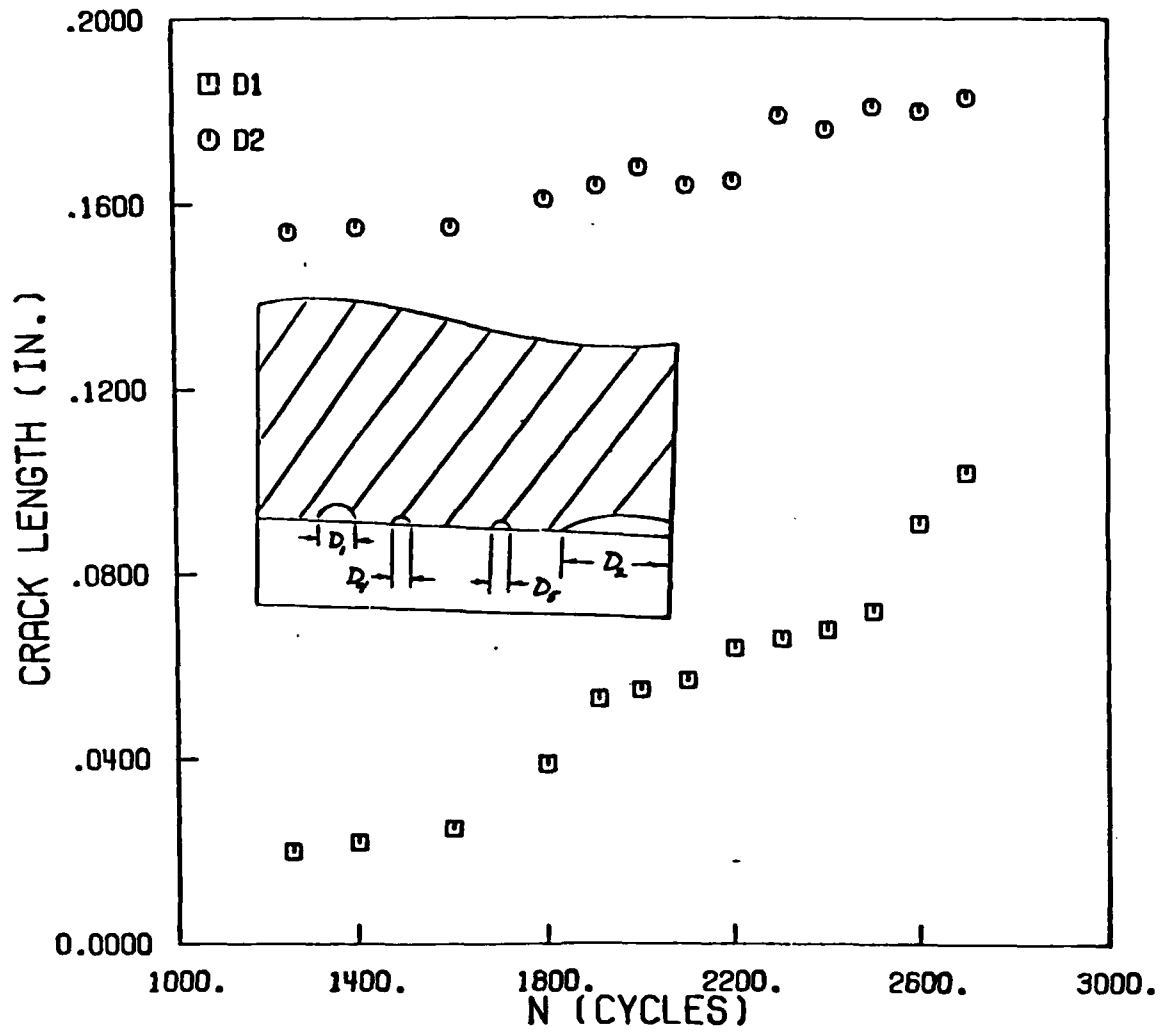


Figure 25c Growth of small fatigue cracks at V-notch in PMMA bend specimen

TEST ST-5

MAX LOAD=600 LB. MIN LOAD=30 LB.

45 DEG. V-NOTCH FREQUENCY 3 HZ.

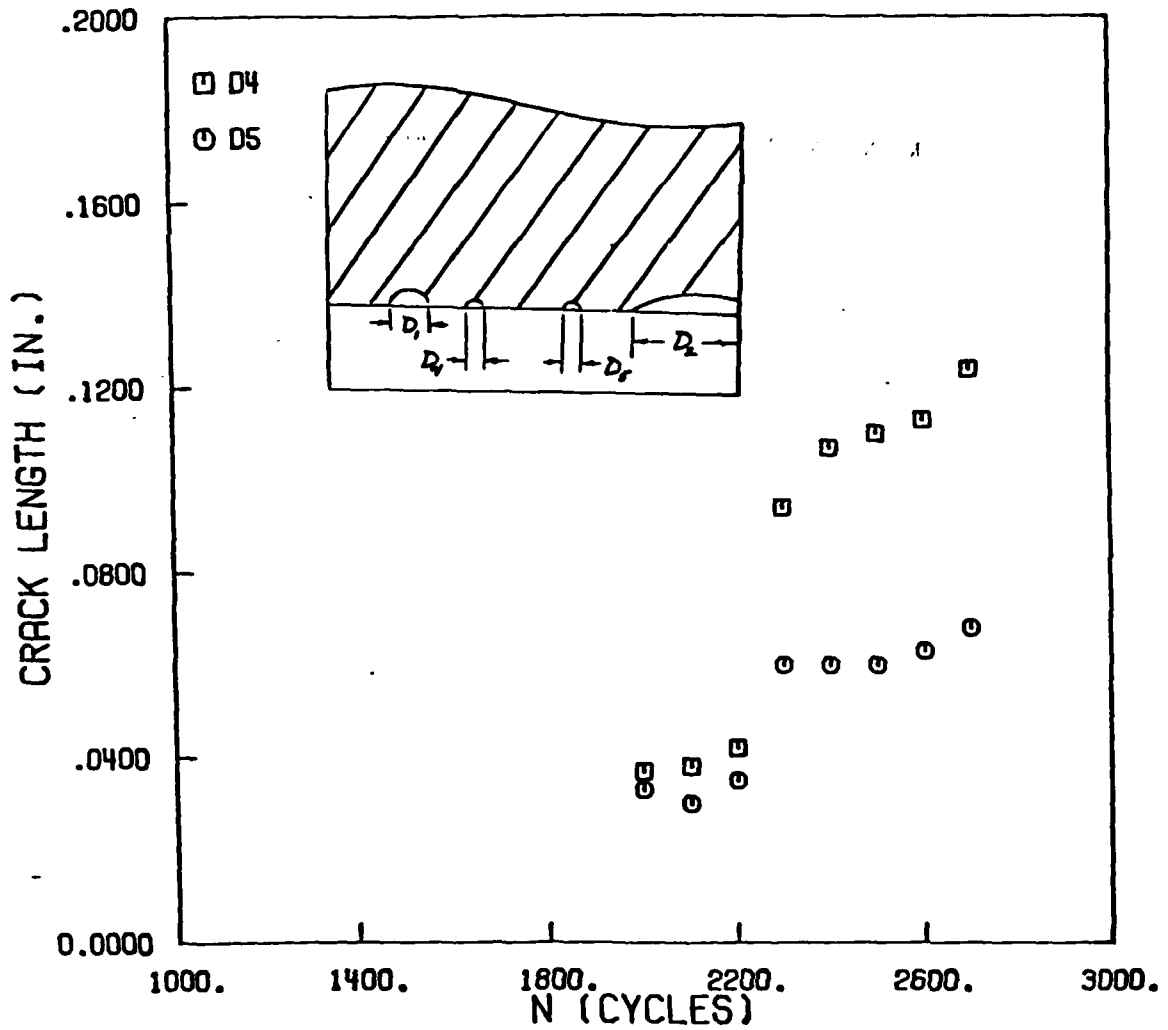


Figure 25d Growth of small fatigue cracks at V-notch in PMMA bend specimen

TEST ST-6

MAX LOAD=600 LB. MIN LOAD=30 LB.

45 DEG. V-NOTCH FREQUENCY 2 HZ.

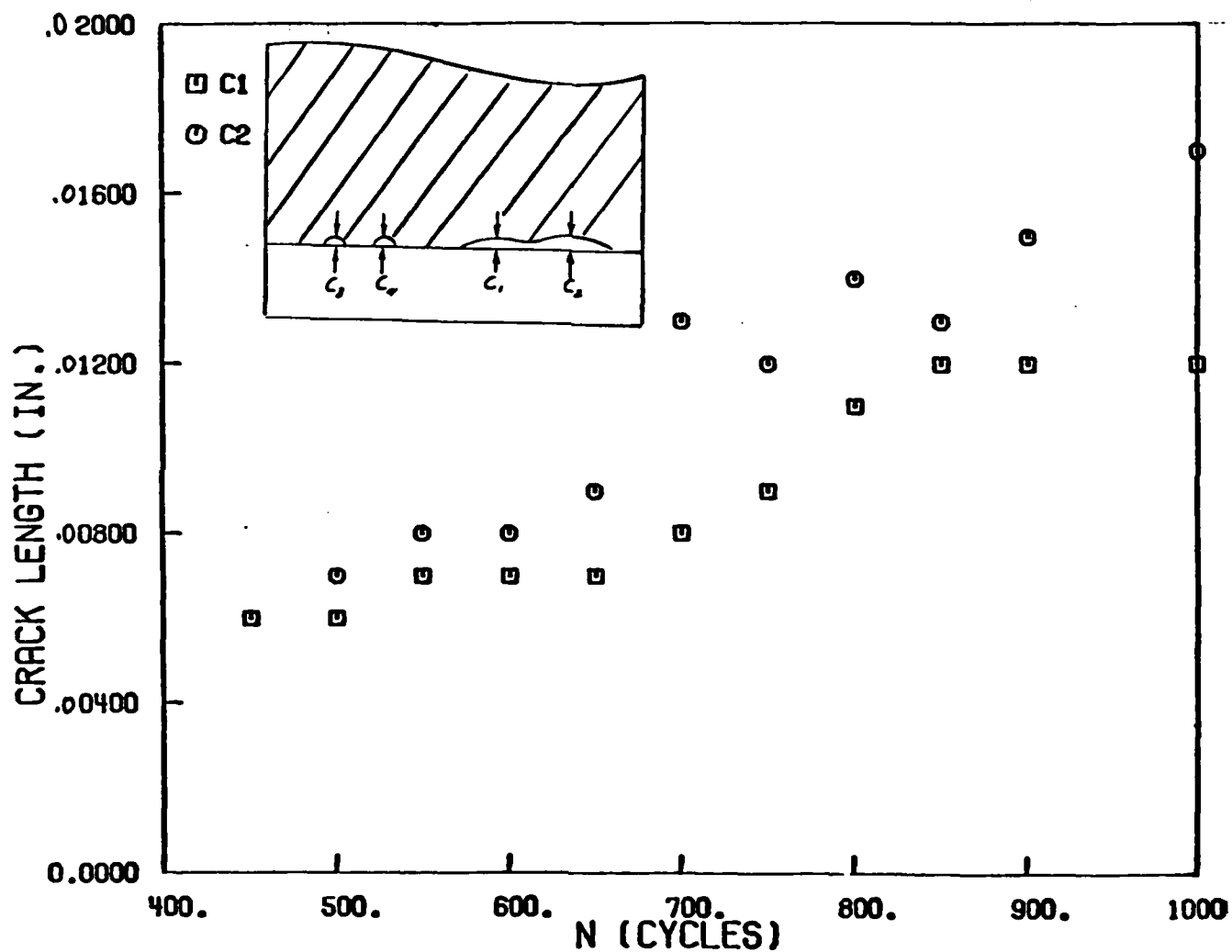


Figure 26a Growth of small fatigue cracks at V-notch in PMMA bend specimen

TEST ST-6

MAX LOAD=600 LB. MIN LOAD=30 LB.

45 DEG. V-NOTCH FREQUENCY 2 HZ.

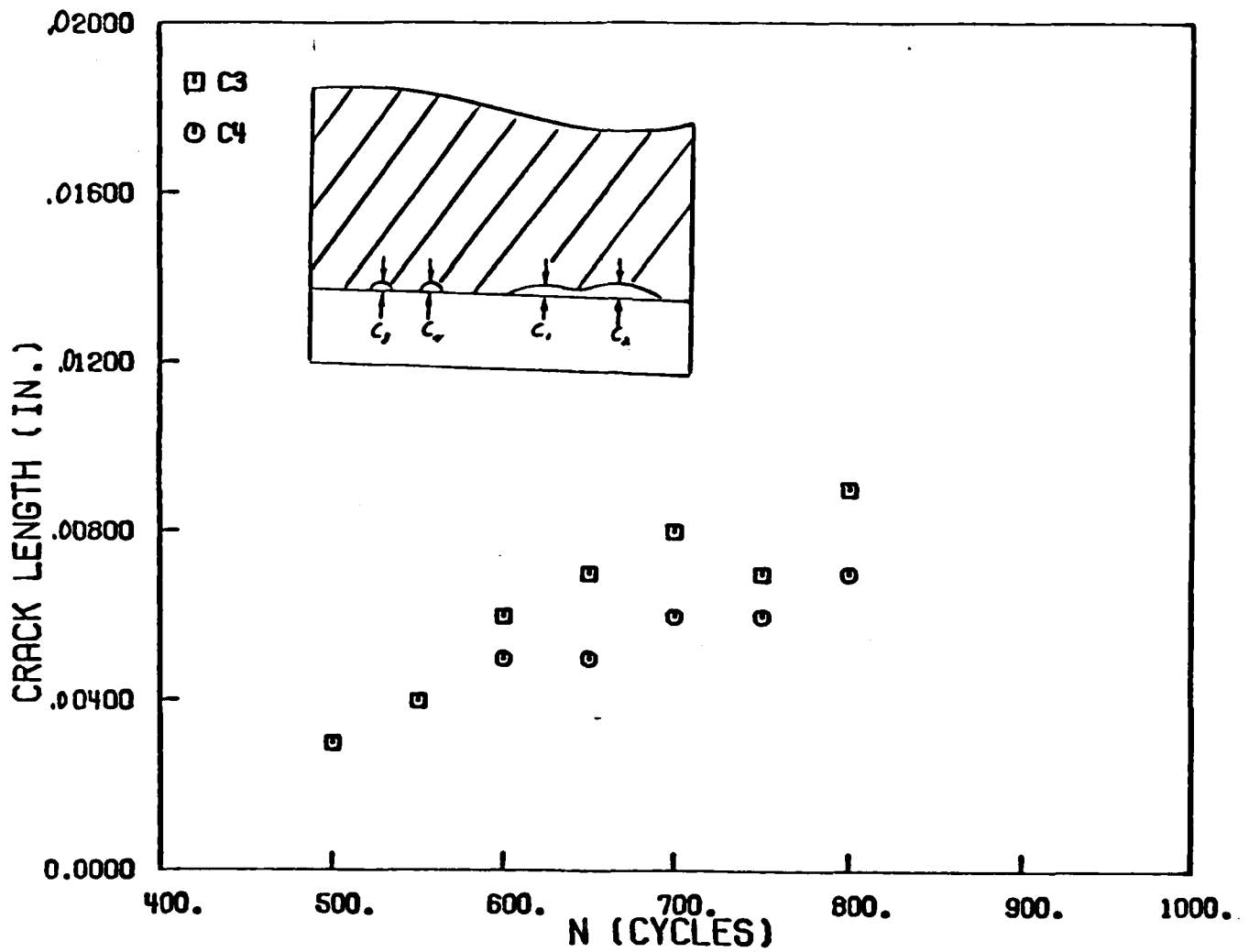


Figure 26b Growth of small fatigue cracks at V-notch in PMMA bend specimen

TEST ST-6

MAX LOAD=600 LB. MIN LOAD=30 LB.

45 DEG. V-NOTCH FREQUENCY 2 HZ.

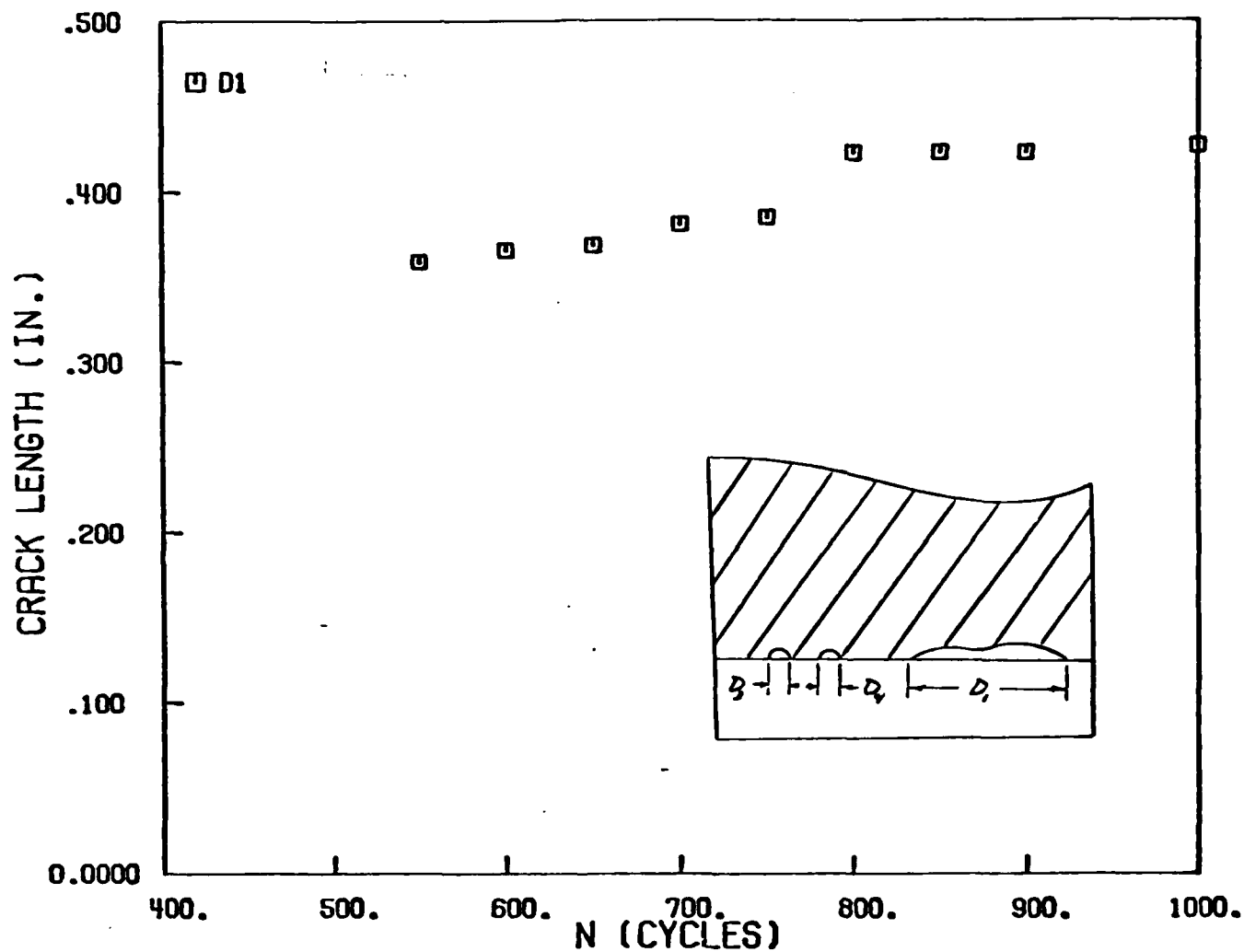


Figure 26c Growth of small fatigue cracks at V-notch in PMMA bend specimen



TEST ST-6

MAX LOAD=600 LB. MIN LOAD=30 LB.

45 DEG. V-NOTCH FREQUENCY 2 HZ.

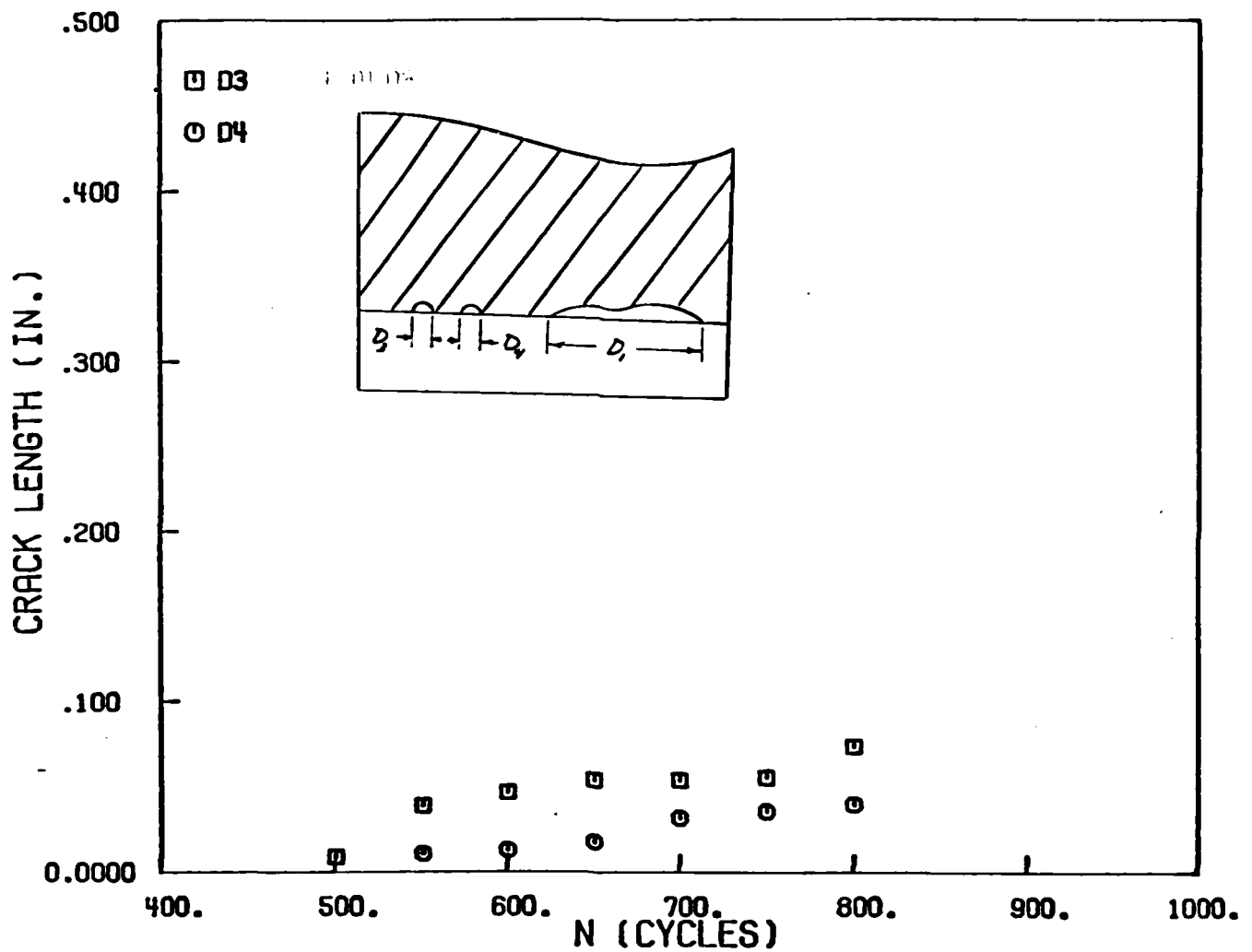


Figure 26d Growth of small fatigue cracks at V-notch in PMMA bend specimen

TEST ST-1

MAX LOAD=600 LB. MIN LOAD=90 LB.

90 DEG. V-NOTCH      FREQUENCY 2 HZ

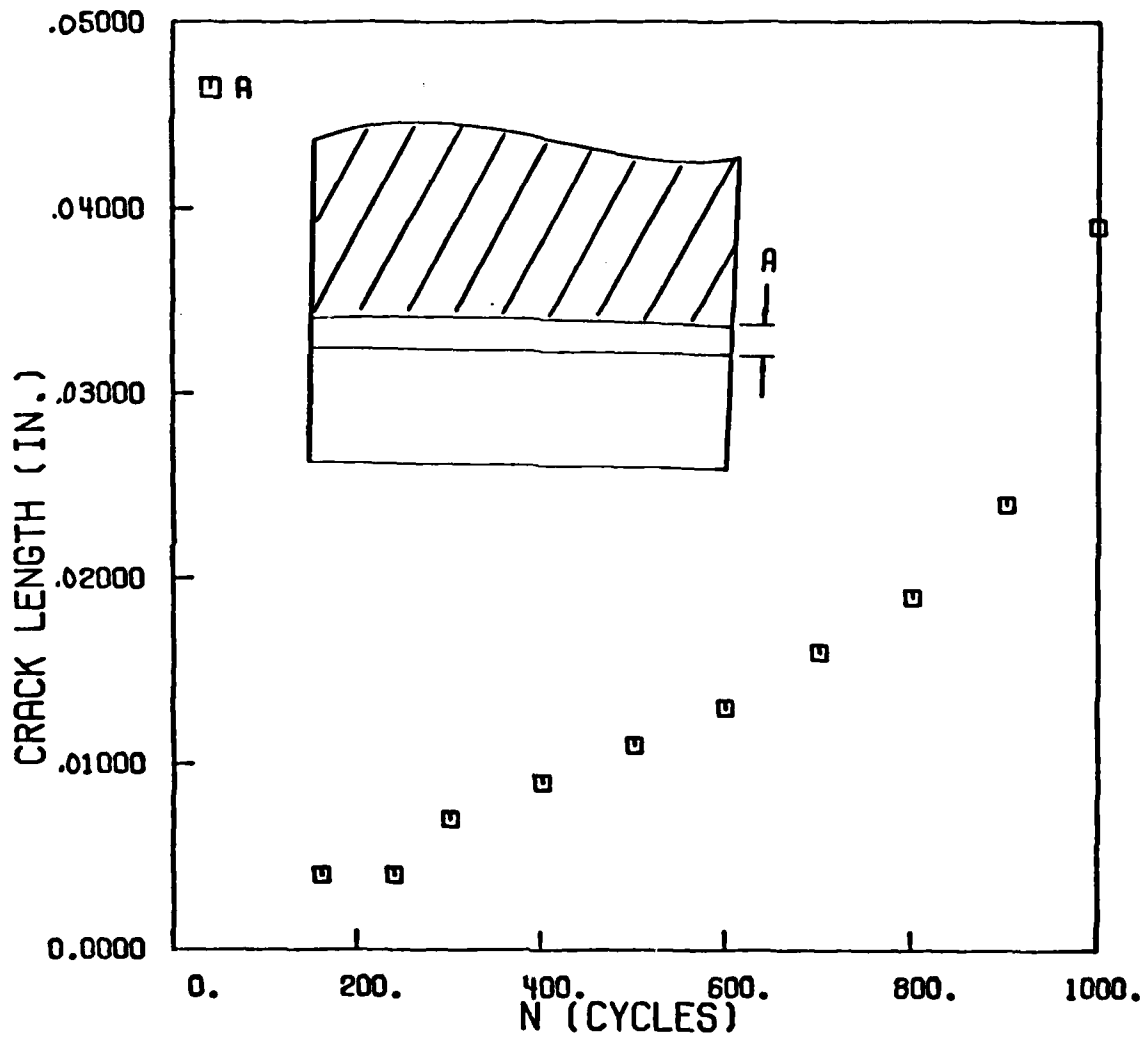


Figure 27 Growth of small through-the-thickness cracks at V-notch in PMMA bend specimen

TEST ST-3

MAX LOAD 500 LB. MIN LOAD 26 LB.

90 DEG. V-NOTCH FREQUENCY 2 HZ

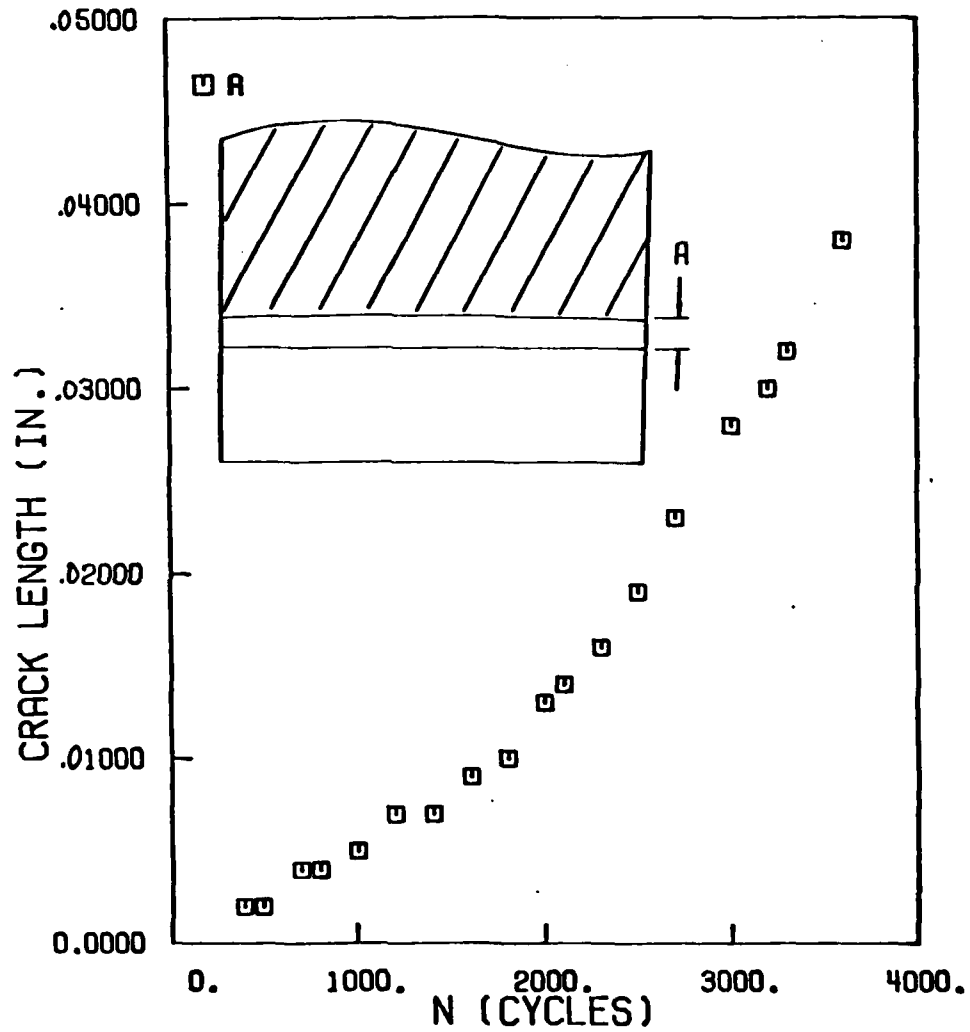


Figure 28 Growth of small through-thickness crack at V-notch in PMMA bend specimen

Stress Intensity Factors for Coalescing  
and Single Corner Flaws along a Hole Bore in a Plate

by

B.J. Heath<sup>1</sup>

and

A.F. Grandt<sup>2</sup>

ABSTRACT

The objective of this paper is to describe the effects of crack interaction on stress intensity factors for two symmetric coplanar corner flaws located along a hole bore. This numerical analysis employs the Finite Element-Alternating Method to determine Mode I stress intensity factors for single and coalescing corner flaws. Using single flaw stress intensity factors as a reference, analysis of crack size and shape effects on  $K_I$  for coalescing corner flaws indicates the stress intensity factor for crack points along the hole bore increases as the crack tip separation distance decreases. Interaction effects are not experienced by hole bore crack points when the crack tip separation distance is equal to or greater than half of the largest corner flaw dimension.

(Paper accepted for publication by Engineering Fracture Mechanics)

---

<sup>1</sup>Graduate research assistant and <sup>2</sup>Associate Professor, School of Aeronautics and Astronautics, Purdue University, W. Lafayette, Indiana 47907.

## INTRODUCTION

Naturally occurring fatigue cracks frequently initiate at several independent points along the bore of fastener holes. These individual flaws then grow and coalesce into a single dominant crack which controls final fracture. Prediction of this coalescence phase of crack growth requires stress intensity factor solutions for the individual cracks prior to their "link up" into a single flaw.

It is known that the stress intensity factor for a crack tip is influenced by the close proximity of an adjacent crack tip [1-4]. Crack interaction effects on Mode I stress intensity factors ( $K_I$ ) have been studied by several authors [1-4]. Various two-dimensional  $K_I$  solutions exist for interaction of coplanar through-the-thickness cracks [3, 4]. Kamei and Yokoburi [3], for example, present a two-dimensional stress intensity factor solution for two asymmetric through-the-thickness cracks in an infinite sheet, while Benthem and Koiter [4] give a two-dimensional  $K_I$  solution for two symmetric edge cracks. Murakami and Nemat-Nassar [1] present an approximate three-dimensional  $K_I$  solution, obtained by the Body Force Method, for coplanar surface flaws in an unbounded solid. None of these solutions, however, consider coalescence of coplanar flaws located along the bore of a hole in a finite thickness plate. Since multiple fastener hole cracks often occur in service [5, 6], the present paper examines crack coalescence along a hole bore.

The objective of this paper is to describe stress intensity factor results for two adjacent cracks located along the bore of a hole in a finite thickness plate. Figure 1 shows typical plate cross sections for the symmetric and single crack configurations considered. Here  $a$  is the crack dimension measured along the hole bore;  $c$  is measured along the

free surface;  $T$  is the plate thickness and  $D$  is the hole diameter. The plate is loaded with a remote stress  $\sigma$  applied perpendicular to the crack plane. The Finite Element - Alternating Method (FEAM) [7-13] is used to compute  $K_I$  for symmetric (coalescing) and single corner cracks along the hole bore.

Results are given in both tabular and graphical form for crack sizes in the range  $0.25 \leq a/T < .5$  for crack shapes  $a/c = 1.11, 1.5, 2.0$  and  $3.0$ . (As described in earlier work [7], numerical programming difficulties prevent analysis of quarter circular cracks,  $a/c = 1.0$ , with the present computer codes.) Crack shape and size effects on  $K_I$  variation around the crack perimeter are presented for coalescing corner flaws. Two and three-dimensional stress intensity factor solutions for other coalescing crack configurations are compared with the stress intensity factors generated for the corner cracked hole geometry.

## NUMERICAL APPROACH

Stress intensity factors for coalescing cracks along a hole bore are obtained by the Finite Element - Alternating Method (FEAM). The present parametric study makes use of computer codes developed by Smith and Kullgren [7]. The original codes were modified here to treat the coalescing crack problem.

The FEAM calculates  $K_I$  based on approximate surface crack boundary conditions. An iterative superposition of two solutions, one a 3-D finite element solution for an uncracked body under prescribed surface loadings, and the second a stress solution for a flat elliptical crack in an infinite body with nonuniform prescribed surface pressure, produce these approximate surface flaw boundary conditions. Earlier applications of the FEAM to various other cracked hole problems are described in Ref. 8-12.

The crack coalescence problem studied here requires modification of the finite element mesh and the elliptical crack stress solution of [7] to produce the symmetric crack finite element model used in conjunction with the coalescence option of the FEAM computer code.

### Single Crack Model

The single crack model is a semi-circular plate with a hole. As in Fig. 2, this model has a hole radius  $R$ . In order to minimize boundary effects in the region of the crack, the same outer plate radius of  $12 R$  ( $R$  = hole radius) used by Smith and Kullgren [7] is used. The single crack model employs 112 20-Node isoparametric finite elements. The hole diameter to thickness ratio ( $D/T$ ) is 0.5. The modulus of rigidity for the plate is  $G = 12 \times 10^6$  psi with a Poisson's ratio of  $\nu = 0.3$ .

### Symmetric Crack Model

Symmetric interacting cracks were studied by imposing a line of symmetry along the  $x = 0.5$  face of the original FEAM model with  $D/T = 1.0$  as shown in Fig. 2. The hole radius, outer radius, and element number are equivalent to the single crack model. In order to account for the line of symmetry, the symmetric crack model has a  $D/T = 1.0$  rather than  $D/T = 0.5$  for the single crack. As shown in Fig. 3, the plane of symmetry imposed along the front surface of the plate, however, effectively doubles the symmetric crack model plate thickness. Thus, the symmetric crack model  $D/T$  equals that of the single crack model ( $D/T = 0.5$ ). Figure 3 shows how an infinite plate with two symmetric cracks along the hole bore is simulated when a corner flaw is applied to the FEAM symmetric crack model.



## DISCUSSION OF RESULTS

Stress intensity factors were generated for crack shapes  $a/c = 1.11$ , 1.5, 2.0, and 3.0 by the FEAM analysis. Each crack varied in size from  $0.25 \leq a/T < 0.5$ . The stress intensity factors for the corner flaw configurations considered are listed in tables 1 and 2. Table 1 lists the stress intensity factor variation for the single crack in 15 degree increments of the elliptic angle  $\phi$  defined in Fig. 1. Stress intensity factor results for the symmetric crack configuration are listed in Table 2.

These results provide a parametric study of size and shape effects on the stress intensity factor variation around the crack perimeter. For a single corner crack with  $a/c = 1.11$ , Figure 4 shows the variation of the dimensionless stress intensity factor ( $K_I/\sigma\sqrt{D}$ ) versus normalized elliptic angle ( $\phi/\phi_{\max}$ ) as the crack size ( $a/T$ ) increases. Note that  $\phi_{\max} = 90$  degrees. Figure 5 shows the variation of  $K_I/\sigma\sqrt{D}$  over the same  $a/T$  range for two symmetric cracks with the same  $a/c = 1.11$ .

Recalling that  $\phi = 90^\circ$  corresponds to the hole bore crack location, notice the increased magnitude of  $K_I/\sigma\sqrt{D}$  along the hole bore for the symmetric configuration compared to the same location for the single flaw as the crack size is increased. Using the single flaw  $K_I/\sigma\sqrt{D}$  as a reference, the influence of  $a/T$  on  $K_I/\sigma\sqrt{D}$  for particular flaw points on the symmetric model crack perimeter is shown in Figs. 6-8. For small crack sizes ( $0.25 \leq a/T \leq 0.3$ ) shown in Figs. 6-8, the single and coalescing configurations differ by a maximum of 4 percent. However, Figures 6 and 7 show a significant increase in the symmetric crack  $K_I/\sigma\sqrt{D}$  as compared to the single flaw  $K_I/\sigma\sqrt{D}$  when the crack size approaches coalescence ( $a/T = 0.5$ ).

Following Murakami [1], a crack interaction factor  $\gamma$  is defined as the ratio of the stress intensity factor for two cracks to the stress intensity factor for a single crack. Kamei and Yokoburi [3] have given two-dimensional stress intensity factor solutions for two asymmetrical through-the-thickness cracks in an infinite elastic sheet. By equating the crack lengths as shown in Figure 9a, and normalizing the crack tip stress intensity factor expression by  $\sigma\sqrt{\pi a}$ , the interaction factor  $\gamma$  for two symmetric through-the-thickness cracks is obtained. The Benthem and Koiter [4] two-dimensional stress intensity factor solution for two symmetric edge cracks (see Figure 9b) may be used to compute the edge crack interaction factor shown in Fig. 10. Here, the double edge-crack solution was divided by the stress intensity factor given by Harris [14] for a single edge-cracked sheet which doesn't bend.

Three-dimensional crack point interaction factors for symmetric semi-circular surface flaws (Fig. 9c) are presented by Murakami and Nemat-Nassar in Ref. [1]. These coplanar flaws exist in an unbounded solid. The present FEAM results were used to compute three-dimensional interaction factors for symmetric corner cracks along a hole bore (Fig. 9d). Figure 10 compares these two-and-three dimensional crack tip interaction factors as a function of dimensionless crack separation distance ( $\frac{t_{sep}}{a}$ ). The through-the-thickness interaction factor of Kamei [3] represents the limiting value of two interacting surface cracks, while the Benthem and Koiter [4] edge-crack factor serves as a limiting value for the present study of interacting corner cracks. Due to a numerical instability in the FEAM code, values of crack interaction factors at coalescence ( $t_{sep}/a = 0$ ) are not obtainable.

Notice the close proximity of the present FEAM results for corner cracked holes to the Murakami [1] interaction factor for surface cracks. As the crack separation  $t_{sep}$  exceeds approximately half of the crack length dimension  $a$ , ( $t_{sep}/a \geq 0.5$ ), the FEAM crack interaction factor stabilize at unity, indicating that the crack tip located along the hole bore is no longer influenced by the adjacent crack. For a given  $t_{sep}/a$ , the maximum difference in all hole bore interaction factors presented in Figure 10 is 10.7 percent. Figure 10 indicates that crack size ( $a/T$ ) dominates the increase in  $K_I$  due to crack interaction at the hole bore, while crack shape ( $a/c$ ) has only a slight influence. The effect of crack shape on the hole bore interaction factors is shown on an expanded scale in Figure 11.

Figure 12 presents the interaction factor at the plate surface ( $\phi = 0$ ). The factors decrease slightly below unity in the range of  $0 < \frac{t_{sep}}{a} \leq 0.5$ . Figure 12 further indicates that the crack is free of influence from the adjacent crack when the hole bore separation distance is greater than half the crack length  $a$ . As the separation distance decreases, the decrease in  $K_I$  at the plate surface is considerably less than the increase in  $K_I$  at the hole bore location (see Figure 10). Thus, the effect of crack coalescence is fairly localized, serving to increase  $K_I$  for crack points in the vicinity of the hole bore. The free surface  $K_I$ , however, is only slightly affected as crack separation approaches zero. Table 3 lists the hole bore and free surface interaction factors for all aspect ratios considered. The decrease in  $K$  for the double cracked case may be caused by elimination of through-the-thickness bending for the symmetric crack configuration.

### SUMMARY AND CONCLUSIONS

Several conclusions can be made about stress intensity factors for two symmetric coalescing corner cracks. First, as two symmetric corner cracks approach coalescence ( $a/T = 0.5$ ), the greatest increase in stress intensity factor occurs at the crack point along the hole bore. The crack point at the free surface does not experience a significant stress intensity factor increase, but shows a slight decrease in  $K_I$  as the crack tips approach along the hole bore.

For crack points along the hole bore, crack interaction (stress intensity factor increase) does not occur until the crack separation distance is equal to or less than half of the crack length  $a$ . The localized effect of coalescence is found to depend strongly on crack size ( $a/T$ ) and only weakly on crack shape ( $a/c$ ). The crack shape dependence indicates that the deeper cracks (smaller  $a/c$  ratios) have a slightly larger  $K$  (maximum 10.7% difference) at the hole bore location than more shallow flaws (larger  $a/c$ ) with the same crack length  $a$ .

#### ACKNOWLEDGMENTS

Research sponsored by the Air Force Office of Scientific Research, Air Force Systems Command, USAF, under grant Number AFOSR-82-0041. The U.S. Government is authorized to reproduce and distribute reprints for Governmental purposes notwithstanding any copyright notation thereon. Captain D. A. Glasgow was the technical monitor. The authors would like to thank T.E. Kullgren for his continued assistance with operation of the finite element-alternating computer codes. His significant help in making the modifications necessary to analyze the symmetric crack problem is especially appreciated. Thanks is also extended to C.T. Malmsten for making the FEAM codes operational on the Purdue computer system.

REFERENCES

1. Murakami, Y., Nemat-Nasser, S., "Interacting Dissimilar Semi-elliptical Surface Flaws Under Tension and Bending," Engineering Fracture Mechanics, Vol. 16, No. 3, 1982.
2. Chang, R., "On Crack-Crack Interaction and Coalescence in Fatigue," Engineering Fracture Mechanics, Vol. 16, No. 5, 1982.
3. Kamei, A., and Yokoburi, T., "Two Collinear Asymmetrical Elastic Cracks," Rep. Res. Inst. Strength Materials, Tohoku Univ., Vol. 10, Dec. 1974.
4. Benthem, J.P. and Koiter, W.T., results reported in Compendium of Stress Intensity Factors, by D.P. Rooke and D.J. Cartwright, The Hillingdon Press, 1976, p. 110.
5. Hyzak, J.M., Reimann, W.H., and Allison, J.E., "The Development of Quantitative NDE for Retirement-for-Cause," AFML-TR-78-198, February 1977.
6. Harris, J.H. Jr., Sims, D.L., and Annis, C.G., "Concept Definition: Retirement for cause of F100 ROTOR Components," AFWAL-TR-80-4118, September 1980.
7. Smith, F.W., Kullgren, T.E., "Theoretical and Experimental Analysis of Surface Cracks Emanating from Fastener Holes," AFFDL-TR-76-104, Feb. 1977.
8. Kullgren, T.E., Smith, F.W., and Ganong, G.P., "Quarter-Elliptical Cracks Emanating from Holes in Plates," Journal of Engineering Materials and Technology, Vol. 100, April 1978, pp. 144-149.
9. Kullgren, T.E., and Smith, F.W., "The Finite Element-Alternating Method Applied to Benchmark No. 2," International Journal of Fracture, Vol. 14, 1978, pp. R319-R322.
10. Kullgren, T.E. and Smith, F.W., "Part-Elliptical Cracks Emanating from Open and Loaded Holes in Plates," Journal of Engineering Materials and Technology, Vol. 101, January 1979, pp. 12-17.
11. Grandt, A.F., Jr., and Kullgren, T.E., "Stress Intensity Factors for Corner Cracked Holes Under General Loading Conditions," Journal of Engineering Materials and Technology, Vol. 103, No. 2, April 1981, pp. 171-176.
12. Grandt, A.F., Jr., "Crack Face Pressure Loading of Semielliptical Cracks Located Along the Bore of a Hole," Engineering Fracture Mechanics, Vol. 14, No. 4, 1981, pp. 843-852.

13. Smith, F.W., "Stress Near a Semi-Circular Edge Crack," Ph.D. thesis, University of Washington, 1966.
14. Harris, J.O., results reported in Compendium of Stress Intensity Factors, by D.P. Rooke and D.J. Cartwright, The Hillingdon Press, 1976, p. 84.

**Table 1** Dimensionless stress intensity factors for single corner crack at open hole in a large plate loaded in remote tension. Results given as a function of crack shape  $a/c$ , crack size  $a/T$ , and position along crack perimeter defined by parametric angle  $\phi$  ( $\phi = 0^\circ$  at front surface and  $\phi = 90^\circ$  at hole bore).

a/c	a/T	$K_I/\sigma\sqrt{D}$						
		$\phi = 0^\circ$	15°	30°	45°	60°	75°	$\phi = 90^\circ$
1.11	.2500	1.156	1.137	1.137	1.215	1.373	1.553	1.665
	.3000	1.238	1.198	1.183	1.259	1.431	1.633	1.765
	.3500	1.299	1.255	1.234	1.308	1.483	1.692	1.831
	.4000	1.388	1.325	1.285	1.355	1.542	1.773	1.933
	.4500	1.479	1.404	1.347	1.398	1.571	1.794	1.952
	.4750	1.496	1.426	1.371	1.422	1.592	1.813	1.968
	.4875	1.519	1.440	1.378	1.428	1.607	1.840	2.007
	.4938	1.540	1.456	1.388	1.433	1.610	1.844	2.014
1.5	.2500	1.184	1.192	1.202	1.260	1.360	1.457	1.513
	.3000	1.270	1.250	1.237	1.292	1.409	1.535	1.617
	.3500	1.317	1.293	1.279	1.337	1.460	1.591	1.676
	.4000	1.394	1.353	1.326	1.385	1.523	1.676	1.780
	.4500	1.448	1.400	1.362	1.411	1.544	1.695	1.799
	.4750	1.482	1.428	1.383	1.427	1.559	1.712	1.819
	.4875	1.519	1.452	1.395	1.437	1.576	1.741	1.859
	.4938	1.531	1.460	1.399	1.439	1.577	1.743	1.863
2.0	.2500	1.150	1.204	1.247	1.302	1.349	1.357	1.349
	.3000	1.268	1.278	1.284	1.330	1.397	1.437	1.458
	.3500	1.308	1.313	1.315	1.365	1.440	1.490	1.518
	.4000	1.400	1.372	1.351	1.400	1.496	1.573	1.623
	.4500	1.435	1.410	1.386	1.432	1.532	1.596	1.645
	.4750	1.458	1.432	1.407	1.451	1.542	1.615	1.665
	.4875	1.480	1.444	1.414	1.460	1.562	1.646	1.705
	.4938	1.486	1.447	1.413	1.460	1.563	1.651	1.711



a/c	a/T	$K_I/\sigma\sqrt{D}$						
		$\phi = 0^\circ$	$15^\circ$	$30^\circ$	$45^\circ$	$60^\circ$	$75^\circ$	$90^\circ$
3.0	.2500	1.202	1.277	1.311	1.322	1.290	1.186	1.100
	.3000	1.237	1.299	1.335	1.370	1.370	1.286	1.209
	.3500	1.275	1.326	1.358	1.400	1.413	1.339	1.267
	.4000	1.333	1.356	1.373	1.427	1.470	1.423	1.368
	.4500	1.402	1.410	1.411	1.455	1.497	1.454	1.403
	.4750	1.421	1.424	1.421	1.465	1.510	1.470	1.421
	.4875	1.429	1.429	1.428	1.480	1.537	1.505	1.461
	.4938	1.431	1.431	1.430	1.484	1.542	1.511	1.467

Table 2 Dimensionless stress intensity factors for symmetric corner cracks located at intersection of hole bore with front and back surfaces of a plate loaded in remote tension. Results given as crack tips approach coalescence ( $a/T = 0.5$ ) in terms of crack shape  $a/c$ , crack size  $a/T$ , and position along crack perimeter defined by parametric angle  $\phi$  ( $\phi = 90^\circ$  at hole bore)

a/c	a/T	Symmetric Cracks $K_I/\sigma \sqrt{D}$						
		$\phi = 0^\circ$	$15^\circ$	$30^\circ$	$45^\circ$	$60^\circ$	$75^\circ$	$\phi = 90^\circ$
1.11	.2500	1.121	1.145	1.182	1.277	1.422	1.555	1.595
	.3000	1.185	1.201	1.229	1.325	1.479	1.627	1.680
	.3500	1.210	1.224	1.262	1.377	1.560	1.733	1.799
	.4000	1.276	1.283	1.317	1.440	1.643	1.841	1.925
	.4500	1.349	1.347	1.381	1.526	1.765	2.001	2.107
	.4750	1.350	1.356	1.415	1.595	1.872	2.137	2.250
	.4875	1.364	1.356	1.425	1.644	1.981	2.300	2.441
	.4938	1.377	1.347	1.424	1.700	2.127	2.534	2.722
1.5	.2500	1.171	1.219	1.254	1.317	1.398	1.457	1.459
	.3000	1.237	1.273	1.296	1.358	1.450	1.526	1.545
	.3500	1.265	1.301	1.332	1.410	1.523	1.617	1.645
	.4000	1.321	1.352	1.382	1.470	1.601	1.715	1.756
	.4500	1.357	1.385	1.426	1.542	1.709	1.854	1.912
	.4750	1.384	1.409	1.458	1.592	1.784	1.948	2.014
	.4875	1.417	1.425	1.474	1.635	1.872	2.081	2.173
	.4938	1.426	1.406	1.464	1.683	2.010	2.302	2.444

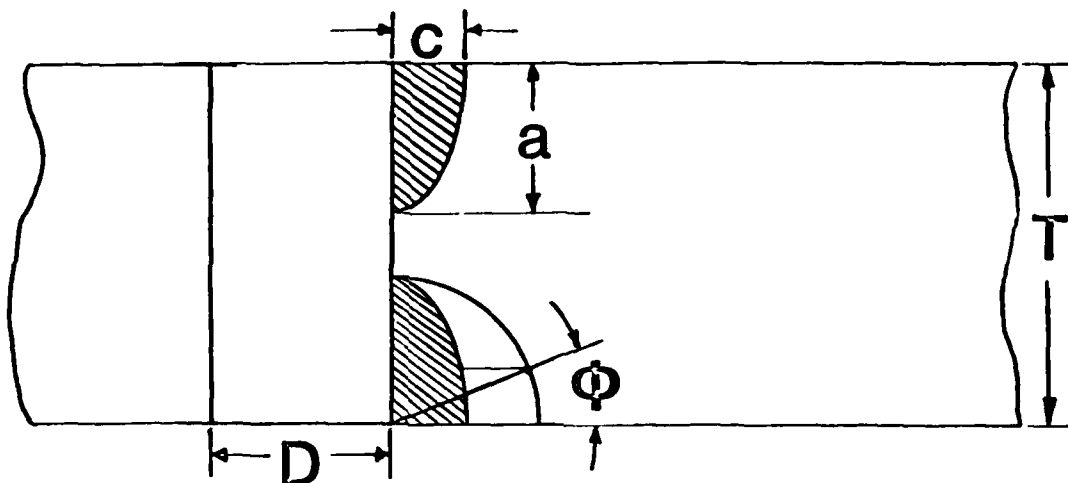
Table 2 Continued

a/c	a/T	$K_I/\sigma\sqrt{D}$						
		$\phi = 0^\circ$	$15^\circ$	$30^\circ$	$45^\circ$	$60^\circ$	$75^\circ$	$90^\circ$
2.0	.2500	1.187	1.261	1.303	1.345	1.373	1.358	1.321
	.3000	1.266	1.326	1.352	1.388	1.422	1.420	1.397
	.3500	1.281	1.345	1.385	1.444	1.501	1.515	1.499
	.4000	1.350	1.394	1.421	1.484	1.562	1.599	1.600
	.4500	1.385	1.432	1.470	1.556	1.661	1.718	1.730
	.4750	1.398	1.446	1.494	1.597	1.719	1.788	1.805
	.4875	1.416	1.452	1.503	1.634	1.797	1.900	1.936
	.4938	1.422	1.433	1.495	1.684	1.932	2.108	2.187
3.0	.2500	1.252	1.357	1.386	1.374	1.313	1.184	1.078
	.3000	1.261	1.372	1.416	1.426	1.386	1.266	1.164
	.3500	1.287	1.387	1.433	1.462	1.450	1.352	1.260
	.4000	1.319	1.418	1.467	1.510	1.516	1.429	1.344
	.4500	1.385	1.458	1.495	1.550	1.585	1.523	1.452
	.4750	1.402	1.472	1.511	1.575	1.622	1.567	1.497
	.4875	1.407	1.471	1.520	1.611	1.690	1.656	1.596
	.4938	1.413	1.460	1.524	1.672	1.823	1.840	1.802

**Table 3** Dimensionless interaction factor,  $\gamma$ , defined as ratio of stress intensity factor for symmetric double crack geometry divided by single corner crack result. Interaction factors given at hole bore ( $\phi = 90^\circ$ ) and free surface ( $\phi = 0^\circ$ ) locations as functions of dimensionless separation along hole bore ( $t_{sep}/a$ ) and crack shape  $a/c$ .

INTERACTION FACTORS $\gamma$									
HOLE BORE ( $\phi = 90^\circ$ )						FREE SURFACE ( $\phi = 0^\circ$ )			
	$a/c$	1.11	1.5	2.0	3.0	1.11	1.5	2.0	3.0
$t_{sep}/a$	.025	1.352	1.312	1.278	1.228	.894	.931	.957	.988
	.051	1.216	1.169	1.136	1.092	.898	.932	.956	.984
	.105	1.143	1.107	1.084	1.053	.902	.934	.958	.987
	.222	1.079	1.062	1.051	1.035	.912	.937	.965	.987
	.500	.996	.987	.986	.982	.919	.948	.964	.990
	.857	.983	.982	.987	.995	.932	.961	.979	1.009
	1.333	.952	.955	.958	.963	.957	.974	.999	1.020
	2.000	.958	.964	.979	.980	.969	.989	1.033	1.041

## Symmetric Corner Crack Configuration



## Single Corner Crack Configuration

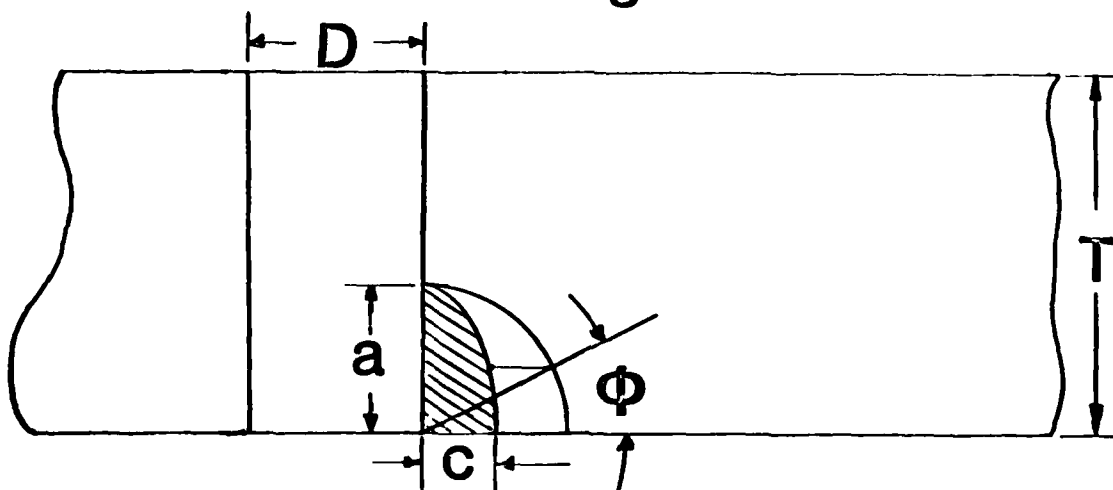


Figure 1 Schematic drawing of crack plane showing location of single and symmetric corner cracks located at bore of hole.

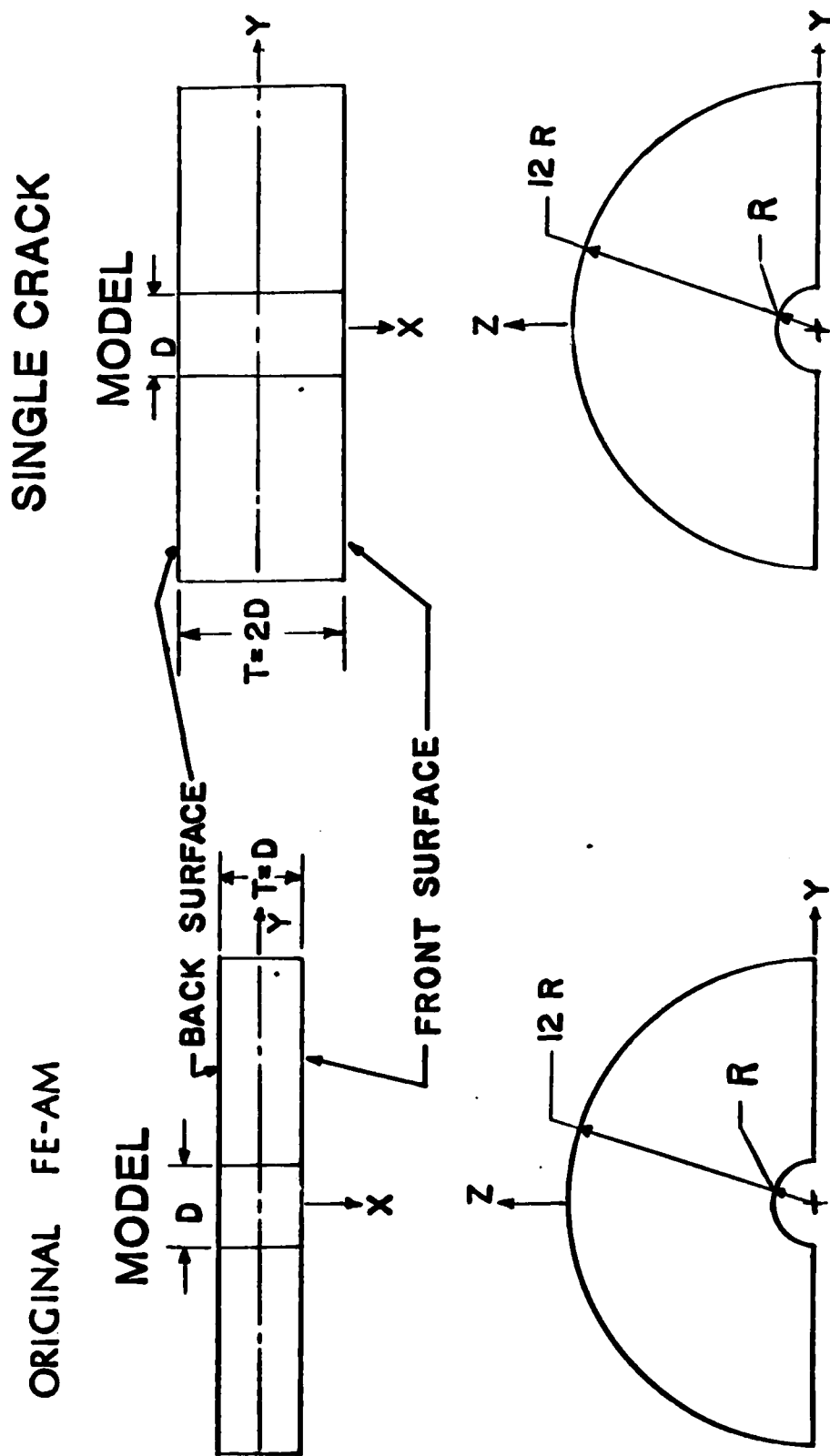


Figure 2 Geometric models employed for uncracked solution in FEAM iterative algorithm. The half ring geometries shown were modeled by 112 three-dimensional finite elements.

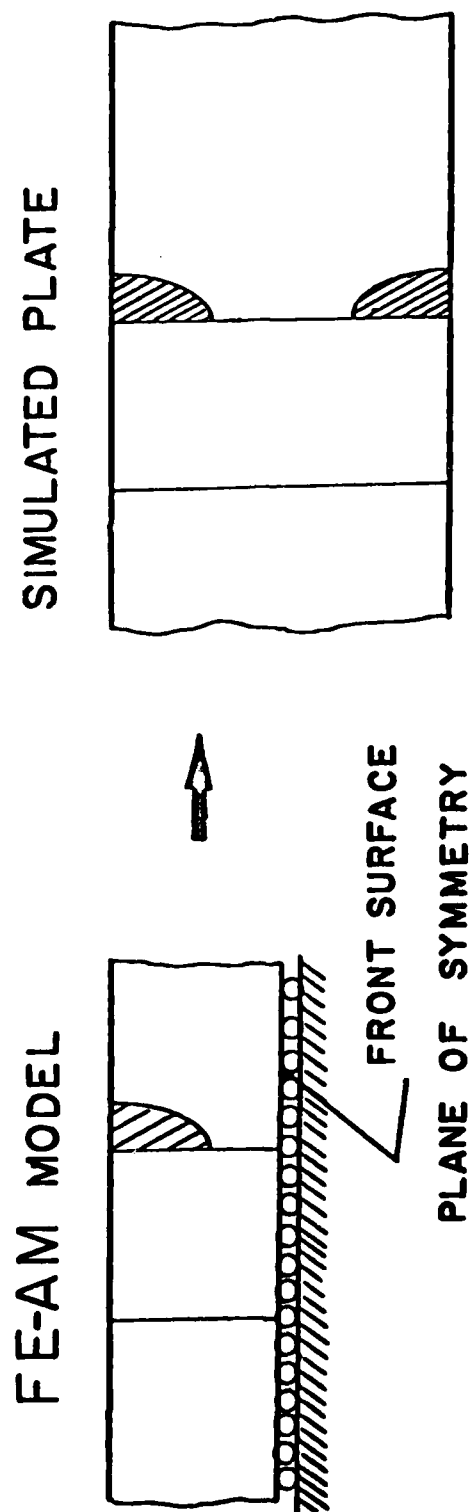


Figure 3 Symmetric crack model showing how front surface plane of symmetry simulates double crack problem.

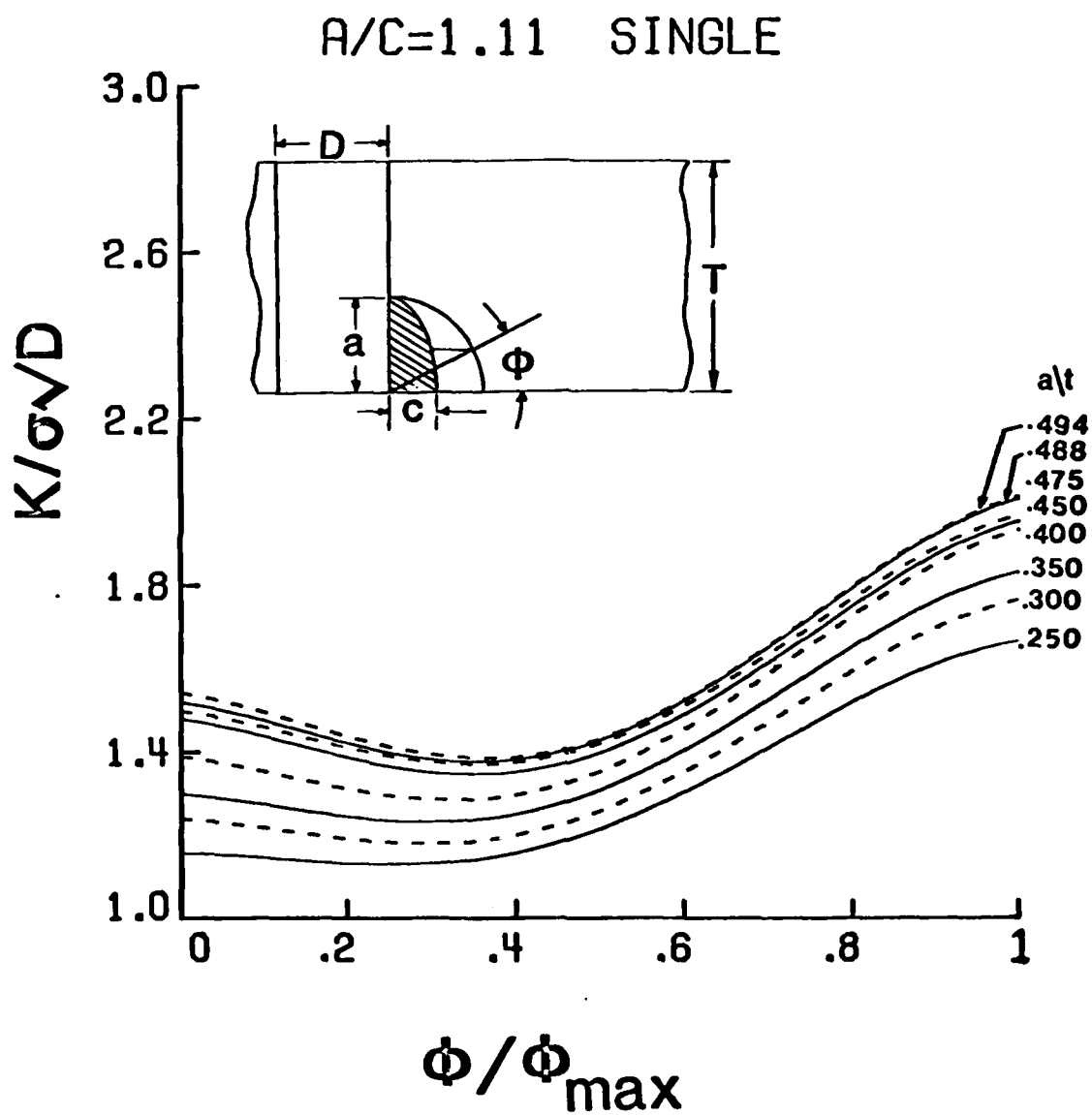


Figure 4 Dimensionless stress intensity factor results for single crack as function of dimensionless parametric angle  $\phi/\phi_{\max}$  ( $\phi = \phi_{\max} = 90^\circ$  at hole bore) and crack size  $a/T$  for crack shape  $a/c = 1.11$ .



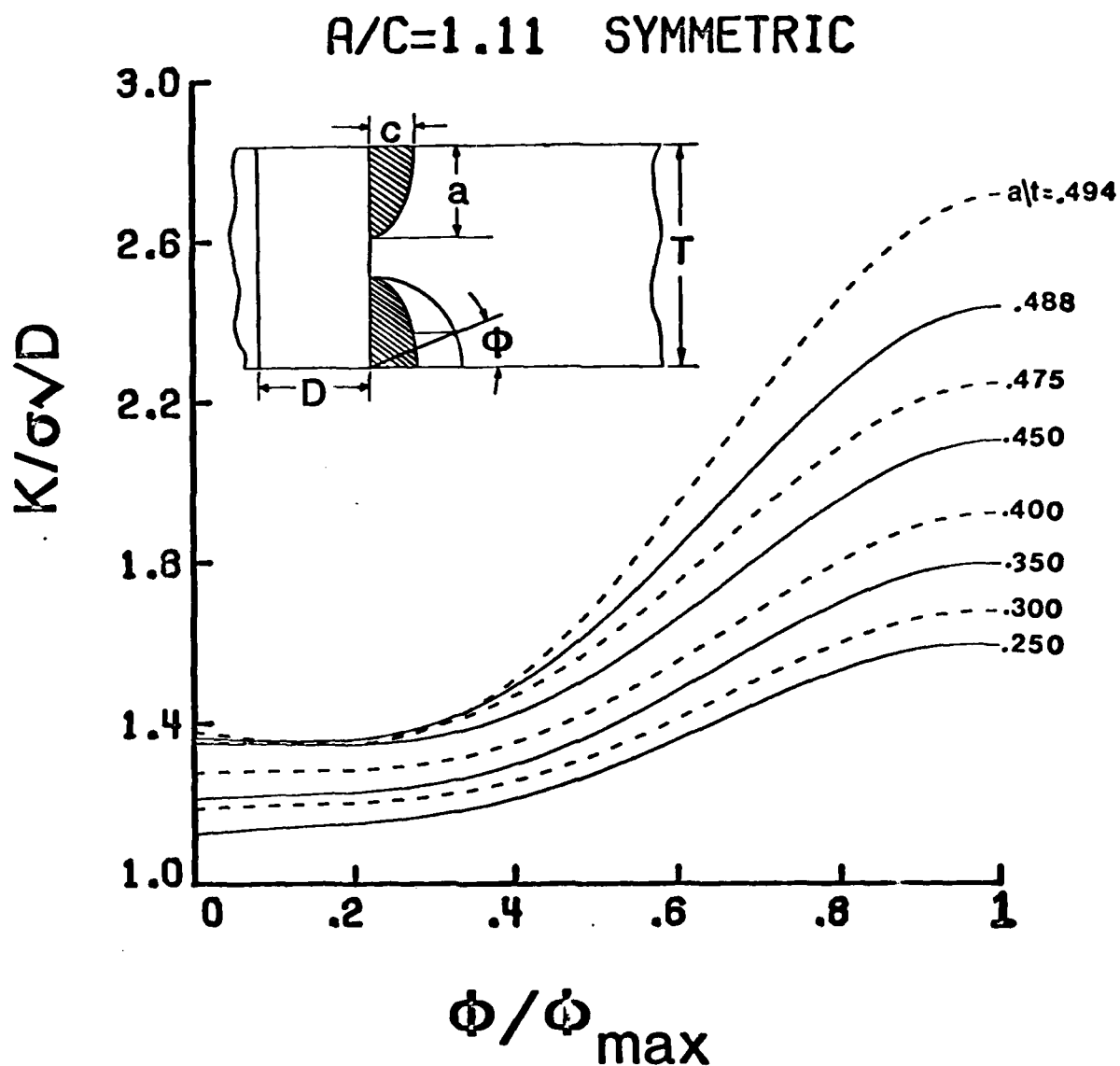


Figure 5 Dimensionless stress intensity factors for symmetric double crack problem as function of dimensionless parametric angle  $\phi/\phi_{\max}$  ( $\phi = \phi_{\max} = 90^\circ$  at hole bore) and crack size  $a/T$  for flaw shape  $a/c = 1.11$ .

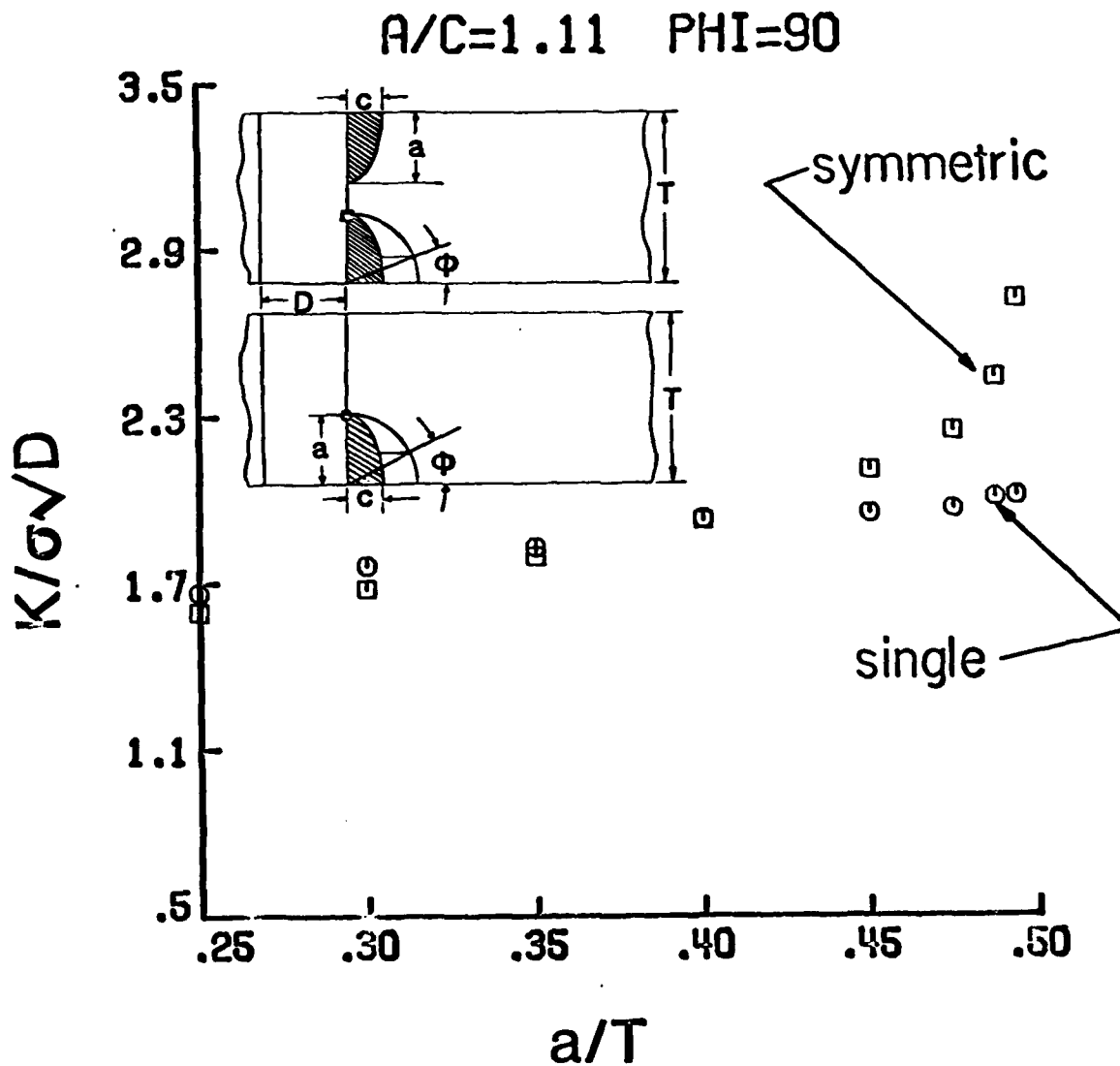


Figure 6 Comparison of dimensionless stress intensity factors for single and symmetric cracks with aspect ratio  $a/c = 1.11$  showing magnification in stress intensity factor at hole bore location ( $\phi = 90^\circ$ ) as crack size  $a/T$  increases.

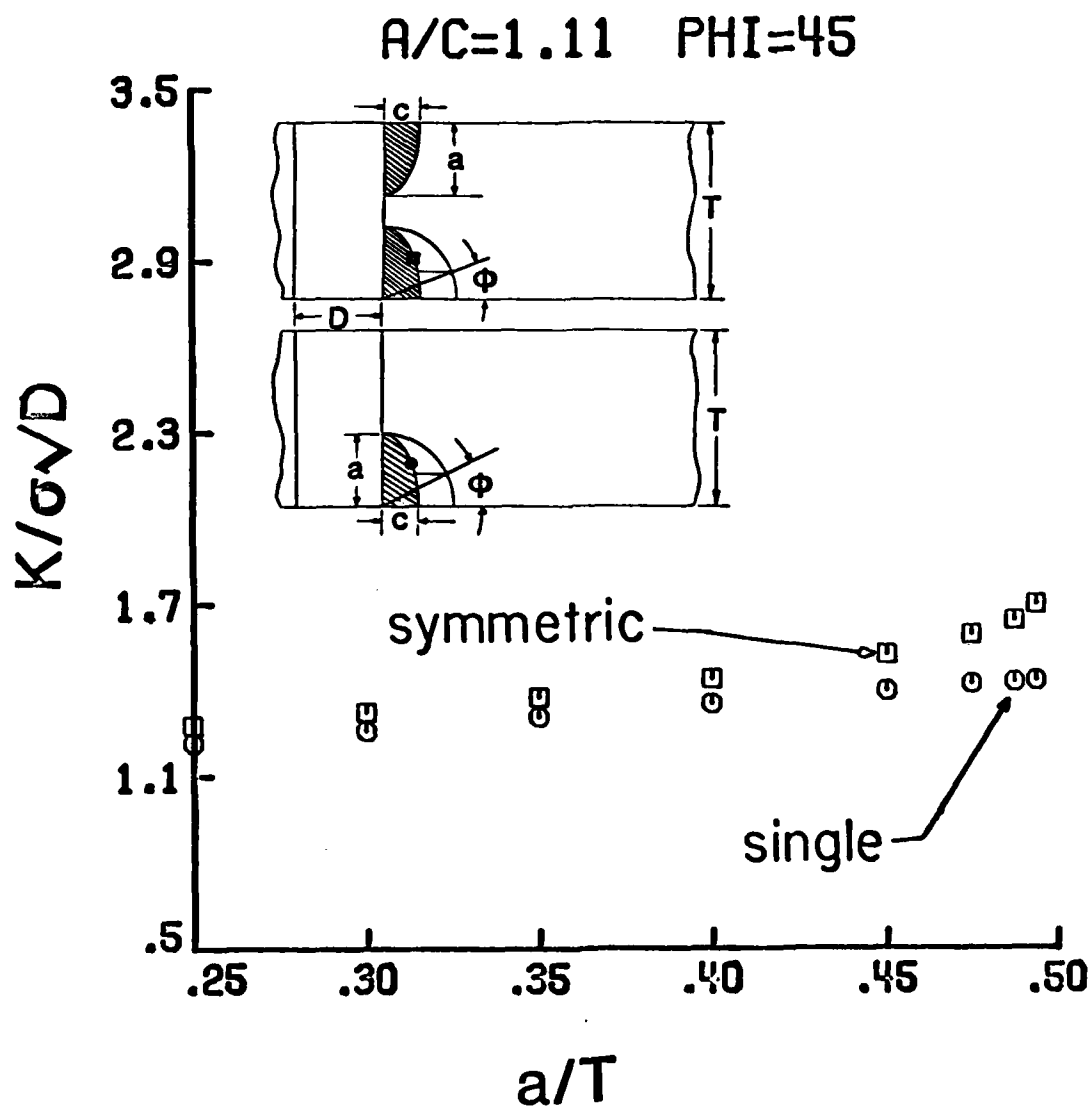


Figure 7 Comparison of dimensionless stress intensity factors for single and symmetric cracks with aspect ratio  $a/c = 1.11$  at crack perimeter location  $\phi = 45^\circ$ .

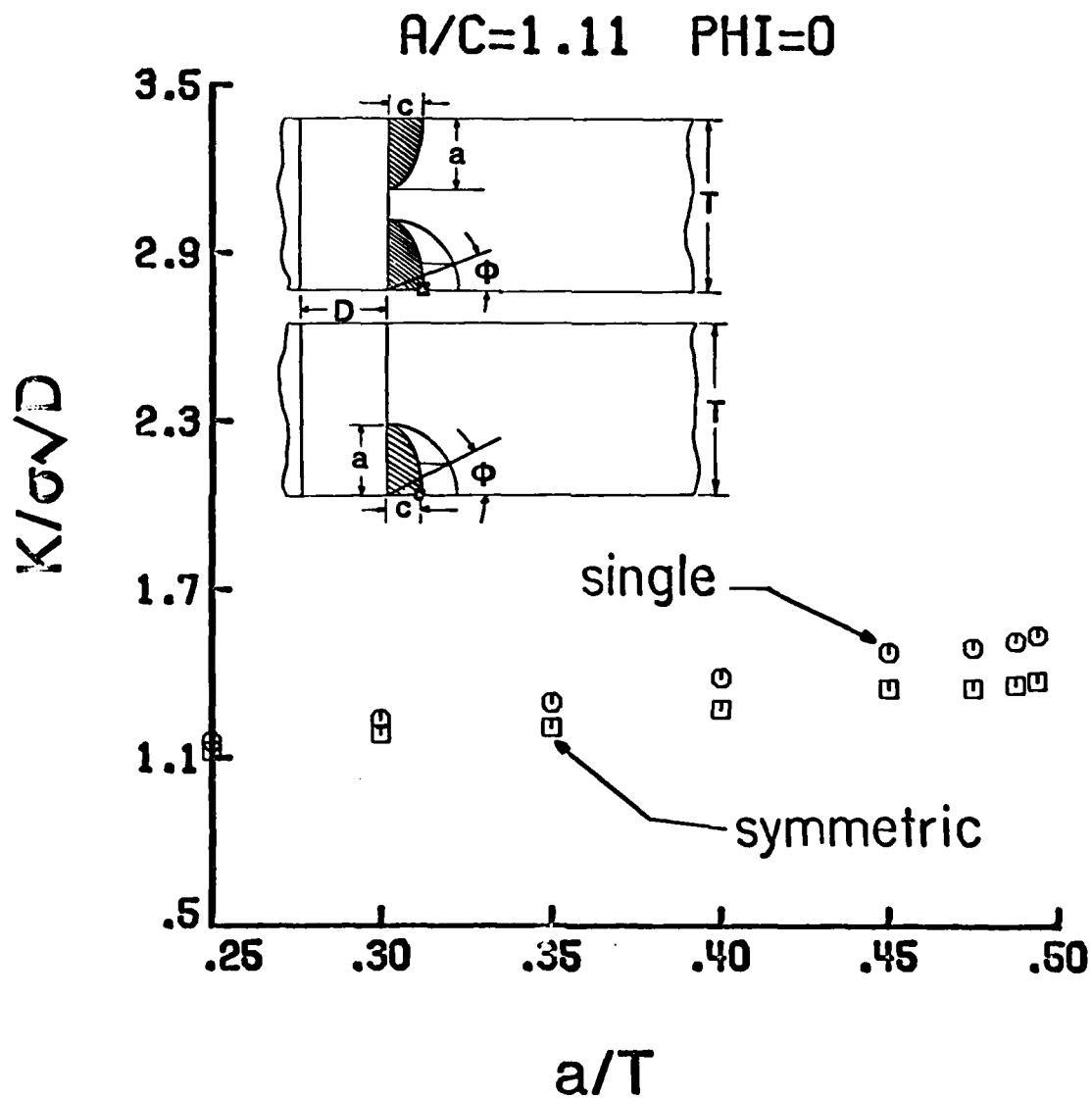


Figure 8 Comparison of dimensionless stress intensity factors for single and symmetric cracks with aspect ratio  $a/c = 1.11$  showing slight decrease in symmetric crack stress intensity factor at surface location ( $\phi = 0^\circ$ ) as crack size  $a/T$  increases.

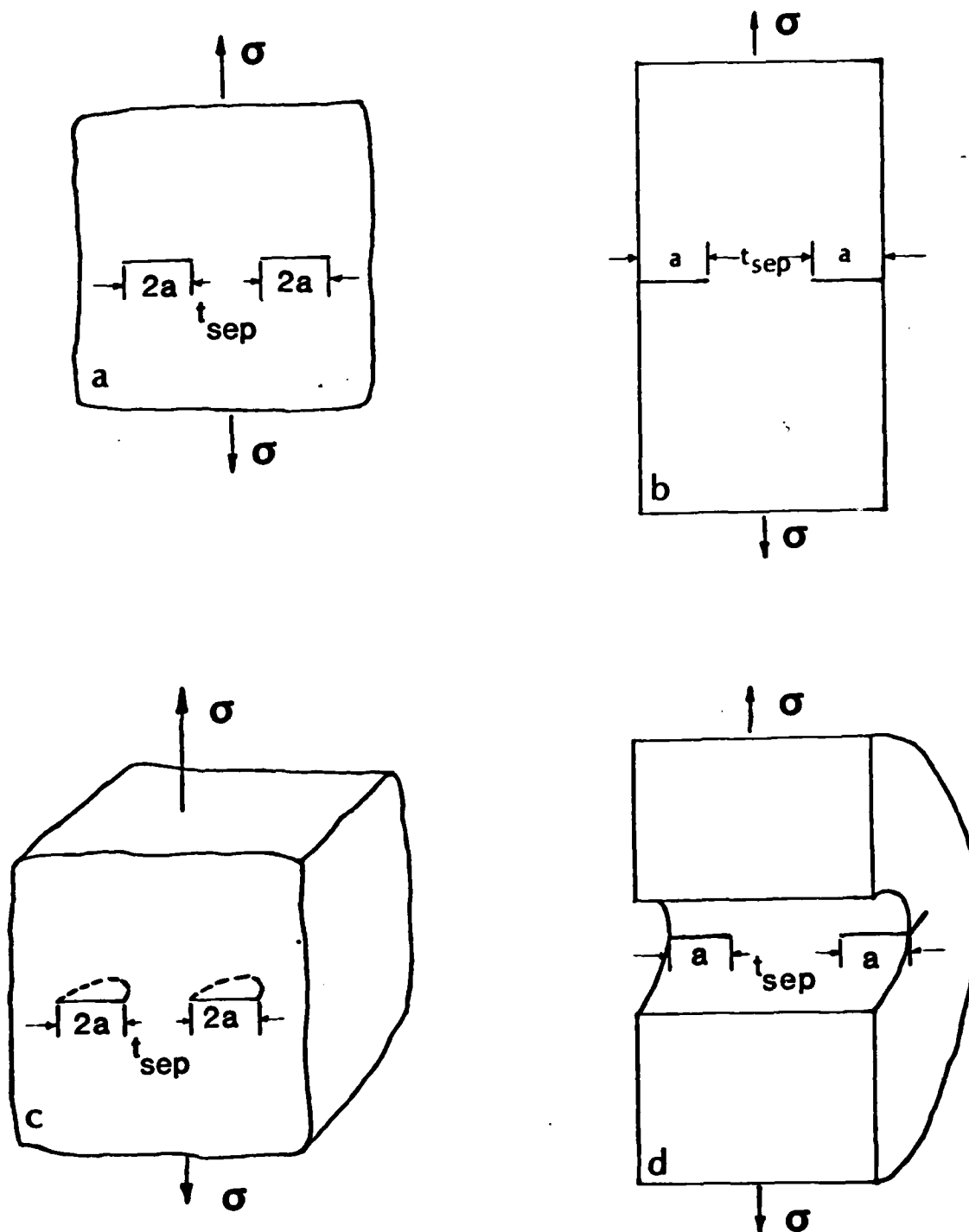


Figure 9 Interacting crack configurations represented by: a. Kamei (through-the-thickness center cracks in a large sheet), b. Koiter and Benthem (through-the-thickness edge cracks), c. Murakami and Nemet-Nasser (surface cracks in a semi-infinite solid), and d. present study (symmetric corner cracks located along hole bore).

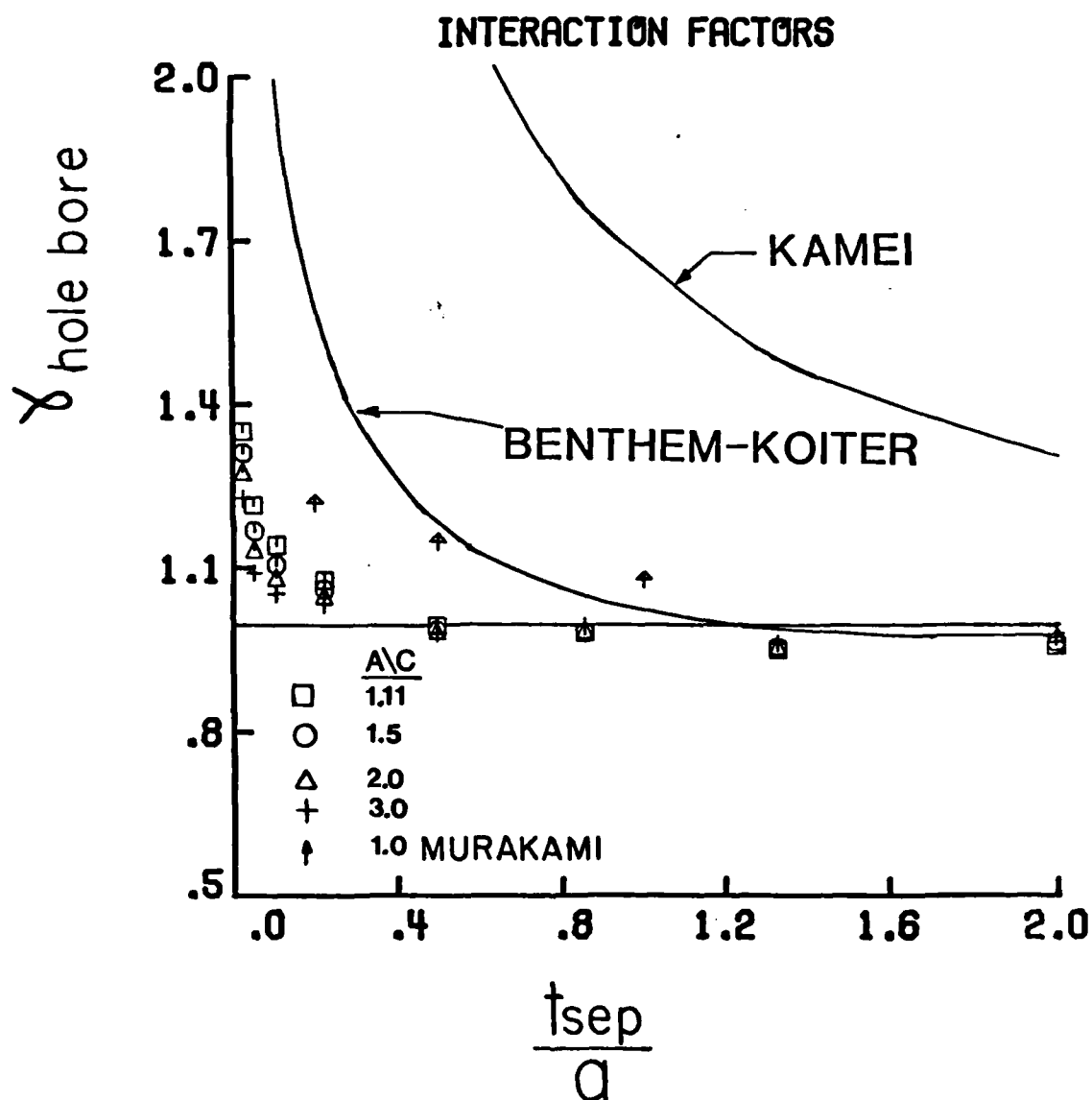


Figure 10 Comparison of effect of crack spacing  $t_{\text{sep}}/a$  on stress intensity factor for various two- and three-dimensional crack configurations. The interaction factor  $\gamma$  is defined as ratio of double to single crack stress intensity factors.

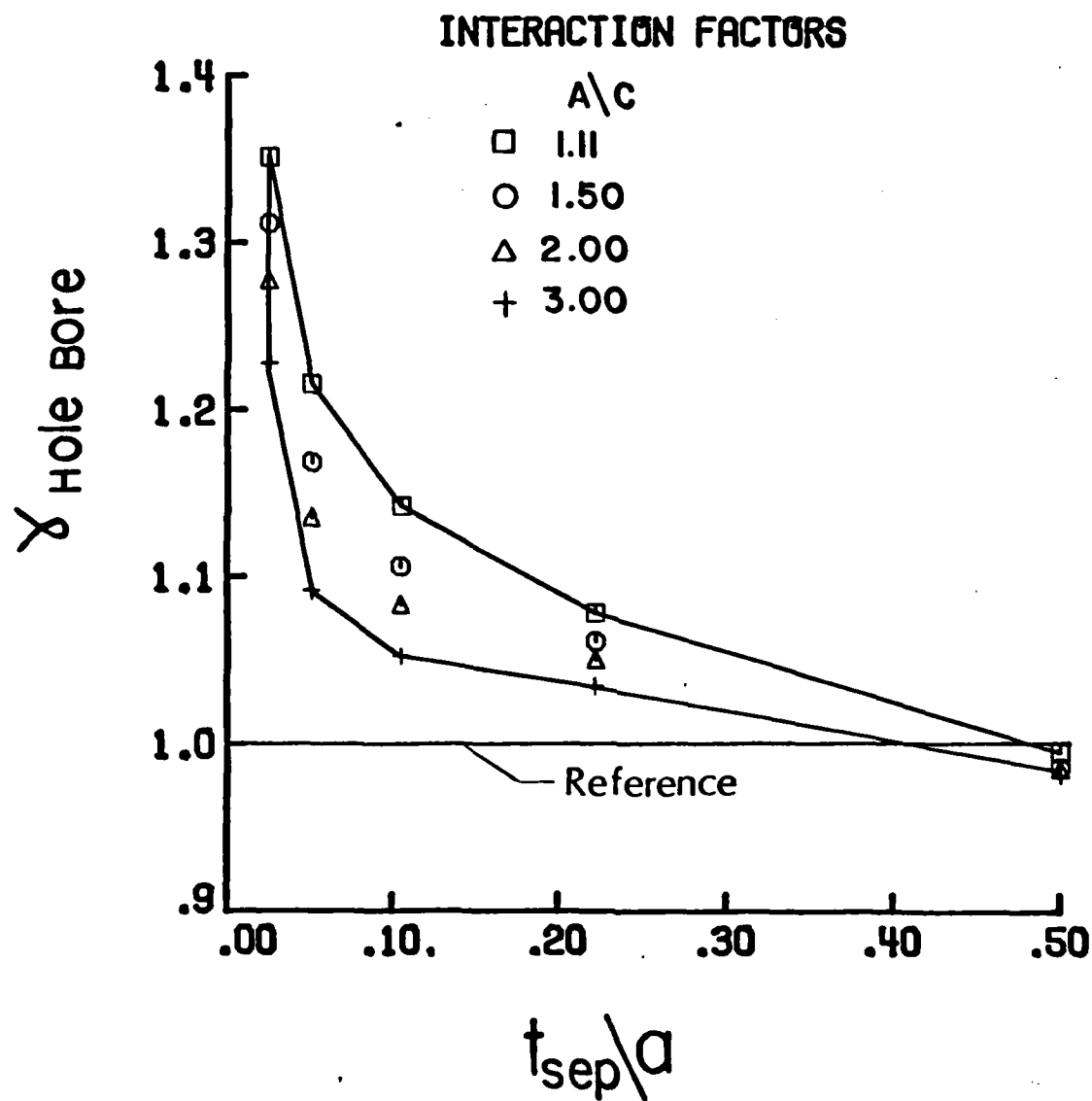


Figure 11 Summary of the effect of crack spacing  $t_{\text{sep}}/a$  and crack shape  $a/c$  on stress intensity factor interaction at hole bore crack location ( $\phi = 90^\circ$ ).

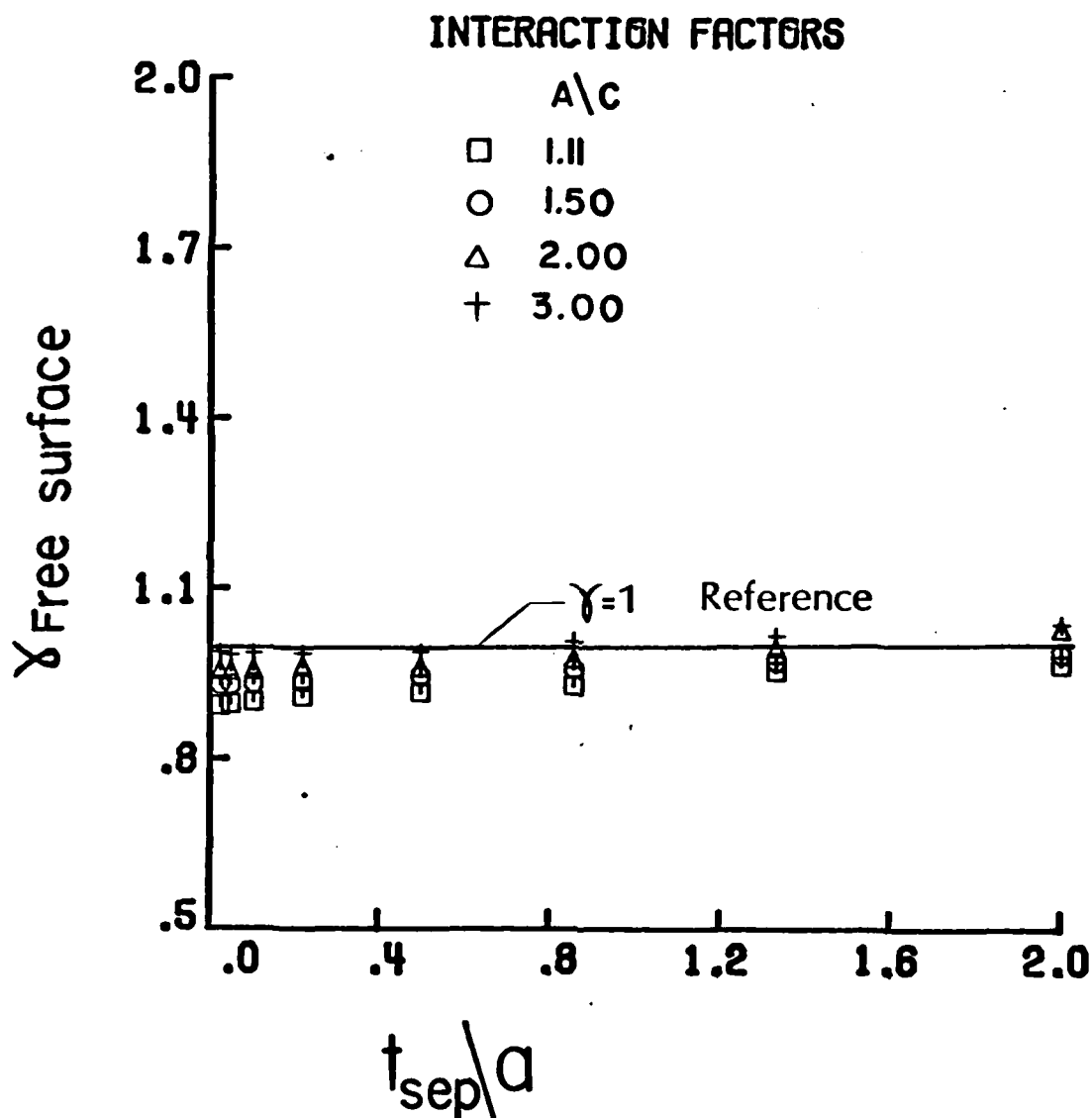


Figure 12 Summary of the effect of crack spacing  $t_{sep}/a$  and crack shape  $a/c$  on stress intensity factor interaction at front surface location ( $\phi = 0$ ) for corner cracked hole.



ED  
8